Horst-Moritz Maus

Towards understanding human locomotion

Towards understanding human locomotion

Horst-Moritz Maus

Universitätsverlag Ilmenau
2013

Impressum

Bibliografische Information der Deutschen Nationalbibliothek
Die Deutsche Nationalbibliothek verzeichnet diese Publikation in der Deutschen Nationalbibliografie; detaillierte bibliografische Angaben sind im Internet über http://dnb.d-nb.de abrufbar.

Diese Arbeit hat der Fakultät für Informatik und Automatisierung der Technischen Universität Ilmenau als Dissertation vorgelegen.

Tag der Einreichung:	04. Juli 2012
1. Gutachter:	Univ.-Prof. Dr.-Ing. Johann Reger (Technische Universität Ilmenau)
2. Gutachter:	Univ.-Prof. Dr. phil. Andre Seyfarth (Technische Universität Darmstadt)
3. Gutachter:	Prof. Dr. Shai Revzen (University of Michigan, USA)
Tag der Verteidigung:	19. Oktober 2012

Technische Universität Ilmenau/Universitätsbibliothek
Universitätsverlag Ilmenau
Postfach 10 05 65
98684 Ilmenau
www.tu-ilmenau.de/universitaetsverlag

Herstellung und Auslieferung
Verlagshaus Monsenstein und Vannerdat OHG
Am Hawerkamp 31
48155 Münster
www.mv-verlag.de

ISBN 978-3-86360-054-9 (Druckausgabe)
URN urn:nbn:de:gbv:ilm1-2012000364

Titelfoto: photocase.com

Preface

Here, in this dissertation, I present my research results from my thesis work in the Lauflabor. Before the actual book starts, I want to take the opportunity to write some personal words and remarks.

Locomotion analysis is an interdisciplinary field of research. Interdisciplinary research areas can benefit from many different fields - but here also lies one of the challenges: every researcher in an interdisciplinary field has his or own strengths and weaknesses in his or her background. Especially when starting research as a graduate student, there are many more things you do not know than things you know. This might be true for all fields of science, but I think that this is especially true for interdisciplinary research areas like locomotion research.

The knowledge I gained during my work was mostly influenced by my colleagues. If I had worked with other colleagues, both my research and my knowledge would have developed in a very different direction. I am grateful to many colleagues and supervisors, because their influence has finally led to the work that is presented here. Without claim of completeness I want to thank and Sten Grimmer, John Guckenheimer, Suzi Lipfert, Karl Kalveram, Johann Reger, Daniel Renjewski, Shai Revzen and Andre Seyfarth, and apologize to all persons that I unfortunately might have forgotten here.

The interdisciplinary nature of this research has left its marks on this thesis. Various methods from different fields are applied, and some new were developed. As interested readers may have very different backgrounds, I give an overview of the applied methods in chapter 2, even if they might be considered common knowledge by some researchers.

Following a proposition on readability from a colleague, this thesis is written mostly in active language and “we”-form. Actually, that specific proposition was meant for journal or conference papers. However, dear reader, as readability is also important for a thesis, let us consider it as follows: here I invite you to follow

my reasoning so that “we” refers to you and me, unless a different meaning is clear from the context[1].

[1] especially in sections 2.2 and 3.3, where published research results from my colleagues and me are presented

for Kerstin
and Magdalena

CONTENTS

Zusammenfassung 13
Summary 15

1 Introduction **17**
1.1 General introduction 18
1.2 Thesis Outline 21

2 Methods overview **23**
2.1 Mathematical Background 24
2.1.1 Principal components analysis 24
2.1.2 Return map computation 26
2.1.3 Identifying main contributors in a linear model 27
2.1.4 Magnitude of the noisefloor in eigenvalue analysis 31
2.1.5 Estimation of significant subspaces 35
2.1.6 Phase estimation by Phaser 37
2.1.7 Detrended Fluctuation Analysis 39
2.1.8 Q-Q-plots 43
2.1.9 State space reconstruction and nonlinear analysis 43
2.1.10 Calculation of Dimension 46
2.1.11 The bootstrap procedure 47

2.1.12 Hypothesis testing with surrogate data 50
2.2 Center of mass estimation 51
2.3 Collection of human treadmill running data 66
2.3.1 Subjects and protocol 66
2.3.2 Experimental setup 67
2.3.3 Basic data processing 67

3 Template models **71**
3.1 Introduction 72
3.2 Calculating SLIP template parameters 74
3.3 A template for stabilization of the posture 75
3.4 Conclusion 86

4 Quantitative gait analysis **89**
4.1 Introduction 90
4.2 Model-free gait characterization 90
4.2.1 Introduction 90
4.2.2 Stationarity and temporal scaling 91
4.2.3 Symmetry of the motion 94
4.2.4 Statistical properties of residuals 94
4.2.5 Spatial scaling 98
4.2.6 Conclusion 98
4.3 Linear Gait analysis 101
4.3.1 Motivation 101
4.3.2 Methods 102
4.3.3 Results 102
4.3.4 Conclusion 107
4.4 SLIP based gait analysis 109
4.4.1 Motivation 109
4.4.2 Methods 109
4.4.3 Results 113
4.4.4 Conclusion 124
4.5 Summary 127

5 General discussion **129**
5.1 Summary: viewing the whole picture 130
5.2 Templates for understanding human locomotion? . . 133
5.3 Physiological aspects of templates and control 135
5.4 Possible applications in machines 138
5.5 Possible applications in gait analysis 139
5.6 Résumé 140

Zusammenfassung

Die zentrale Frage, die in der vorliegenden Arbeit untersucht wurde, ist, wie man die komplizierte Dynamik des menschlichen Laufens besser verstehen kann.

In der wissenschaftlichen Literatur werden zur Beschreibung von Gehen und Rennen oft minimalistische “Template”-Modelle (Full and Koditschek, 1999) verwendet. Diese sehr einfachen Modelle beschreiben nur einen ausgewählten Teil der Dynamik, meistens die Schwerpunktsbahn. In dieser Arbeit wird nun versucht, mittels Template-Modellen das Verständnis des Laufens voranzubringen.

Die Analyse der Schwerpunktsbewegung mittels Template-Modellen setzt eine präzise Bestimmung der Schwerpunktsbahn im Experiment voraus. Hierfür wird in Kapitel 2.2 eine neue Methode vorgestellt, welche besonders robust gegen die typischen Messfehler bei Laufexperimenten ist.

Die am häufigsten verwendeten Template-Modelle sind das Masse-Feder-Modell (Blickhan, 1989; McMahon and Cheng, 1990) und das inverse Pendel (Alexander, 1976; Cavagna et al., 1977), welche zur Beschreibung der Körperschwerpunktsbewegung gedacht sind und das Drehmoment um den Schwerpunkt vernachlässigen. Zur Beschreibung der Stabilisierung der Körperhaltung (und damit der Drehimpulsbilanz) wird in Abschnitt 3.3 das Template-Modell “virtuelles Pendel” für das menschliche Gehen eingeführt und mit experimentellen Daten verglichen. Die Diskussion möglicher Realisierungsmechanismen legt dabei nahe, dass die Aufrichtung des menschlichen Gangs im Laufe der Evolution keine große mechanische Hürde war.

In der Literatur wird oft versucht, Eigenschaften der Bewegung wie Stabilität durch Eigenschaften der Template-Modelle zu erklären. Dies wird in modifizierter Form auch in der vorliegen Arbeit getan. Hierzu wird zunächst eine experimentell bestimmte Schwerpunktsbewegung auf das Masse-Feder-Modell übertragen. Im Anschluss wird die Kontrollvorschrift der Schritt-zu-Schritt-Anpassung

der Modellparameter identifiziert sowie eine geeignete Näherung angegeben, um die Stabilität des Modells, welches mit dieser Kontrollvorschrift ausgestattet wird, zu analysieren. Der Vergleich mit einer direkten Bestimmung der Stabilität aus einem Floquet-Modell zeigt qualitativ gute Übereinstimmung. Beide Ansätze führen auf das Ergebnis, dass beim langsamen menschlichen Rennen Störungen innerhalb von zwei Schritten weitgehend abgebaut werden.

Zusammenfassend wurde gezeigt, wie Template-Modelle zum Verständnis der Laufbewegung beitragen können. Gerade die Identifikation der individuellen Kontrollvorschrift auf der Abstraktionsebene des Masse-Feder-Modells erlaubt zukünftig neue Wege, aktive Prothesen oder Orthesen in menschenähnlicher Weise zu steuern und ebnet den Weg, menschliches Rennen auf Roboter zu übertragen.

Summary

The central question in this thesis is: “How can we better understand the complex dynamics of human locomotion?”

Often in scientific literature minimalistic template models (Full and Koditschek, 1999) are used to describe locomotion. These very simple models describe only a select part of the dynamics, often the motion of the center of mass. Here, we try to improve the understanding of locomotion using these template models.

Analyzing the motion of the center of mass using template models requires a precise reconstruction of this trajectory from experimental data. For this problem, a new method is presented in chapter 2.2 which is especially robust against typical measurement errors in experimental data.

The most commonly used template models are the spring-loaded inverted pendulum model (Blickhan, 1989; McMahon and Cheng, 1990) and the inverted pendulum model (Alexander, 1976; Cavagna et al., 1977), which are intended to describe the motion of the body’s center of mass, thereby neglecting the body’s angular momentum. To address the stabilization of the posture of the body (the body’s angular momentum), the “virtual pendulum” template model is introduced in chapter 3.3 for human walking and compared to experimental data. The discussion of possible mechanisms that could realize this template suggests that the erection of human posture during evolution likely posed no major mechanical or control challenge.

In literature, sometimes templates are used to explain properties of the observed motion by properties of the template. This is also done in a modified form here. First, an experimentally observed center of mass trajectory is transferred to the spring-loaded inverted pendulum. Next, a step-to-step parameter adaptation scheme is identified, and suitable approximations are given that allow a stability analysis of the model when it is equipped with the identified control scheme. Comparison with the direct analysis of stability

using a Floquet model shows qualitatively good agreement. Both approaches show that in slow human running, disturbances are typically rejected within two steps.

Summarizing, we demonstrate how template models can contribute to enhance the understanding of human locomotion. We will also put our results into a broader context, and discuss their potential impact on technical devices like protheses, orthoses and bipedal robots.

1

Introduction

We have found a strange footprint on the shores of the unknown. We have devised profound theories, one after another, to account for its origins. At last, we have succeeded in reconstructing the creature that made the footprint. And look! It is our own.

Sir Arthur Eddington (1882-1944)

1.1 General introduction

”Life Is Motion“ - this is the title of a poem from Wallace Stevens. Although this claim is scientifically not correct - motion is not part of most definitions of life - how would human life without motion, without locomotion, look like? It is hard to imagine, at least for healthy people. For most people, walking is so rooted in their daily life, that they would never specify it when asked what they did this day. However, when people loose their ability to walk, it becomes obvious what a large impairment this would be. Especially under such circumstances, the importance of locomotion for human life is undisputed.

For healthy humans, walking and running are trivial tasks. If we stumble or fall, we do not doubt the reliability of our locomotor system but rather look at the floor to see if we overlooked an obstacle or an unexpected slippery part of the surface. The opposite is true for today’s bipedal robots, even for the most advanced ones: a failure is primarily attributed to the robot itself unless other reasons are obvious.

There has been remarkable progress in the last few years in bipedal robots - PetMan from Boston dynamics (Petman), new developments in Honda’s ASIMO (ASIMO, 20.11.2011), and the quasi-planar robot Mable (Sreenath et al., 2011, 2012), to give some prominent examples. The reasons for building legged robots are many. Besides academic interests like the verification of control concepts, there are many practical applications. Bipedal robots could potentially reach areas that are not accessible by wheeled robots, in disaster zones as well as in typical apartments with stairs. Further, building a humanoid robot with truly human-like gait would likely promote the development of prostheses and ortheses. But what is the current state of the art, compared to humans?

Today, human performance in terms of speed, endurance, versatility and efficiency, and especially the combination of these features in a single system, is unrivaled. There are specialized bipedal robots

that perform excellent in single tasks - eaibert's famous legged robots for example, described in the famous book by Raibert (1985), which could even perform somersault in 1992 (Playter and Raibert, 1992), and the passive and nearly-passive dynamic walkers, starting in the 1990s from McGeer (1990), have now reached a remarkable level of energy efficiency in walking that is close to or even better than humans (Collins et al., 2005; Bhounsule and Ruina, 2009). Yet, so far a healthy human would easily outperform every modern bipedal robot in everyday situations, where disturbance recovery, adaptation (e.g. wearing a backpack), moderate energy efficiency and versatility are required - not talking at all of path planning or related tasks.

What are the reasons for this seeming low performance, especially if in contrast industrial robots show performance in terms of speed combined with accuracy that a human could never reach? This is because -in contrast to industrial robots- most complications a roboticist would imagine are present in autonomous bipedal robots: disturbances due to impacts, underactuation and actuator limitations, to give some important examples. The design of a robot that is strong, powerful and light enough to show human-like locomotion is a complex, challenging - for example, the selection of actuators must be very accurate and precisely adapted to the geometry and desired motion, and leaves almost no freedom of choice (Radkhah et al., 2011; Radkhah and von Stryk, 2011). However, finding the "optimal" control of such a system is probably an even more demanding challenge.

One of the difficult tasks in finding an "optimal" control is the proper definition of an optimality criterion - when do we consider a motion to be "optimal"? Many researchers have shown that humans tend to "somehow" optimize their gait with respect to energetic costs (Alexander, 1984, 1991; Donelan et al., 2001; Ortega and Farley, 2005), but the inexact match of optimal configurations on the one hand and the variability of human gait (Ludwig, 2010) on the other hand indicate that there is no single optimal solution

that humans try to adapt to. In other words: There seems to be no single optimality criterion. Liu and Todorov (2007) have shown this for a different motion task (reaching). This might not be too surprising, because in nature the optimality criterion might depend on the situation: muscle fatigue might lead to a gait with higher stress on bones, whereas safety requirements in cluttered environments might lead to a more exhausting gait pattern.

Around 1990, Blickhan (1989) and McMahon and Cheng (1990) came up with the idea to describe human running with a "behavior", namely by the bouncing of a point mass on top of a spring. Later, it was shown by e.g. Seyfarth et al. (2002), Seyfarth et al. (2003), Geyer et al. (2006), Rummel et al. (2010) that this behavior, namely elastic leg operation, offers convenient features like stability and robustness for running and walking. This idea of describing a "complex, high-dimensional, non-linear" motion with highly abstract models in the first approach was discussed in detail in the well-known article of Full and Koditschek (1999), where these kind of models were named "templates". These templates improved our understanding of how locomotion is organized and how it could be controlled (e.g. Blum et al. (2010)), and can further offer a way to transfer human-like locomotion principles into legged robots (e.g. Westervelt et al. (2003), Poulakakis and Grizzle (2007)).

Other researchers have tried to characterize human gait with the tools of dynamical system theory and nonlinear time series analysis. There have been attempts to describe locomotion as asymptotically stable limit cycle (e.g. Hurmuzlu and Basdogan (1994)) or as chaotic motion (e.g. Dingwell and Cusumano (2000); Dingwell et al. (2001); Dingwell and Kang (2007)). However, there are doubts to what extent these parameters are suited to assess the human gaits (Granata and Lockhart, 2008; Bruijn et al., 2012).

To this day, many aspect of the organization of human locomotion are still unknown or not well understood. When does control happen - continuously or at discrete times? To what extend are supraspinal levels involved in control? Is there a unique control law

for a certain situation, or do grown up humans continously adapt their locomotion control scheme? How does control change in impaired or elderly people? I cannot give answers to these questions, but in this dissertation I present new contributions to the characterization of the human gaits that will further enhance our understanding of this complex topic.

In section 1.2, an outline of this work is presented, giving a brief overview of every chapter, and pointing out each chapter's contribution.

1.2 Thesis Outline

This thesis is organized as follows:

In chapter 2, we give an overview of the applied methods. Here, also new contributions are presented, namely a new way to estimate the motion of the center of mass from measurement data with typical error profile, and a contribution to estimate the noise floor of the eigenvalues in regression matrices.

In chapter 3, we introduce the notion of template models for describing gaits. Here, a new template, namely the Virtual Pivot Point (VPP), is presented with its possible implications for human gait and its evolution.

In chapter 4, we perform a quantitative analysis of an experiment on human treadmill running. This chapter is partitioned into three main sections: First, in section 4.2 the dynamics around the average motion are analyzed in order to gain basic knowledge on the kind of the dynamical system. Second, in section 4.3, a linear approximation of the dynamics (that is, a Floquet model), is fitted to the data and its eigenvalues are analyzed. Third, a template-based investigation of the control of the center of mass dynamics in humans is performed in section 4.4.

We will summarize and discuss the main results, putting the findings into a broader context, in the final chapter 5.

2

Methods overview

Smoking is one of the leading causes of statistics.
Fletcher Knebel (1911 - 1993)

This thesis draws upon a diverse collection of mathematical tools for data analysis. Most methods are summarized in this chapter and will be referred to in the text when they are used. Here, general methods are presented first with corresponding links to the literature (except section 2.1.4 where a new contribution is presented). Next, a new method for estimating the center of mass (CoM) trajectory from experimental data is presented. Finally, in section 2.3 the experimental setup for data analyzed in chapter 4 is presented.

2.1 Mathematical Background

In this section, I briefly summarize mathematical methods used in this thesis. References to the literature are presented, but the main points of every method should be understandable from the text. The methods are not presented with all details, for example the complex valued cases are (mostly) neglected. Nonetheless, relevant aspects for the future chapters are included.

2.1.1 Principal components analysis and singular value decomposition (PCA, SVD)

Principal component analysis (PCA) is a commonly used method to identify the main components, that is the directions of largest variation of a multidimensional dataset. It is very closely related to the singular value decomposition (SVD) of a matrix.

Let us start with a real-valued data matrix $\hat{M}$ of dimension $d \times n$. Without loss of generality assume $n \geq d$ (transpose matrix $\hat{M}$ if

$d < n$). The singular value decomposition of this matrix (Eckart and Young, 1936; Golub and Reinsch, 1970) is:

$$\begin{aligned} \hat{M} &= \hat{U}\hat{\Sigma}\hat{V} && \text{with} \\ \hat{U}^T\hat{U} = \hat{U}\hat{U}^T &= \mathbb{1} && \hat{U} \text{ is a } d \times d \text{ orthogonal matrix} \\ \hat{\Sigma} &= \mathrm{diag}(\sigma_i) && \hat{\Sigma} \text{ is a } d \times d \text{ diagonal matrix with non-negative entres} \\ \hat{V}\hat{V}^T &= \mathbb{1} && \hat{V} \text{ is a } d \times n \text{ matrix with orthogonal rows} \end{aligned} \tag{2.1}$$

The entries σ_i of Σ are ordered by descending magnitude: $\sigma_1 \geq \ldots \geq \sigma_d$.

Let us now assume that the data are centered, that is the mean of each row of $\hat{M}$ is zero. Then, the SVD is related to the covariance matrix $\hat{C}$ of $\hat{M}$. The element c_{ij} of the covariance matrix is the covariance of the the data rows i and j. $\hat{C} = \frac{1}{(N-1)}\hat{M}\hat{M}^T$ is symmetric. Using the SVD, we obtain:

$$\hat{C}(N-1) = \hat{M}\hat{M}^T = \hat{U}\hat{\Sigma}\underbrace{\hat{V}\hat{V}^T}_{=\mathbb{1}}\hat{\Sigma}\hat{U}^T = \hat{U}\hat{\Sigma}^2\hat{U}^T \tag{2.2}$$

Here, the SVD gives an orthogonal diagonalization of the (scaled) covariance of the data $\hat{M}$. Now, we interpret the columns of $\hat{U}$ as new, orthogonal coordinate axes. The covariance matrix is diagonal in these coordinates. The tranformation of the matrix $\hat{M}$ to the basis $\hat{U}$ gives the "scores" $\hat{\Sigma}\hat{V}$, which are by construction linearly independent. The first axis covers the largest part of the variance, the second axis the second largest part, and so on. Thus, we call these new axes the **principal components** of the data. The fraction

$v(k)$ of the total variance that is captured by the first k principal components is

$$v(k) = \frac{\sum_{i=1}^{k} \sigma_i^2}{\sum_{i=1}^{d} \sigma_i^2}. \tag{2.3}$$

Plotting $v(k)$ over k can give an estimate of how many principal components are required to capture the desired amount of the total variance.

2.1.2 Return map computation

Periodic systems can be analyzed by investigating a stroboscopic view of their state, taken once per cycle when the dynamics cross a predefined hyperplane in the phase space (Guckenheimer and Holmes, 1983). These hyperplanes are called Poincaré-sections. A map that maps the state x_n at the n^{th} crossing of the Poincaré-section to the state x_{n+1} at the $n+1^{th}$ crossing is called a return map. In the following, when we refer to a return map we mean a linear approximation of the potentially nonlinear return map.

We can compute a linear approximation of the return map from experimental data as that linear map $\hat{A}$ that best (in a least-squares sense, see below) maps the experimental data at a given Poincaré-section to the next crossing of that Poincaré-section. Here, we are interested in the dynamics *around* a hypothetical limit cycle, thus the term "data" refers to the residuals after subtracting the average gait cycle. We thus assume that the mean of the data has been removed, that is, the data are centered.

Let $\hat{X}$ denote the $d \times k$ data matrix containing the input data, and $\hat{Y}$ denote the $d \times k$ data matrix that we want to predict using $\hat{X}$. Note that the formalism does not change when general least-squares regressions are performed, that is, when $\hat{Y}$ is of dimension $p \times k$ with $p \neq d$. In this thesis, each column of $\hat{Y}$ represents the data one stride ahead of the corresponding column of $\hat{X}$. For example,

the 5th column of $\hat{Y}$ contains the data one stride ahead of the data in the 5th column of $\hat{X}$. This least-squares problem can be formulated as the minimization of $\min_{\hat{A}} \|\hat{Y} - \hat{A}\hat{X}\|_F$. Minimizing the Frobenius norm of a matrix is equivalent to minimizing the sum of squares of its elements.

There is a general solution to this problem (e.g. Kiebel and Holmes, 2003):

$$\hat{A} = \hat{Y}\hat{X}^{-}, \tag{2.4}$$

with $\hat{X}^{-}$ denoting the Moore-Penrose pseudo-inverse of $\hat{X}$, which can be computed using the SVD $\hat{X} = \hat{U}\hat{\Sigma}\hat{V}$:

$$\hat{X}^{-} = \hat{V}^{T}\hat{\Sigma}^{-}\hat{U}^{T}. \tag{2.5}$$

Here, the elements of $\hat{\Sigma}^{-}$ are σ_i^{-1} if $\sigma_i \neq 0$, and 0 otherwise. It is easily verified that if $\hat{X}$ is an invertible matrix (that is, $\hat{V}$ is square and thus orthogonal, and all $\sigma_i > 0$), then $\hat{X}^{-}$ is the inverse of $\hat{X}$.

In this thesis, a modification is used to make the computation more robust against measurement noise. A potential problem is that small σ_i become very large numbers when being inverted. However, when the σ_i are small, this typically means that the variance along the corresponding axis is rather low, and that noise might dominate the data along that axis. Thus, the inversion might lead to large matrix elements which are however determined mostly by noise. In numerical considerations, this problem of strong dependence of the solution on the data is known as the condition of a problem. Here, we can express the condition as the "condition number" of the matrix which is defined as $\frac{\max \sigma_i}{\min \sigma_i}$. In order to avoid the condition problem, σ_i that are smaller than $10^{-4}\sigma_1$ are not inverted in return map computations but set to 0.

2.1.3 Identifying main contributors in a linear model

Here, we are interested in extracting the main factors (linear combinations of the input in a linear model) that explain most of the

variance in a dataset that we want to predict. That is, we ask the question: Can we reduce the dimension of the input data in a linear regression to get the same or almost the same variance of the output data explained?

Let's assume we have some data $\hat{P} \in \mathbb{R}^{d \times n}$ that we want to predict using the data $\hat{X} \in \mathbb{R}^{m \times n}$. We interpret these data as having n measurements of P, each with dimension d, and having also n measurements of X, each with dimension m. Here, we assume that $n > m, n > d$, and that the mean of each row in $\hat{P}$ and $\hat{X}$ is zero.

We formulate the linear model as

$$\hat{P} = A\hat{X} + \eta, \tag{2.6}$$

with A being the matrix that minimizes $||\hat{P} - A\hat{X}||_F$, and η beeing the remaining prediction error.

The general solution to this problem is $A = \hat{P}\hat{X}^-$, with $\hat{X}^-$ denoting the (Moore-Penrose) pseudoinverse of $\hat{X}$ (see section 2.1.2).

Generally, any matrix Y that is formed by another matrix y by $Y := y^- y$ is an orthogonal projector, that is, $Y^2 = Y$ and $Y^T = Y$. Using this, we can easily compute the covariance of the unpredicted data η from the prediction $A\hat{X}$:

$$\begin{aligned}(n-1)\mathrm{cov}(A\hat{X}, \eta) =& A\hat{X}\,\eta^T \\ =& (\hat{P}\hat{X}^-\hat{X})(\hat{P} - A\hat{X})^T \\ =& (\hat{P}\underbrace{\hat{X}^-\hat{X}}_{=:Q})(\hat{P}^T - \underbrace{\hat{X}^T(\hat{X}^-)^T}_{=Q^T=Q}\hat{P}^T) \\ =& \hat{P}Q(\hat{P}^T - Q\hat{P}^T) = \hat{P}Q\hat{P}^T - \hat{P}\underbrace{Q^2}_{Q^2=Q}\hat{P}^T = 0\end{aligned} \tag{2.7}$$

As expected, the prediction $A\hat{X}$ is uncorrelated with the remainder η. It follows that the covariance of $\hat{P}$ can be expressed as sum of the covariance of $A\hat{X}$ and the covariance of η (which we identify

as that part of the covariance that cannot be predicted from $\hat{X}$), and the total variance of $\hat{P}$ which can be expressed as the trace of its covariance matrix equals the total variance of $A\hat{X}$ plus the total variance of η.

We now ask "How much of the predictable variance (that is, variance of $A\hat{X}$) can we get when we use only k input dimensions?" and "What are these dimensions?".

Let now USZ be a singular value decomposition of $\hat{X}$. The matrix S is diagonal with the elements $\sigma_1, \ldots, \sigma_r, 0, \ldots, 0$. Let S^- be the diagonal matrix with elements $\sigma_1^{-1}, \ldots, \sigma_r^{-1}, 0, \ldots, 0$. (that is, S^- is a pseudoinverse of $S : SS^-S = S$). We know by construction of USZ and $n > m$ that $ZZ^T = 1, U^T = U^{-1}$ and see that $US(S^-U^T)USZ = USZ = \hat{X}$. We can now express the covariance of $A\hat{X}$ as:

$$\begin{aligned}(n-1)\mathrm{cov}A\hat{X} =& (A\hat{X})(A\hat{X})^T \\ =& A\hat{X}\hat{X}^T A^T \\ =& \underbrace{AUS}_{=:B}\underbrace{ZZ^T}_{=1}\underbrace{S^TU^TA^T}_{=B^T} = BB^T. \end{aligned} \tag{2.8}$$

The variance of $A\hat{X}$ is now $(n-1)$ times the trace of BB^T, which itself is sum of the squared singular values of B. We can interpret Z as a scaled and rotated representation of $\hat{X}$, having orthogonal rows. Let now $U_B\Sigma_B V_B = B$ denote a singular value decomposition of B. When we decide to project the data Z onto the first k rows of V_B, and set the remainder to 0 (that is, we select a k-dimensional subspace of the input data), we see that this can easily be achieved by setting all but the first k singular values $\sigma_{B,i}$ in Σ_B to 0. The relative remaining variance $v(k)$ of BZ_k is then

$$v(k) = \frac{\sum_{i=1}^{k} \sigma_{B,i}^2}{\sum \sigma_{B,i}^2}. \tag{2.9}$$

In other words, if we decide to restrict ourselves to have k regressors, we still can explain the fraction $v(k)$ of the total variance.

One can plot $v(k)$ over k to see how many regressors are necessary to obtain the desired amount of predictable variance. Interestingly, because B can be expressed as product of $\hat{P}$ and $\hat{X}^-$, the rank of B is smaller or equal to $\min(\mathrm{rank}(\hat{P}), \mathrm{rank}(\hat{X}^-)) = \min(\mathrm{rank}(\hat{P}), \mathrm{rank}(\hat{X}))$. That is, no matter how large the rank of $\hat{X}$, we never need more factors than the rank of $\hat{P}$.

Let's say we have chosen to keep k factors. We now want to examine these factors, which we already identified as the first k rows of V_B, in the space of $\hat{X}$. We compute B' as $U_B \Sigma'_B V_B$, with $\sigma'_{B,i} = \sigma_{B,i}$ for $i \leq k$, and 0 otherwise. B' is a reduced version of B that takes only the projection onto the first k rows of V into account. Now, assuming that S is invertible (e.g. due to some noise in $\hat{X}$), we can write $Z = S^- U^T \hat{X}$ and obtain

$$B'Z = \underbrace{B'S^-U^T}_{=:C}\hat{X} = U_C \Sigma_C V_C \hat{X}. \tag{2.10}$$

As the rank of B' is k, the rank of C and the number of nonzero singular values σ_C is also k. That is, only data that are projected on the space that is spanned by the first k rows of V_C contribute to the result of CX. By construction, the rows of V_C are orthonormal, so we can interpret the first k rows of V_C (V_C^k) as basis in the space of our factors, and the rows themselves as factors. As we could choose another basis in that subspace, the choice of factors is not unique. Note that these k axes need not coincide with the first k principal axes of $\hat{X}$.

We might be interested to see if there are a few linear combinations of the input data $\hat{X}$ that give especially large contributions for the prediction $A\hat{X}$. To analyze this, we can normalize $\hat{X}$, perform the factor analysis as mentioned above, and investigate which columns of V_C^k have large magnitude. Each column of V_C^k is a linear combination of the columns of $\hat{X}$, and all have the same variance. Thus, columns with large magnitude are major contributors to the variance of the prediction $A\hat{X}$.

2.1.4 Estimating the diameter of the the noise floor in the eigenvalue analysis

When eigenvalues of least squares regression matrices are computed, errors in the regression will also lead to errors in the eigenvalues. Here, in order to quantify this phenomenon, the expected eigenvalue distribution of regression of random data using other random data is computed. This eigenvalue distribution is what we would expect if there is absolutely no structure in the data.

Some approximations are performed, and their validity in the region of interest is verified in numerical examples. These results allow a comparison to what extent the observed eigenvalues could be explained by noise. In a first step, we analyze the regression of random data using a permutation of the same random data. Then, we argue under which circumstances these results can be transferred into the more general case of two different sets of random data.

Let $\hat{X}$ be a $d \times n$ matrix, $n \geq d$, that represents a single d-dimensional measurement in each column. Let the mean of each row of $\hat{X}$ be 0. Further, let π_i be a random permutation of the numbers $1 \ldots n$, and $\hat{Y} = (Y_{i,j}) = (X_{\{i,\pi_j\}})$ be a random permutation of the measurement data that only permutes the position of each measurement (that is, it permutes the position of the columns). Let $\hat{A}$ be a solution for $\min_{\hat{A}} \|\hat{Y} - \hat{A}\hat{X}\|_F$, a least squares regression matrix (see section 2.1.2). What can we say about the eigenvalues of $\hat{A}$?

First, we notice that $\hat{X}$ and $\hat{Y}$ describe the same n points in $\mathbb{R}^d$ (only in different order) and thus have common principal axes, and the same variance along these axes. Consequently, a partially common singular value decomposition is possible: $\hat{X} = \hat{U}\hat{\Sigma}\hat{V}_x$ and $\hat{Y} = \hat{U}\hat{\Sigma}\hat{V}_y$. $\hat{U} \in \mathbb{R}^{d\times d}$ is an orthogonal matrix, $\hat{\Sigma} \in \mathbb{R}^{d\times d}$ is a diagonal matrix with non-negative entries σ_i, and $\hat{V}_x, \hat{V}_y \in \mathbb{R}^{d\times n}$ are matrices with orthogonal rows. ($\hat{V}_y$ has orthogonal rows if $\hat{V}_x$ has orthogonal rows, because its columns are the permuted columns of $\hat{V}_x$, that is, $\hat{V}_{y_{i,j}} = \hat{V}_{y_{i,\pi(j)}}$. The dot product of the rows m and n of $\hat{V}_y$ is now $\sum_j \hat{V}_{y_{m,j}}\hat{V}_{y_{n,j}} = \sum_j \hat{V}_{xm,\pi(j)}\hat{V}_{xn,\pi(j)} = \sum_{\pi(j)} \hat{V}_{xm,j}\hat{V}_{xn,j} = \delta_{mn}$.)

Let us now assume that $\sigma_i > 0 \, \forall i$, that is Σ is invertible, which is almost-sure for experimental data because of measurement noise.

A least squares regression map $\hat{A}$ can be computed by $\hat{A} = \hat{Y}\hat{X}^{-}$, where $\hat{X}^{-}$ is the Moore-Penrose pseudo inverse of $\hat{X}$. Using the partially common singular value decomposition, this reads

$$\hat{A} = \hat{U}\hat{\Sigma}\underbrace{\hat{V}_x\hat{V}_y^{\,T}}_{=:\hat{V}'}\hat{\Sigma}^{-1}\hat{U}^T. \tag{2.11}$$

The eigenvalues of $\hat{A}$ are now the eigenvalues of $\hat{V}'$, because $\hat{A}$ and V' are related via a similarity transformation.

What can we say about the variance of the entries of $\hat{V}'$? Let us recall how the elements of $\hat{V}'$ are computed: A column from $\hat{V}_y^{\,T}$ is projected onto a row of $\hat{V}_x$. We can interpret this formally as a projection of a unit-length vector $y \in \mathbb{R}^n$ onto another random (unit-length) vector $x \in \mathbb{R}^n$. Actually, the direction of x is not completely random, because all vectors x that we project y on are perpendicular to each other by construction. Here, we make an approximation: we assume that the directions of the d different vectors x are random and statistically independent. This approximation will get reasonable for $n \gg d$.

Now, we denote the coordinates of y with p (there are n of them), and from the unit-length it follows that $\sum_{i=1}^{n} p_i^2 = 1$. We can interpret this vector as a random point in $\mathbb{R}^n$. Because of the random direction, we expect that its expected total variance (that is just the squared sum of its elements, that is, 1) spreads equally over all all axes. It follows that the expected variance along each axis in $\mathbb{R}^n$ is $\frac{1}{n}$. This is just the expected variance of the projection of x on y, or, in other words, of each matrix element of $\hat{V}'$.

Knowing the variance, we can now compute the eigenvalue distribution according to the circular law (Tao et al., 2010). The circular law requires independent elements of $\hat{V}'$, an assumption that might be quite reasonable for $n \gg d$. Given that, the circular law states that the expected eigenvalue spectrum of $\sqrt{d^{-1}}$-scaled real or com-

plex $d \times d$ random matrices of whose elements have unit variance is the uniform distribution on the unit disc (in the limit $d \to \infty$; for small d, there is a concentration on the real axis besides other possible effects like a blurred border of the disc, see also Fig. 2.1.). The variance of each matrix element is of a $\sqrt{d^{-1}}$-scaled matrix is $\frac{1}{d}$. The elements of the regressed matrices V' have variance $\frac{1}{n} = \frac{d}{n}\frac{1}{d}$. Thus, we expect a uniform distribution of the eigenvalue on the unit disc if we scale the matrix V' or the matrix $\hat{A}$ by factor $\sqrt{\frac{n}{d}}$. Alternatively, we expect a uniform distribution on a disc with radius $\sqrt{\frac{d}{n}}$ if we do not rescale the regression matrix.

So far, we have considererd the case where the matrix Y is a pemutation of X. How do these results extend towards the more general case, when we are trying to fit random data with other random data that stems from the same distribution? This could for example be the case for two independent measurements from repeated experiments. Here, the partially common singular value decomposition is not exactly true anymore, that is the matrix V' is now transformed by a transformation that is not exactly a similarity transformation any more. However, if the data stem from the same distribution, the principal components will be approximately equal, and thus the transformation may be (in some sense) "close to" a similarity transformation. Indeed, numerical experiments indicate that the $\sqrt{\frac{n}{d}}$ scaling law remains approximately valid, as shown in Fig. 2.1. The expected diameter of the eigenvalue distribution of a regression matrix on $d \times n$ random data consequently is $\sqrt{\frac{d}{n}}$.

When the input data are bootstrapped (see section 2.1.11), we have to take into account that the n points in the bootstrapped ensemble are actually not all different. In fact, the chance for each of the n measurements not being selected in the n selections is $(1 - \frac{1}{n})^n \approx \frac{1}{e}$. We thus have only $\approx n(1 - \frac{1}{e})$ different elements in our n selected data points. Consequently, these points only span a $(1 - \frac{1}{e})n$-dimensional subspace. Following the argumentation above and replacing n by $(1 - \frac{1}{e})n$, this yields an expected diameter of the

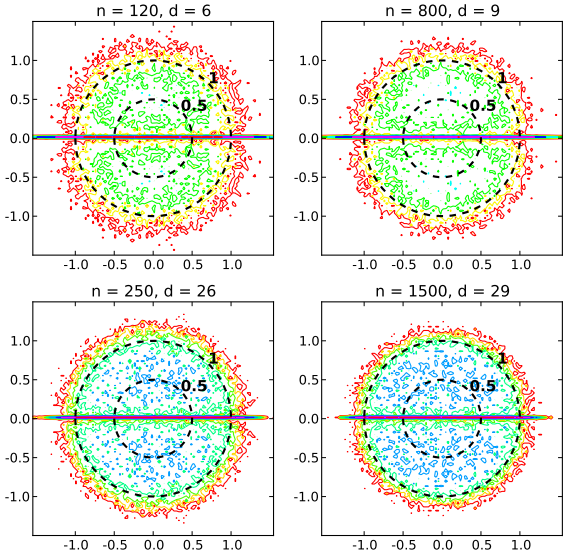

Figure 2.1: Distribution of eigenvalues of regression matrices on random data in the complex plane. Matrices have been scaled with the expected diameter $\left(\sqrt{\frac{d}{n}}\right)^{-1}$, that is the expected diameter of the distribution of eigenvalues is 1. The approximation of the unit disc gets better for larger d, as predicted by the circular law. The situation with $n = 1500, d = 29$ is typical for the data analyzed in section 4.3.

eigenvalue distribution of $\sqrt{\frac{d}{(1-e^{-1})n}}$, which is $\approx 25\%$ larger than the original diameter. In the bootstrapped case, additional factors

that are not considered by this rough argumentation might come into play. However, a numerical experiment with matrix dimension similar to those of the experimental data is given in Fig. 2.2, indicating that this adaptaion is at least roughly valid.

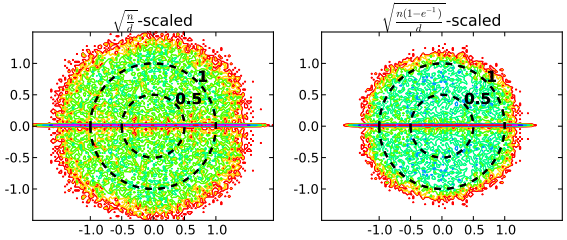

Figure 2.2: Distribution of eigenvalues of bootstrapped regression matrices on random data ($n = 1500, d = 29$ in both cases) in the complex plane, after normal (left) and adapted (right) scaling has been applied. The expected diameter of the eigenvalue distribution is 1. The theoretical additional scaling of $\sqrt{(1 - e^{-1})}$ appears to be a reasonable approximation.

2.1.5 Estimation of significant subspaces

This section describes an idea which was originally proposed by Revzen and Guckenheimer (2011).

According to the hypothesis of Full and Koditschek (1999), one might expect that the "collapse of dimensions" is also visible in the dynamics of the system. To be more precise, one might expect that in some few dimensions, there are comparatively large amplitudes of the dynamics, and in the remaining dimensions, the dynamics decay quickly. This might be reflected in the eigenvalues of the linearized return maps, with some few large eigenvalues (correspond-

ing to slowly decaying dynamics), accompanied by a larger set of small eigenvalues (corresponding to quickly decaying dynamics). A statistical test to estimate how many "slow eigenvalues" are present - which can be interpreted as estimating the dimension of a template - is to compare the distribution of the magnitudes of the eigenvalues of the computed return maps to the corresponding distributions of a null model.

The algorithm is described in detail in (Revzen and Guckenheimer, 2011), and is briefly summarized here:

Compute a bootstrapped set of return maps (see section 2.1.11). For every map, compute the magnitude of the p eigenvalues, and order them. Now, for every number $1 \dots p$ we have a distribution of the magnitude of the corresponding eigenvalue. Compute for each ordinal a certain selected quantile (here: 95-percentile) to obtain an upper bound $q(k),\ k \in 1 \dots n$. $q(k)$ states that in 95% of all matrices, k eigenvalues have smaller or equal magnitude than $q(k)$.

Now compute the same quantiles $q'(k)$ for a set of null models. This can be for example a set of random matrices of dimensions $1 \dots k$, or regression matrices of random data. As the hypothesis is that the lowest k' eigenvalues can be described by this null model, and higher eigenvalues do not fit, we construct the following p null models: $q'_k(k'),\ k \in 1 \dots p,\ k' \in 1 \dots k$. In our case, we construct for every dimension p' a specific null model from $p' \times p'$ regression matrices of random data.

In the final step, one has to compare these two quantities $q(k)$ and $q'(k)$, for every k. If we find that there is a good match up to dimension $\tilde{p}$, but for higher dimensions the distributions poorly, we can say that the null model explains low eigenvalues up to dimension $\tilde{p}$, and our slow dynamics have dimension $\tilde{p} - p$.

In order to account for possible different scalings of the same distributions, the comparison is done without comparison of the absolute scale: Only the relative increase from $q(k)$ to $q(k+1)$ is compared to the relative increase from $q'(k)$ to $q'(k+1)$ by computing the differences of the logarithms. In detail, the quality of fit

statistic Ξ_k for every possible null-model dimension k is computed as:

$$\Xi_k := \sum_{k=1}^{d-1} \xi_d^2(k) \tag{2.12}$$

$$\xi_d(k) := (\log q(k+1) - \log q(k)) - \tag{2.13}$$

$$(\log q'_d(k+1) - \log q'_d(k)) \tag{2.14}$$

This quantity Ξ_k is then plotted against k. If a sudden increase for some value k_0 is visible, then $p - k_0$ is considered as significant dimension of the slow dynamics, or alternatively as dimension of the template.

2.1.6 Phase estimation by Phaser

To analyze return maps of the system, those instances where the system is in the same phase have to be identified. Often, the gait cycle is defined to start at touchdown, and phase implicitly progresses with constant speed until 2π at the next touchdown of the same leg (e.g. Perry, 1992; Braune and Fischer, 1900). Instead of touchdown, any event of the gait cycle could be used. This method appears intuitive, however it has some problems: if, for example, a touchdown occurs too early due to a disturbance, but the gait cycle was typical up to the instant of touchdown - what would this phase estimate give? The stride would be "stretched", and there might be doubts if this really reflects a "true" phase. Here, a different phase estimation is performed, which was proposed by Revzen and Guckenheimer (2008). A comparison of the variance as a function of phase in Fig. 2.3 shows that this new approach gives a more reliable phase estimate.

The Phaser algorithm is described in detail in (Revzen and Guckenheimer, 2008). Here, I present the main ideas in an overview. The algorithm assumes that we are investigating a system of synchronized stable oscillators, that these oscillators are disturbed and that

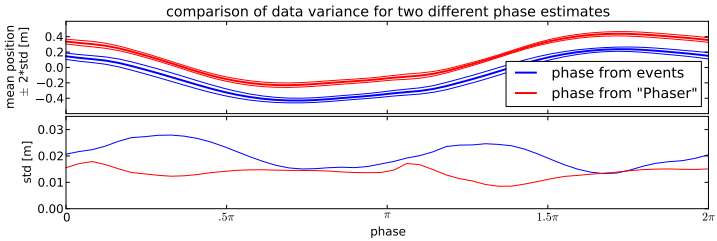

Figure 2.3: Exemplarily, the mean and standard deviations for each phase are presented for the difference between left and right knee anterior position in human running ($n = 317$ subsequent strides). For better visualization, position data have been shifted, and the standard deviation was scaled by factor 2 (upper plot).
The variance of the data depends strongly on the computation of the phase (lower plot). In general, an error in the phase estimate would increase the variance at the affected sections, because in addition to the true variability at that phase, variability that stems from the error in phase is introduced. The expected increase of the variability would be larger if the motion is faster. This is clearly the case for event-based phase estimates, but not for the “Phaser”-based phase estimate.

we have measurement noise. Without disturbances, we would observe a limit cycle. The phase of a system at a given state can be now defined: All points in a set of system states that will asymptotically converge to the single recurrent point of that set are considered to have the same phase. This set is called an isochron (Guckenheimer, 1975). Because the recurrent point is on the limit cycle, a phase can be assigned to it, and consequently to the isochron. The proposed algorithm is a way to estimate this phase from experimental time series data. It consists of three main steps:

- **Finding Protophases** In a first step, candidates for so-called protophases have to be identitied. A protophase can be any variable that progresses monotonically, not necessarily with a constant rate, from 0 to 2π during a complete gait cycle. For example, plotting a cyclic variable and its derivative against each other, and taking the angle with respect to any fixed axis is a candidate for a protophase if the variable cycles smoothly, as exemplarily shown in Fig. 2.4. Here, we take the argument of the complex Hilbert transformation of selected cyclic variables as protophases.
- **Imposing constant phase velocity** On the limit cycle, phase should progress with constant speed. To achieve this, a Fourier model is fitted to the average of each protophase, and inverted. Applying this inverted Fourier model to the protophase now results in a straightened protophase, that progresses with approximately constant speed.
- **Combining corrected protophases** The n straightened protophases ϕ_i^s have now to be combined into a single common phase estimate. For this, a cyclic motion is created in a $2n$ dimensional space, with $x_{2i-1} = r_i \sin(\phi_i^s), x_{2i} = r_i \cos(\phi_i^s)$, with r_i denoting a scaling parameter for each protophase that depicts our confidence in that coordinate. If all protophases would give the correct phase, the artificial motion would result in a circle, from which the phase could easily be read off. As this is typically not the case, we project this motion on its first two principal components, and obtain a combined phase estimate which we then have to straighten once more as described above.

2.1.7 Detrended Fluctuation Analysis (DFA)

Peng et al. (1994) introduced the tool of detrended fluctuation analysis (DFA), which makes it possible to identify long-range correlations in the data (Kantelhardt et al., 2001). Long-range correlations

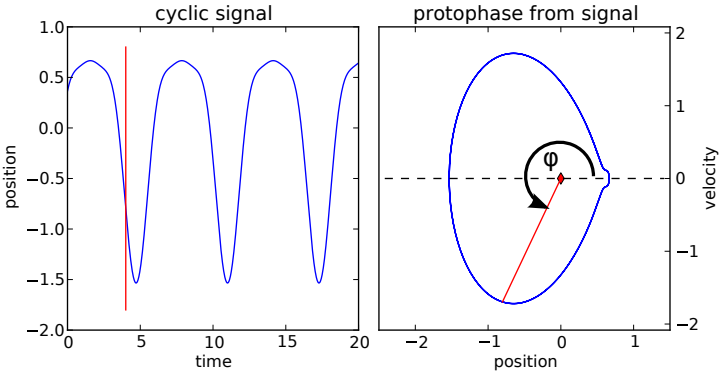

Figure 2.4:
A protophase from this cyclic signal can be computed for example by plotting the derivative of the signal against the signal itself and taking the angle with respect to the horizontal axes. This is shown here for $t = 4$ sec.

in biological data (with finite variance) typically indicate a long-memory process, that is a process whose future states do not depend only on the current state but also on previous states (these are non-Markovian processes)(Kantz and Schreiber, 1997). These long-range correlations are typical for biological systems (Ward and Greenwood, 2007; Goldberger et al., 2002) and have been demonstrated in human walking (Hausdorff et al., 1995, 1996, 1997, 2001) and standing (Duarte and Zatsiorsky, 2001).

DFA analyzes the self-affinity of a given signal, that is, loosely speaking, it investigates in how time and amplitude have to be scaled in order to appear self similar (see Fig. 2.5 for clarification). For Brownian motion, we know that $\langle (x_t - x_0)^2 \rangle \propto t$, that is, its variance scales linearly with time, and its standard deviation (which corresponds to the “amplitude”) scales with the square root

of the time. Processes with long-range correlations typically show a different behavior: $\langle (x_t - x_0)^2 \rangle \propto t^{2H}$, with the Hurst exponent $H > .5$. The goal of the DFA is to identify the Hurst exponent.

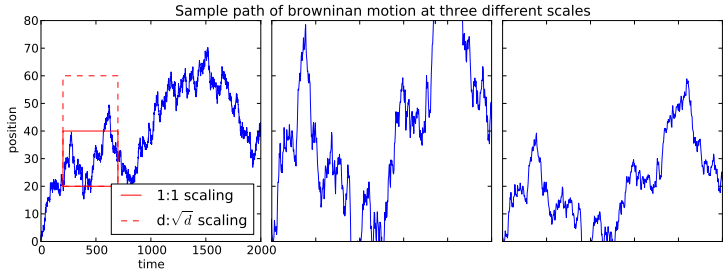

Figure 2.5: A sample path of the Brownian motion is shown at three different scales.
The original scale (left) is chosen such that the graph fits into the plot. Two windows with different ratios of time and ordinate are selected: "1:1 scaling" means that time and ordinate are scaled by the same factor, namely .25 (center). "d:$\sqrt{d}$ scaling" means that time is scaled by some factor d (here: .25), but the ordinate is scaled by factor $\sqrt{d}$, here: .5 (right). Only the "d:$\sqrt{d}$ scaling" shows the same "roughness" as the original scaling.

The idea of DFA is now to analyze the variance as a function of the window length. Here, we consider one-dimensional data x_i that fluctuate around some mean value. To analyze the long- range correlation, in a first step we create a diffusion process X_i by cumulatively summing up the values x_i: $X_i := \sum_{k=1}^{i} x_i$. Next, we split this diffusion process into windows of length L. A linear trend is removed from the each data window, and the fluctuation F (standard deviation of the residuals) is computed. Higher order detrending is also possible, but not commonly used. For different window lengths L, one obtains fluctuations F. These fluctuations now re-

flect the scaling behavior: $F \propto L^{\alpha}$. In the absence of statistical and systematic errors, the scaling exponent α is the Hurst exponent H.

To compute α from given $F(L)$ data, typically $F(L)$ is plotted on a double-logarithmic plot, as in Fig. 2.6. The scaling exponent α is then computed from a linear fit of $\log(F) = \alpha \log(L)$.

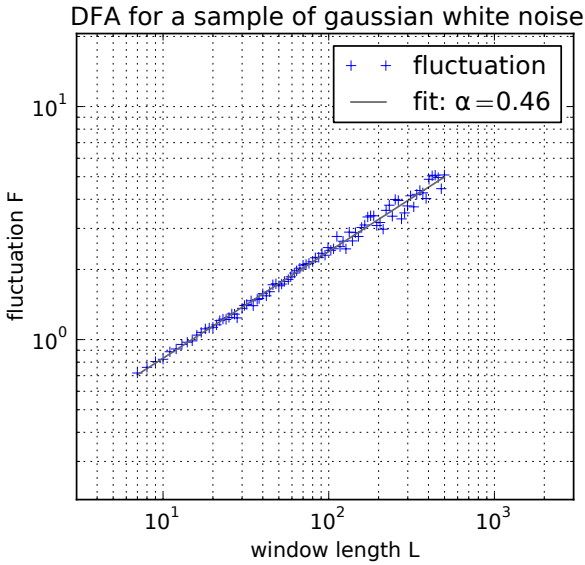

Figure 2.6:
The DFA is performed for the increments of the Brownian path in Fig. 2.5. The scaling exponent α is computed as linear fit of $\log(F) = \alpha \log(L)$. The result of .46 is close to the expected value of .5 for Gaussian white noise.

A useful feature of the DFA is that due to the detrending, scaling behavior might be recovered even in the presence of trends and

non-stationarities (Kantz and Schreiber, 1997; Kantelhardt et al., 2001).

2.1.8 Q-Q-plots

Wilk and Gnanadesikan (1968) introduced a method to visually investigate whether or not a random sample is from a given distribution. For this, the quantiles of the two distributions (typically the experimental sample and the expected distribution) are plotted against each other. When the distances between adjacent quantiles in both distributions are similar, then the resulting graph will be a straight line.

In practice, the following approach can be used: The random sample of length n is ordered first, yielding values for the $\frac{1}{n} \ldots 1$ quantiles q_n. Then, the corresponding quantiles from the given probability distributions are computed. In the plot, a dot is placed at $(q_{n,\text{exp.}}, q_{n,\text{theor.}})$. However, because in many distributions, the 0- and/or 1-quantiles are at $\pm\infty$, appropriate thresholds have to be chosen here. In general, the outer quantiles will be more inaccurate for finite sample sizes.

If the distributions are of the same type, but maybe have different scale and/or a different mean, then the Q-Q-plot will still show approximately a straight line. Deviations from a straight line indicate different underlying distributions. An example is presented in Fig. 2.7.

2.1.9 State space reconstruction and nonlinear analysis

In a closed-loop system without external input (explicitly without dynamical noise), two fundamentally different cyclic motions can exist: Periodic/quasiperiodic and aperiodic motions. Periodic motions are typically an asymptotically stable limit cycle, which is what we assume in later chapters. Aperiodic bounded “cyclic” motions

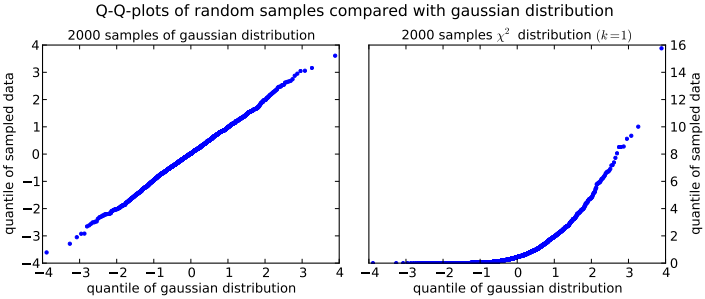

Figure 2.7: Examples of a Q-Q-plot:
Left: A random sample from a Gaussian distribution is plotted against a Gaussian distribution. A nearly straight line is visible, indicating a good fit of the sample with the distribution.
Right: A random sample from a χ^2-distribution is plotted against a Gaussian distribution. The differences are apparent.

were initially discovered by Jules Henry Poincaré (1890), and became famous in the work of Lorenz (1963). Typically aperiodic motions are associated with chaos, that is, sensitivity to initial conditions and positive Lyapunov exponents. However, Grebogi et al. (1984) showed that there exist strange non-chaotic attractors, and Romeiras and Ott (1987) showed that they are "typical", too. As human running is not exactly periodic even in the absence of apparent external disturbances, one might assume that it is a chaotic motion, and thus be interested in the properties of the corresponding chaotic attractor.

Several related dimensions can be defined for chaotic attractors. Whitney (1936) proved that smooth manifolds of dimension $r \in \mathbb{Z}^+$, can be embedded in euclidean space of dimension $d = 2r + 1$; analogous results for attractors were established first by Takens. Us-

ing d not much larger than required is often beneficial for recovering the structure of the attractor (Kantz and Schreiber, 1997). The question remains how to construct such an embedding. Packard et al. (1980) proposed the delay-embedding method for creating such an embedding, a method that works even if only a scalar quantity of the system is observed. This was independently detected and generalized by Takens (1981). Finally, Sauer et al. (1991) showed that "almost every" delay embedding can be used in principle (although some are more suited than others, for example more robust with respect to noise).

The delay-embedding goes as follows: From any given scalar or multi-dimensional observation $x(t)$ of the system at time t, a vector

$$X(t) = [x(t), x(t-\tau), x(t-2\tau), \ldots, x(t-n\tau)] \tag{2.15}$$

can be formed with a constant time delay $\tau > 0$ for arbitrary many $n \in \mathbb{N}$. The trajectory of X is now diffeomorphic to the original attractor if the dimension of X is sufficiently high. Quantities of interest like dimensions, entropy and Lyapunov exponents (see e.g. Eckmann and Ruelle (1985)) can be estimated.

Here, in chapter 4.2 we will see that human running is not stationary in our experiments, which is however a prerequisite for the validity of these methods. Thus, despite commonly used for gait analysis, these algorithms will not be applied here. However, an important result that will be used is the following: If a lower-dimensional motion exists, this can be reconstructed from the data. Although in principle a one-dimensional observation can be sufficient using the delay-embedding, a higher-dimensional observation without delay embedding can also be used and might be more robust against measurement noise (Kantz and Schreiber (1997); Sauer et al. (1991)). Thus, we see that the calculation of dimension as presented in section 2.1.10 will give approximately correct results using data from a sufficiently high-dimensional section of the state space.

2.1.10 Calculation of Dimension

Often, the attractor of a chaotic system is a low-dimensional object in the state space. Thus, it is of interest to compute attractor dimensions. Because a low-dimensional set can nevertheless extend in every (linear) subspace of a given phase space, it is not sufficient to look for small principal components. Instead, we have to compute the dimension in another way.

Different definitions of the dimension of an attractor have been proposed and applied to data(for a review see e.g. Kantz and Schreiber (1997, chap. 6)). Here, we use the widely adopted *box counting* dimension. To define this, we count the number $N(r)$ of balls of radius r required to cover the attractor. As $r \to 0$, we expect $N(r)$ to increase at a rate comparable to r^{-d}. If $N(r) = cr^{-d}$, then

$$d = \lim_{r \to 0} -\frac{\log N(r)}{\log r}. \tag{2.16}$$

Thus the slope of a $\log - \log$ plot of $N(r)$ vs r estimates the box-counting dimension. Implementation of this formula for finite data sets is problematic because the largest possible value of $N(r)$ is the number of observations. If r is too small, N(r) does not change with r. Moreover, the effects of noise create a larger apparent dimension on small scales. On the other hand, $N(r) = 1$ if r exceeds the radius of the attractor and the slope is again 0. In practice, one looks for a "scaling region" in which the $\log - \log$ plot is approximately linear and uses this slope as a dimension estimate. This is exemplarily demonstrated for the Lorenz (1963) attractor with standard parameters ($\rho = 28, \sigma = 10, \beta = \frac{8}{3}$) in Fig. 2.8

To further verify this method, the observed trajectory was embedded in a 10-dimensional space. Subsequently, a new random orthogonal coordinate system was chosen. Here, we expect the same scaling behavior of $n(r)$, because the distance is not affected by this transformation. Also, the data still reside in a 3-dimensional linear subspace. To spread the data into all 10 dimensions, the coordinates on each axis were sine-transformed: $\tilde{x_i}(t) = \sin 3\frac{x_i(t)}{\sup\, x_i(t)}$. However,

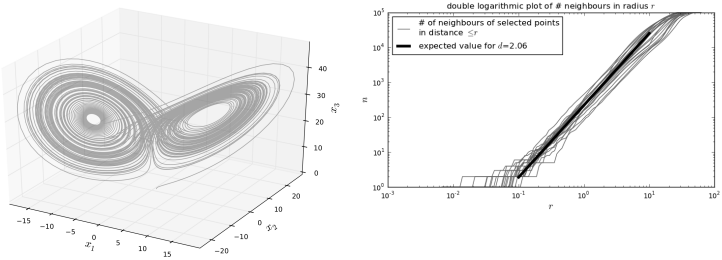

Figure 2.8: Left: typical trajectory on the Lorenz attractor. It's dimension d is $\approx 2.06 \pm .01$ (Grassberger and Procaccia, 1983). Right: observed slopes and expected slope of number of neighbors as a function of the radius. A linear fit in the scaling region ($\approx .25 \ldots 6$) yields a dimension $d \approx 1.99 \pm .16$, which is in good agreement with the expected value.

as we have a smooth mapping, the dimension of the set should not be affected by this procedure, and we can expect the algorithm to recover the underlying low dimension of the data, although the data spread in every direction of the space. The corresponding results are shown in Fig. 2.9, indicating the validity of our approach in this case.

2.1.11 The bootstrap procedure

When working with experimental data, the limited sample size is always a problem for the accuracy of the results. Often, no analytical expression for the accuracy of a computed quantity is known, so other methods to compute the accuracy in terms of confidence intervals have to be used.

Here, the bootstrap method (Efron, 1979; Efron and Tibshirani, 1986; Efron, 1994) comes into play. It is based on a resampling

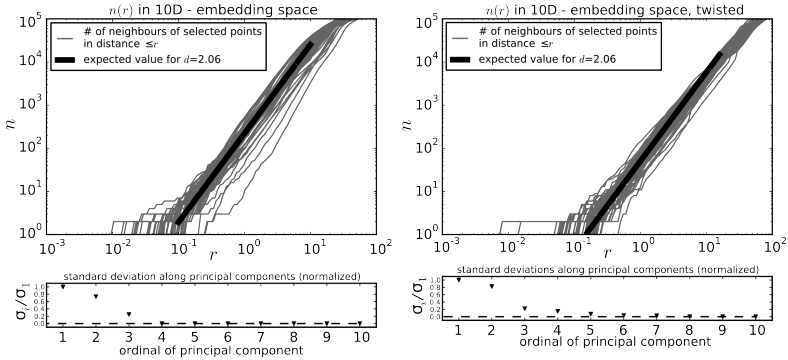

Figure 2.9: The dimension algorithm is able to identify the low-dimensional ($d \approx 2.06$) dataset in higher embedding space (left), even when the data are nonlinearly transformed such that they cannot be projected into a lower-dimensional space without data loss (right). The dimension estimation yields $d \approx 2.00 \pm .11$ (left) and $d \approx 1.92 \pm .17$ (right).

approach, that is from the measured data we select a new random sample (with replacement) of the same length as the original data set. We then compute the quantity of interest for each "bootstrapped" data set, and obtain a distribution of that quantity which reflects its inaccuracy. For scalar quantities, the quantiles give a good approximation of the corresponding confidence intervals. The bootstrap is not limited to scalar quantities - later, we will use the bootstrap method for example to obtain a distribution of matrices, similar to the work of Revzen and Guckenheimer (2011).

An example is presented in Fig. 2.10. Here, an artificial data set was created by $y = .4x + \eta$, where x is evenly spaced between 0 and 3, and $\eta \propto .1\mathcal{N}(0, 1)$ is a scaled Gaussian random variable with zero mean and .01 variance. We now perform a linear regression and want to know how accurately we can determine the parame-

ters. The first step is to compute a linear least-squares fit, and compute also the residuals. Next, we have to choose bootstrapped samples. Assuming that the residuals are random, we obtain new bootstrapped data sets by resampling the residuals as described above, and adding the linear fit to these residuals. We can interpret these data as "new data" that represent another noisy measurement of the original system, with the same noise distribution. Recalculating the quantities of interest will give us an impression of how much these quantities are influenced by noise, finally yielding confidence intervals for these quantities.

Here, we compute a linear fit to each of the bootstrapped data sets. The distribution of the parameters gives a confidence interval for the estimates. In our example (Fig. 2.10), the true values are within the confidence interval.

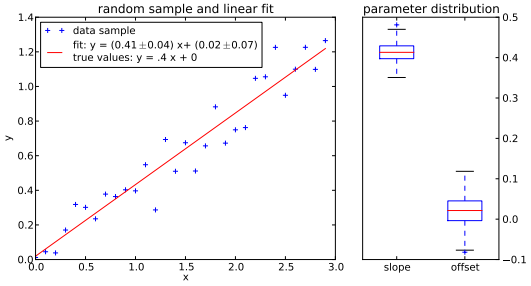

Figure 2.10: Example of applying the bootstrap method to create a confidence interval on the parameters of a linear fit. For the sample of 30 points, 500 bootstrapped samples were created; the corresponding distribution of the parameters is shown on the right. Confidence intervals refer to the 2.5 and 97.5 percentiles.

As mentioned above, we can also apply the bootstrap to obtain a distribution of regression matrices instead of just a single least squares estimate. Let's assume we have X and Y and want to compute A in the linear model $Y = AX + \eta$ (see section 2.1.2). We resample X and Y in the same way, that is, we select exactly that columns from Y that we select from X (in the same order), and compute A. We repeat this procedure with different samples and obtain a distribution for A.

2.1.12 Hypothesis testing with surrogate data

In practice, it is often difficult to find an analytic expression for a statistical test whether or not a given result is significant. A convenient method which is closely related to resampling methods like the bootstrap (section 2.1.11) is using surrogate data. A specific version of surrogate data test for testing nonlinearity in a process underlying experimental data was proposed in a well- recognized article by Theiler et al. (1992); here, however, we are interested in the general idea.

The idea of hypothesis testing with surrogate data is as follows: At first, we compute the quantity of interest. This can be a dimension, a physical quantity or whatever scalar quantity of interest. Next, we create surrogate data that are consistent with our null hypothesis but also "similar" to the original data set. This is the tricky part; we have to think carefully how to compute them. Third, we compute the quantity of interest on the surrogate data. We iterate this process several times, and obtain a distribution of the quantity of interest under the null hypothesis. We can now directly read out the significance level of the original value from that distribution: it is just the probability under the null hypothesis with its corresponding distribution (which we obtained by Monte-Carlo simulation) to obain the observed or a more extreme value. For example, if the observed value is in the 99.9-percentile of the distribution corresponding to the null hypothesis, the significance level (p) is .001 .

Coming back to the tricky part: An example of how the method of surrogate data can be used is given in section 4.2.2. There, we investigate the presence of a slow drift. Our hypothesis is that the data are not completely random, but instead their local average changes with time. Our selected quantity of interest is the standard deviation of a moving average, because we expect that the moving average varies more when indeed a drift is present. We construct a set of surrogate data with similar statistical properties but without such a trend by randomizing the order of the measurements, and compute the same quantity for each surrogate data set.

2.2 Center of mass estimation

This section was published as an article in the Journal of Experimental Biology:
"Combining forces and kinematics for calculating consistent centre of mass trajectories"
(Maus et al., 2011)

For biomechanical studies on animal and human locomotion as well as for clinical gait assessment, a precise estimation of the body center of mass (CoM) trajectory is crucial. In general, the CoM motion is calculated either from kinematic data ("kinematic method"), often by incorporating an anthropometric model, or by double integration of the acceleration obtained from ground reaction forces (GRF, "dynamic method").

The kinematic methods can be subdivided into pure marker methods and segmental analysis methods. Pure marker methods use a single marker (Saini et al., 1998) or a minimalistic marker set (Forsell and Halvorsen, 2009; Halvorsen et al., 2009) to estimate the CoM coordinates. However, some uncertainty arises in these minimalistic estimates because limb motion is not accounted for (Whittle, 1997).

The segmental analysis methods rely on full-body marker sets e.g. Helen-Hayes (cf. Castagno et al. (1995); Kadaba et al. (1990); Sutherland (2002)) and calculate the CoM trajectory by assuming the masses and center of mass locations of each segment (Eames et al., 1999). For humans, segmental data are usually obtained from anthropometric literature (Dempster, 1955) or individually determined from a reference measurement (Forsell and Halvorsen, 2009). However, for animals biometric data is much less available.

The accuracy of the segmental analyses relies on the correct marker placement and the correct estimation of segment properties (cf. Shan and Bohn (2003)). In addition, potential errors arise from unrecorded dynamics of segment masses, i.e. wobbling masses (Gruber et al., 1998; Günther et al., 2003; Schmitt and Günther, 2010) and motion of the viscera (Minetti and Belli, 1994).

In the dynamic method these problems do not occur. According to Newton's second law, the CoM motion is fully determined by the body's mass, external forces, the initial velocity and the initial position. Therefore, the accuracy of the dynamic method is limited by the precision of the measured forces and the precision of the integration constants (Cavagna, 1975). While the initial position can be estimated quite well, the determination of the initial velocity is a common problem in practice. Gutierrez-Farewik et al. (2006) and Günther and Blickhan (2002) showed that the calculated trajectory strongly depends on the body's mass measurement and the estimated initial velocity.

It is possible to optimize the guess for the initial velocity with the path matching method, i.e. the CoM initial conditions are estimates on a reference marker (Daley et al., 2006; McGowan et al., 2005). Yet, as this marker-based criterion itself is only a guess, the optimization is prone to error. In addition, due to systematic errors in the force signals (Mack, 2007) high-pass filters have to be applied on the force signals for long-time integration of acceleration. Another method to correct the integration constants on a per-stride basis has been proposed by Saibene and Minetti (2003). Here, the

mean velocity of each stride is replaced by a kinematic estimate, thus attenuating the long-term drift. However, it remains unclear to what extent typical systematic errors in both kinematic and dynamic measurements bias the results.

The sources of errors in kinematic and dynamic methods are of different kind. While the dynamic method has drawbacks on long time scales, the kinematic methods do not well capture some effects on short time scales, e.g. wobbling masses. Thus, typical inherent errors of both methods can be regarded as opposed, resulting in systematic mismatches of kinematic and dynamic CoM estimates (Gard et al., 2004). Gard et al. (2004) further proposed that a combination of kinematic and dynamic methods could potentially lead to more accurate results.

Here, we present a simple yet powerful approach to calculate CoM trajectories from measured kinematic and dynamic data. It is based on the combination of low-frequency content of kinematic data and high-frequency content of GRF to calculate a more accurate CoM velocity. From this velocity, the CoM trajectory and a corrected GRF are calculated by integration and derivation, respectively. Figuratively speaking, this method combines the strengths of both approaches by taking the coarse motion from the kinematic and adding the fine structure from the GRF. The proposed method is tested on simulation data and subsequently applied to real measurements. The resulting CoM trajectory and GRF are physically consistent and closely resemble the original measurements.

In the following, the new CoM algorithm and the simulation model used for verification are presented. Further, real measurements to which the algorithm is applied are described.

The CoM algorithm The main idea of the algorithm is to compute the CoM velocity based on kinematic and dynamic velocity estimates, taking only the frequencies of each estimate into account that we consider to be reliable. From this combined velocity, the GRF and CoM trajectory are calculated. The algorithm is summa-

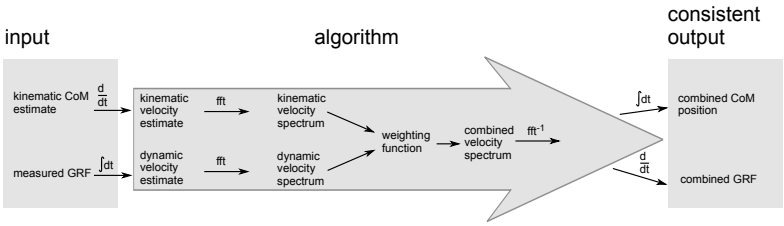

Figure 2.11: Summary of the proposed algorithm: The velocity of the CoM is computed from a combination of force and kinematic data. The corresponding trajectory and GRF are obtained by integration and derivation, respectively.

rized in Fig. 2.11. The individual steps are as follows and hold for each coordinate separately.

- We computed two estimates of the CoM velocity, a kinematic estimate v_k by differentiating the kinematic CoM estimate and a dynamic estimate v_d by integrating the GRF (taking gravity and body mass into account), respectively. Here, it is important that the mean force is accurate. For a subject standing at the beginning and the end of a trial, we set the mean force to exactly zero, because here the mean GRF exactly compensates gravity.
- We computed the Fourier transform $\tilde{\mathrm{v}}_k$ and $\tilde{\mathrm{v}}_d$ of the kinematic and dynamic velocity estimates.
- We select a weighting factor w between [0,1] as a function of the frequency, i.e. w(f) expressing the confidence in each method with respect to the frequency. The choice of w can be dependent on the experiment and the equipment. Here, we used a sigmoid function that is close to 0 for low frequencies and close to 1 for high frequencies (Fig. 2.12). Because the Fourier spectrum is symmetric, this function must also be

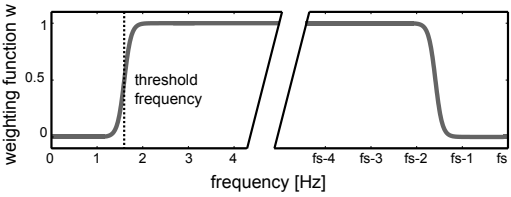

Figure 2.12: **Weighting function**
The selected weighting function expresses the relative reliability of the signals expressed in the frequency domain. We chose a sum of two sigmoid function w = $(1 + e^{(-(f-f_0)s)})^{-1}$ + $(1 + e^{(-((f_s-f_0)-f)s)})^{-1}$, w(0) = 0, with f_s and f_0 denoting the sampling frequency and the threshold frequency, respectively. The steepness of the slope was s = 10 Hz^{-1}.

symmetric. For the appropriate selection of the threshold separating high and low frequencies, see Fig. 2.13 and text.

- We use the weighting factor w to create a combined spectrum $\tilde{v}_c$(f) = w(f)$\tilde{v}_d$(f) + (1-w(f))$\tilde{v}_k$(f), which is a weighted sum of the low frequencies of the kinematic estimate and the high frequencies of the dynamic estimate.
- We computed the combined velocity v_c as the inverse Fourier transformation of the combined spectrum $\tilde{v}_c$.
- We computed the combined CoM position and GRF from the combined velocity by integrating or differentiating, respectively.

Selection of the weighting function Some parts of the segment dynamics, primarily the composition of soft and rigid body structures, are not well recorded in the kinematics. As this segment-internal motion mainly affects harmonics of the stepping frequency and higher frequencies (Günther et al., 2003), we expect the part of motion concerning frequencies below a certain threshold to be well

captured, and that this threshold is not substantially lower than the stepping frequency.

In contrast, errors in force measurement usually are of a type that mainly affects low frequencies, e.g. drift and slowly varying offset (Mack, 2007; Nigg and Herzog, 1999). This is why integration of acceleration obtained from measured GRF without filtering gives reasonable results only if trials are short, i.e. very low frequencies are not present. On the other hand, we have no reason to assume systematic errors in the force measurement in high frequencies. An exception may be the eigenfrequency of the measurement system. In our system, the eigenfrequency is 120 Hz, which corresponds roughly to the 40^{th} harmonic of the stepping frequency and thus is far out of the region of interest (Racic et al., 2010).

These arguments lead us to use a weighting function that takes low frequencies from the kinematics and higher frequencies from the dynamics. As we expect that the wobbling masses move approximately with the frequency of the driving force (i.e., the stepping frequency) and their harmonics, we assume that a threshold frequency slightly below the dominant frequency of the motion would be optimal. The validity of this argument is strongly supported by our simulation results as shown in Fig. 2.13.

Verification using simulated data In order to verify the accuracy of the CoM estimate, we used a simulation model of a bipedal walker to create an artificial dataset with precisely known dynamics. Subsequently, we added virtual measurement errors that resemble errors we expect from real-world measurements, including errors concerning the wobbling masses.

Model description We used the model of a human walker (mass = 80 kg) from Geyer and Herr (2010), which is able to predict typical human-like GRF, CoM motion and even muscle activation patterns. We modified this model by setting $\frac{1}{4}$ of each segment's mass to a wobbling mass, which is connected to the segment by

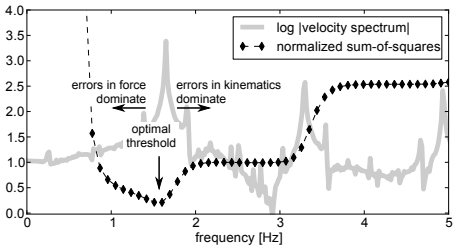

Figure 2.13: To assess the accuracy of the CoM estimation, the residual sum of squares with respect to the real CoM motion of the model was calculated as a function of the threshold frequency (black diamonds). The values were normalized to the apparent plateau after the dominant motion (2.5 Hz). Additionally, the amplitude of the velocity spectrum is shown (solid gray line). The optimal threshold frequency is slightly below the dominant frequency of the motion. Therefore, a reasonable threshold frequency should be selected below this dominant frequency. In this case, appropriate threshold frequencies are approximately ranging from 1.0 Hz to 1.6 Hz. If the threshold is below or above this range, errors in the measured force or measured kinematics become dominant and decrease the estimation quality.

a spring-damper-element (roughly according to Minetti and Belli (1994)). The spring and damping constants are chosen such that the eigenfrequency is $\sim$10 Hz for the limbs and $\sim$3 Hz for the head-arms-trunk segment, with a decay time of 0.4 seconds. Our modified model walked in an aperiodic manner with a dominant motion frequency of 1.64 Hz. Data were sampled every 1 ms simulation time.

Virtual measurement errors and CoM estimation The kinematic CoM estimate of the model was computed using standard segmental analysis (Winter, 2009), including only measurements of the position of the rigid segments, and neglecting wobbling masses. Additionally, white noise with a rms of 0.5 mm was added. The force data were modified by (1) adding a non-stationary noise signal with an amplitude of 5 N, (2) adding white noise with a rms of 5 N, (3) applying a small nonlinear scaling. In detail, these corruptions were calculated to:

1. $R_i^1 = 5N \sin(\sum_i^i 0.01\eta_i)$
2. $R_i^2 = 5N\eta_i'$
3. $F_i' = .98(F_i^0)^{1.02}$,

where η_i, $\eta_i' \sim \mathcal{N}(0,1)$ are Gaussian distributed, and F_i^0 is the real ground reaction force in units of bodyweight. Then, the virtually measured force is $F_i^m = F_i' + R_i^1 + R_i^2$.

The dynamic estimate of the CoM was computed by a double integration of the acceleration obtained from ground reaction force, thereby applying a 0.35 Hz high-pass filter for the force and obtained velocity. The cut-off at 0.35 Hz was chosen because in this model it resulted in the most accurate CoM reconstruction. Lower cut-offs lead to increased long-term oscillation whereas higher cut-offs lead to an underestimation of the oscillation amplitude. For the CoM estimation using the proposed algorithm, the threshold frequency was set to 1.5 Hz, which is below the dominant frequency of the motion at 1.64 Hz.

Analysis of experimental data In order to demonstrate the new method we calculated the CoM trajectories of human running and walking and compared these with kinematic and dynamic CoM estimates. We further calculated the "kinematic GRF" as second derivative of the kinematic CoM estimate to compare kinematic GRF, measured GRF and calculated GRF.

Measurement setup and protocol All measurements were conducted on an instrumented custom-built treadmill (ADAL, HEF Medical Development, Andrézieux-Bouthéon, France). We further used a marker-based kinematic system (Qualisys, Gothenburg, Sweden) to capture the subject's motion. Force data were sampled at 1000 Hz, kinematics were sampled at 240 Hz.

The subject walked at 1.8 ms^{-1} and ran at 2.7 ms^{-1} on the treadmill. Each trial started and ended with 5 seconds of quiet standing. The total trial duration was 50 and 55 seconds, respectively.

Data pre-processing A linear drift in the total vertical and total horizontal force was removed from the raw data. Kinematic data was linearly interpolated from 240 Hz to 1000 Hz to match the treadmill sampling frequency. We do not expect relevant numerical errors from the interpolation because we used only kinematic frequencies up to $\sim$1.5 Hz, which are well over-sampled and thus hardly affected by this interpolation.

CoM estimation with kinematic, dynamic and new method The kinematic CoM estimate was obtained using a standard segmental analysis (Winter, 2009). Corresponding GRF were calculated by computing the second derivative of the CoM estimate after applying a second order Butterworth filter with a cut-off frequency of 15 Hz.

The dynamic CoM estimate was obtained by twice integrating the GRF. To avoid spurious drifts in the resulting trajectory, components below 0.35 Hz were removed before integration by applying a first order Butterworth filter to GRF and computed velocity.

Finally, we applied the proposed algorithm to calculate the combined CoM and GRF. We used the measured GRF and the kinematic CoM estimate as inputs for the algorithm. The threshold frequency was set to 1.5 Hz.

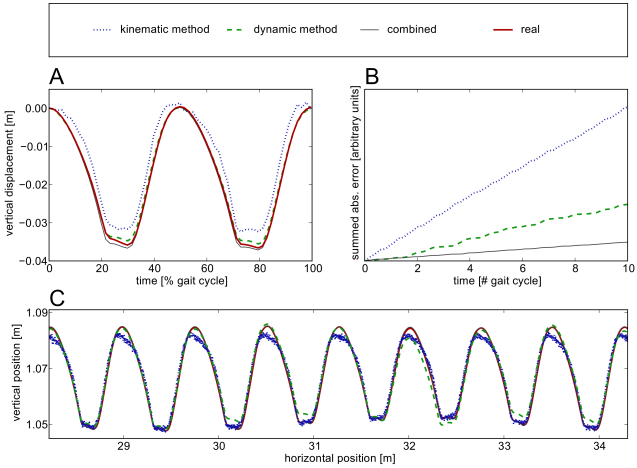

Figure 2.14: Comparisons of the real model CoM and the different calculation methods. **(A)** Simulation results for the real, measured and reconstructed time courses of the vertical CoM over one gait cycle. For better comparison, only the displacement relative to the initial (apex) position is shown. **(B)** The accumulated absolute errors over 10 strides. While the error in the kinematic estimate accumulates regularly, the error in the dynamic method accumulates unregularly (see e.g. t $\sim$3.5 gait cycle). This behavior is due to the different nature of the errors. **(C)** Sagittal plane movement of the CoM. While the kinematic estimate has a systematic wrong shape, it keeps well track of the motion. The contrary is true for the dynamic estimate. The combined estimate performs best as it keeps track of the motion and also shows good match of the shape.

Results and Discussion The analysis on the simulated data shows that the proposed method reconstructs the CoM motion with greater accuracy than the pure kinematic or dynamic methods (Fig. 2.14). For better visual comparison, only the displacement relative to the first apex position is shown in Fig. 2.14(A). Also, we applied the new method to the forward motion. The results show a proper tracking of the motion (Fig. 2.14(C)). While the differences of the kinematic estimate are apparent in every step, the tracking problem of the dynamic method accumulates the error on the long term (Fig. 2.14(B)). These slow drifts are not present in the combined estimate.

The results of applying the algorithm to walking and running data are shown in Fig. 2.15. Here, we focused on the vertical CoM component, but the method is applicable to any CoM component. The calculated data resemble both the kinematic CoM estimate and the measured GRF. Because of this and its inherent physical consistency (i.e. the combined GRF equals the second derivative of the combined CoM minus gravity), this method provides a suitable enhancement to common kinematic CoM estimations. These consistent data can then be used for further analysis, e.g. of external work and external power, with greater confidence.

Our results show systematic deviations of the GRF obtained directly from kinematics compared to the measured GRF. This comprises mainly an underestimation of the GRF after lift-off in running, which is accompanied by an overestimation of the GRF during stance (Fig. 2.15). Similar results were shown by Racic et al. (2010). As negative vertical GRF cannot occur in typical running and hopping experiments, this indicates a systematic shortcoming of kinematic GRF estimates, which also extends to the corresponding CoM estimate according to Newton's second law. The combined CoM/GRF estimates do not show this systematic deviation but closely resemble the measured forces. Later, we show that this property also holds for very simple kinematic CoM estimations like a single marker, both in human walking and dog trotting. Thus, ac-

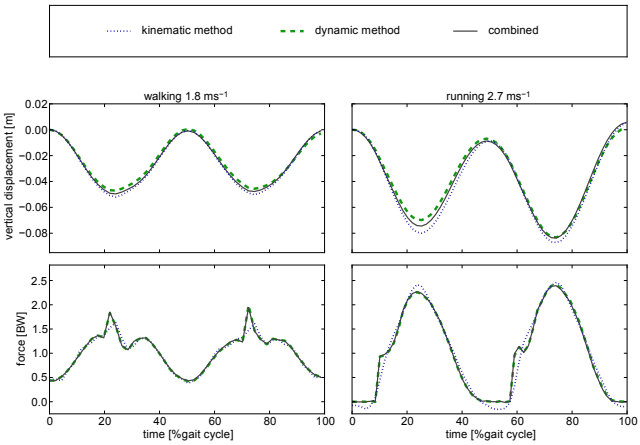

Figure 2.15: Results of applying the new algorithm (grey solid line) to human walking and running in comparison to the classical approaches. Shown are the vertical CoM motion and the derived GRF for one gait cycle. In general, the kinematic estimate shows slightly larger oscillation than the dynamic and combined estimates of the CoM trajectory. The difference between dynamic and combined estimate, showing smaller oscillation amplitude in the dynamic estimate is agreement with simulation results. This is also reflected in differences in the corresponding GRF, indicating that this systematic deviation is a shortcoming of the kinematic estimate.

curate CoM trajectories can be obtained without knowing segment properties using this algorithm. Further, this also allows highly reduced experimental effort for some gait analyses.

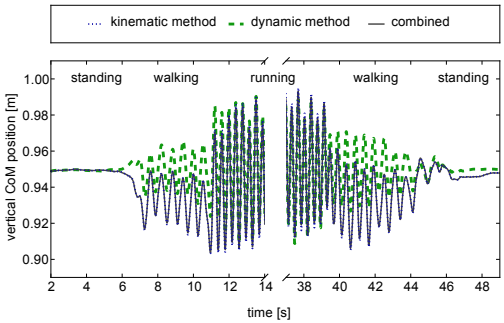

Figure 2.16: Results of different CoM methods for a 55 seconds trial with standing, walking and running. Comparing the dynamic estimate of the CoM trajectory with kinematic and combined CoM trajectories during the running trial shows the drawback of discarding the low-frequency parts (here: < 0.35 Hz) of the dynamics: the descent of the CoM during walking compared to standing and running is not captured, whereas the combined CoM closely resembles the kinematic estimate during the whole trial. Also, the different CoM height at the end of the trial cannot be captured using only force data. On this scale the combined and kinematic estimate appear to be very close.

The proposed method accounts also for wobbling masses (Gruber et al., 1998; Günther et al., 2003; Schmitt and Günther, 2010), because their motion is included in the GRF. Wobbling masses are not necessarily captured by the kinematic measurement. This can lead to differences especially when the wobbling mass motion is substantial or out of phase with respect to the skeletal motion (Minetti and Belli, 1994). Conversely, it appears plausible that this soft tissue

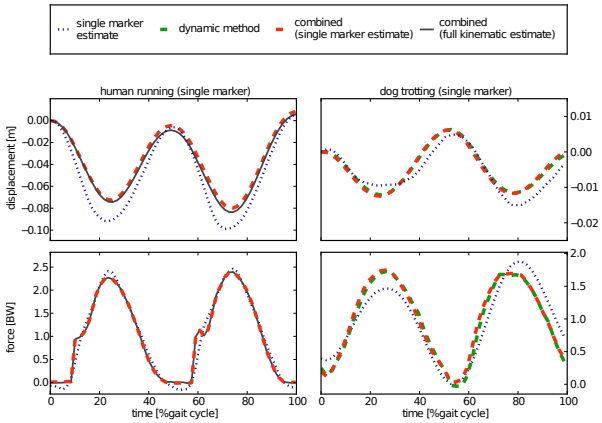

Figure 2.17: Applying the proposed algorithm to a CoM estimate using only a single marker. The markers were placed at the sacrum on the human runner (2.7 $\frac{m}{s}$) and the back (mid thorax height) on a trotting dog (2.5 $\frac{m}{s}$). Despite the rough kinematic estimate, the combined data match well the data obtained using a full marker set and the algorithm (human) or the measured GRF (dog) and corresponding dynamic estimate, respectively. The selected threshold frequency was 1.5 Hz in both cases.

motion could be estimated by calculating the difference of the calculated CoM and the kinematic CoM estimate. Thus, this method could also provide a basis for analyzing soft tissue motion.

A standard method in engineering to combine both kinematic and dynamic input to obtain a more reliable CoM estimate is the Kalman filter (Kalman, 1960). Loosely speaking, the main idea is to propagate the trajectory based on a system model using the GRF as input (so-called estimate $x_i^- = f(x_{i-1}^+, \text{GRF})$), and updat-

ing this estimate with each measurement y_i of the CoM trajectory $x_i^+ = x_i^- + K(y_i - x_i^-)$. The relative weight K of the update is based on the relative confidence in the estimate and the measurement, respectively. Under certain restrictions on the measurement errors, the Kalman filter or its modifications give an optimal estimation. However, this does not apply here as both the kinematic and GRF measurement errors have a systematic structure that renders them very different from these restrictions. In order to use Kalman filtering here, a model of the measurement errors would have to be included. In contrast, the proposed method offers a convenient and intuitive and way, namely the selection of a threshold frequency, to account for the typical structure in the measurement errors.

Physical consistency in long trials can also be obtained by the dynamic method, when low frequencies are discarded. When low frequencies are not discarded, spurious slow oscillations with high amplitude occur. However, when low frequency components are discarded, slow changes like the descent of CoM in walking compared to standing cannot be captured (Fig. 2.16). Our approach solves this problem by adequately replacing the low frequency components by those obtained from the kinematics. This is similar to cutting the long trial into short trials and taking the initial conditions for each short trial from kinematics (see also the method of Saibene and Minetti (2003)). In our case, the length of each short trial would then be 1/(threshold frequency). However, in our method the kinematic estimate does not only influence the initial value of each short trial but reshapes the result equally over time. Therefore, the wider applicability of this method to accelerated (Segers et al., 2007; Williams et al., 2009) and unsteady (McGowan et al., 2005) conditions is given. Further, the need for repeated estimates of the CoM velocity from kinematics is omitted. Thus, the proposed method can be regarded as extension of the dynamic method that enables its application especially for long trials, when low-frequency components become important or non-periodic movements where estimation of integration constants is difficult.

Using a single marker as kinematic CoM estimate When multi-segment kinematics are not available or the segment properties are unknown, the proposed algorithm still can be applied to improve the resulting CoM estimate. Here, we demonstrate the result when we take the sacral marker as kinematic CoM estimate, and compare it to the CoM and GRF obtained when using the full maker set. Further, we show the results of computing the CoM and GRF using a single marker on the back of a trotting dog (Fig. 2.17). For human data (Fig. 2.17, left), a substantial overestimation of the CoM amplitude by the sacral marker estimation is visible, which is also reflected in substantial differences in the GRF. For animal data (Fig. 2.16, right), differences of the single-marker estimate and the combined estimate are apparent. However, in both situations, taking the single marker as input for the algorithm results in reliable CoM and GRF estimates, which is reflected in both cases by close resemblance to the measured GRF. However, it is clear that especially slow or permanent, unrecorded motions (like e.g. a change of posture when using a single marker) induce an offset in the simplified kinematic CoM estimate that transfers to a corresponding offset of the combined estimate. This has to be taken into account when designing the experiment.

2.3 Collection of human treadmill running data

In chapter 4, we will perform several analyses of human running, including the attempt to extract the human gait controller. For this, we need experimental data, which are described here.

2.3.1 Subjects and protocol

10 trained subjects (9 male, 1 female) participated in the experiments after they gave informed written consent prior to experi-

ments. Three subjects were excluded from further analysis because of pronounced fatigue, very frequent loss of markers during the experiment, or technical failure of the setup.

After a warm-up phase, subjects ran continuously on the treadmill. The experiment consisted of three sections: free running, metronome running and disturbance experiments.

In chapter 4, we will only analyze data from the free running section. In this section, six trials of each 4 minutes duration were recorded. Subjects did not notice beginning and end of an individual trial as they ran continuously. Between two subsequent trials, an interruption of the recording for $\approx$ 30-60 seconds was necessary due to technical constraints. In total, the free running section lasted $\approx$ 28 minutes.

2.3.2 Experimental setup

31 reflective markers were placed at prominent anatomical landmarks on the subject (see Figs. 2.18 and 2.19). The motion of the markers was captured using a Qualisys (Qualisys, Gothenburg, Sweden) Oqus camera system with 10 cameras at 250 Hz.

Subjects ran on a custom-built instrumented treadmill (ADAL, HEF Medical Development, Andrézieux-Bouthéon, France). Ground reaction forces were recorded at 1000 Hz (see also Fig. 2.19, right).

Additionally, EMG data were recorded using the MyoMonitor system from Delsys (Delsys Inc., Boston, MA, United States of America). These data will not be used here. However, it should be mentioned that including these measurements in the experimental setup lead to partial occlusion of markers and additional sweating of the subject and consequently impaired the quality of kinematic data.

2.3.3 Basic data processing

After recording and kinematic tracking using the supplied Qualisys software, data were preprocessed with the following steps:

- If a marker was not captured in a particular time window, we linearly interpolate its trajectory between the edges of that window.
- To estimate velocity, we filter the data using a 75Hz zero-lag Butterworth and compute the one-sample difference of the lowpassed data.
- We calculate phase using the Phaser algorithm outlined in section 2.1.6). For this, we use the following cyclic inputs (the minus refers to the difference in Cartesian coordinates, cf. Fig. 2.18):
  - R_Kne - L_Kne : position and velocity in a/p[1] direction
  - R_Trc - R_AnL : position in a/p direction
  - L_Trc - L_AnL : position in a/p direction
  - L_Elb - L_MtV : velocity in a/p direction
  - R_Elb - R_MtV : velocity in a/p direction
  - R_MtV - L_MtV : position and velocity in a/p direction; lateral position

  We define the Poincaré-section corresponding to phase 0 at that instant when L_MtV passes R_MtV in anterior direction.
- In order to compensate a slow drift in the force sensors, we detrend the measured ground reaction force by subtracting a second order polynomial fit to the force data during flight over the duration of a trial. We detrend each sensor separately.
- We compute the motion of the center of mass using the novel method described in section 2.2.

[1] anterior-posterior

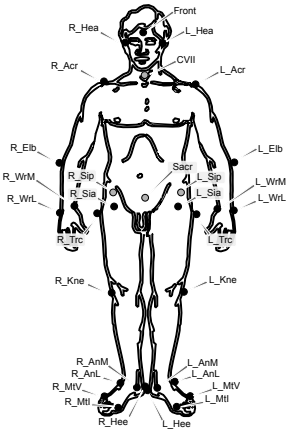

meaning of marker abbreviations	
{R|L}_Acr	acromion (shoulder)
{R|L}_Anl	ankle joint, lateral
{R|L}_Anm	ankle joint, medial
CVII	7^{th} cervical vertebra
{R|L}_Elb	elbow (lateral epicondyle)
Front	forehead
{R|L}_Hea	lateral head (zygomatic process)
{R|L}_Hee	heel
{R|L}_Knl	knee joint, lateral
{R|L}_MtI	1^{st} metatarsal joint
{R|L}_MtV	5^{th} metatarsal joint
Sacr	os sacrum
{R|L}_Sia	spina iliaca anterior
{R|L}_Sip	spina iliaca posterior
{R|L}_Trc	greater trochanter
{R|L}_WrL	lateral wrist (ulnar styloid process)
{R|L}_WrM	medial wrist (radius styloid process)

Figure 2.18: Markers were placed on prominent anatomical landmarks. The prefix L or R indicate the left and right side, respectively.

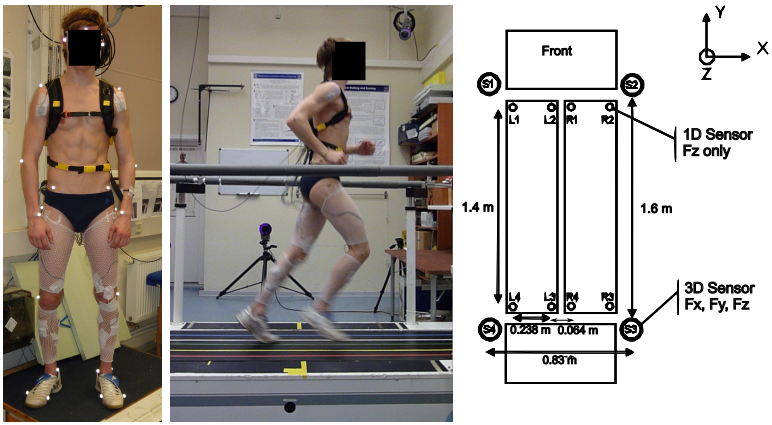

Figure 2.19: A subject after preparation with reflective markers and EMG electrodes placed on selected muscles, standing (left) and running on the treadmill (center). A schematic top-view of the treadmill is given on the right.

3

TEMPLATE MODELS

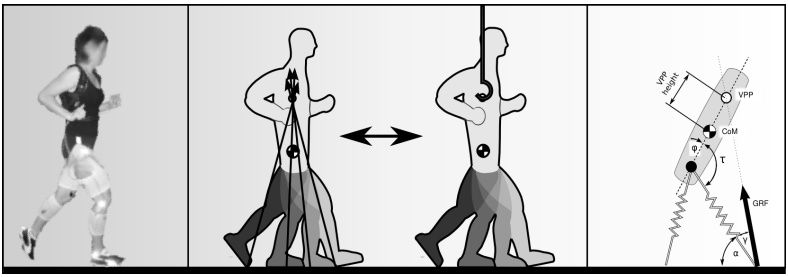

Everything should be made as simple as possible, but not simpler.

Albert Einstein (1879 - 1955)

3.1 Introduction

Human locomotion results from complex, high-dimensional, nonlinear, dynamically coupled interactions between the body and its environment (Full and Koditschek, 1999). To understand the dynamics of the motion, a common approach is to use reduced order models. Specifically, we are looking for simple, comprehensible models that describe the aspects of interest. This simplifying approach is not unique to biomechanics, but also used in engineering for designing control systems. Here, the dynamics of the system to be controlled are splitted into a low-dimensional "main" part and a fast decaying complement, for example in the framework of hybrid zero dynamics (Westervelt et al., 2003; Poulakakis and Grizzle, 2007) or the more general immersion and invariance approach from Astolfi and Ortega (2003). In biomechanics, we are looking for explicit mechanical models, that is, models that we could build. As general hypothesis for animal locomotion, Full and Koditschek (1999) proposed that simple mechanical models –so-called templates– can well capture the center of mass (CoM) motion, and that out of the variety of all possible motions only the subset that corresponds to these templates is selected. Here, we are interested in models that describe the main aspects of human locomotion, namely the CoM dynamics in a first step and pitch dynamics in the sagittal plane as a second step.

Explicit mechanical gait models are typically derived by physiological reasoning. What is the main task for the leg during a running motion? Obviously, it is a general repulsive functionality, that pushes the body from stance into an aerial phase at each step. Several constraints have to be considered: Due to the limitation of maximal force, there is a finite contact time, in which the force has to be applied. Because the contact time is roughly known in advance, and also the task of inverting the vertical motion is the same at every stance phase, a harmonic oscillator would be a good starting point for such a simplified gait model. A harmonic oscillator has the con-

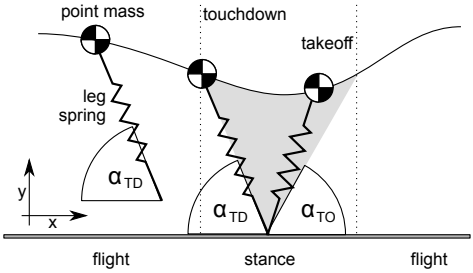

Figure 3.1: The spring-loaded inverted pendulum (SLIP) model: The runner's leg is represented by a simple linear spring, the runner's body by a point mass.

venient property that the time required to invert the motion (that is, half a period) is independent of the amplitude of the motion.

Extending the harmonic oscillator to the sagittal plane leads to the spring-mass model, which is simply a point mass mounted on a linear spring (Fig. 3.1). This model has been proposed to explain CoM dynamics in running and other bouncy gaits by Blickhan (1989) and McMahon and Cheng (1990), and it has been shown by Geyer et al. (2006) that this model can also explain CoM dynamics in human walking. However, it should be mentioned that despite its simplicity, there exists no closed-form analytical solution to this model because of elliptic integrals in the solutions (Schwind and Koditschek, 2000; Whittaker, 1904), and only approximations to explicit solutions exist (Geyer et al., 2005; Schwind and Koditschek, 2000).

Next, we will investigate how a specific recorded experiment can be represented using the SLIP model, and we will introduce another template that accounts for postural stability in human walking and is compatible with the SLIP, that is, both templates can be implemented in a single model.

3.2 Calculating SLIP template parameters

When we want to describe human gait using the SLIP template, the question arises what would be the correct leg parameters (spring stiffness, leg rest length, angle of attack) for the model for a given step? Here, we will use the approach proposed by Ludwig et al. (2012 (accepted)). We modify the original SLIP model in two ways: first, we introduce a lateral angle of attack to account for lateral motion (in the same way like Carver et al. (2009)). The model is now extended from the sagittal plane to 3D. Second, we allow energy changes in the model to account for energy fluctuations in real-world data. For this, we allow an instantaneous change of the spring stiffness and rest length at the lowest point in stance, with the additional constraint that the total ground reaction force must not change. This gives a unique solution for the parameter change (for details, see Ludwig et al. (2012 (accepted))).

The computation of the five leg parameters (leg stiffness k, rest length L_0, angles of attack during flight α, β, energy change ΔE, see Fig. 4.10, page 110) follows an idea from Carver et al. (2009). First, we split experimental data into steps that go from one apex to the next. Then, we are looking for SLIP parameters that exactly reproduce the experimentally observed step in simulation in five criteria, when the model starts from the experimentally observed initial conditions. These five criteria are the total step duration, final apex height and velocity (in running direction and lateral direction), and the minimal height during stance. As this defines an implicit function, we can find locally unique solutions for the model parameters. Note that horizontal and lateral positions are not required to be matched.

Using this method to compute the SLIP parameters, we obtain excellent agreement with experimental trajectories when using these parameters in forward simulation, for both forefoot and rearfoot running (Fig. 3.2). That indicates that we have a method to approximate the CoM motion using a set of only five parameters and three

initial conditions. In section 4.4, we will see how these parameters can be used to further analyze human locomotion, for example in terms of stability and control.

3.3 A template for stabilization of the posture

This section was published as an article in Nature Communications:
"Upright human gait did not provide a major mechanical challenge for our ancestors."
(Maus et al., 2010)

Habitual terrestrial bipedalism has often been considered the evolutionary event that separated humans from apes (Pontzer et al., 2009; Ward, 2002). Because bipedalism enhances the ability to gather small fruit from short trees and frees the hands for tool use, bipedalism might have not only been an adaptation to an ecological niche, but also a prerequisite for cultural development and the evolution of modern human (Weaver and Klein, 2006; Du Brul, 1962). However, an important selection criterion in evolution is the efficiency of gait (Pontzer et al., 2009; Wang and Crompton, 2004), and efficient bipedal gait requires straightened legs and an upright trunk as opposed to "bent-hip-bent-knee walking" (Wang et al., 2003). Early habitual bipeds such as Australopithecus afarensis and perhaps even Ardipithecus ramidus ("Ardi") presumably already utilized an upright gait (Crompton et al., 2008, 1998; Lovejoy et al., 2009a,c). Walking upright entails advantages but also raises new challenges including load distribution on two legs only and stabilization of the upright posture. While the increased load per leg can be compensated by extended legs (Du Brul, 1962), the intuitively expected instability of bipedal gait seems to be a rather complex challenge.

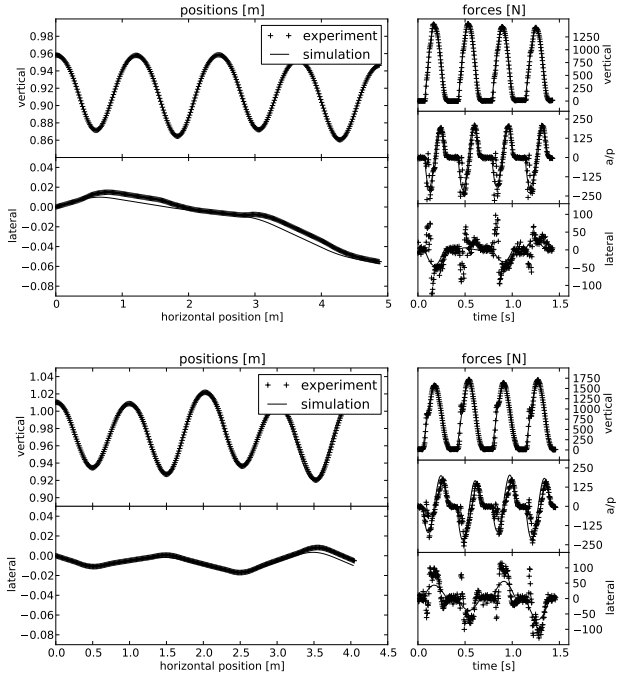

Figure 3.2: Comparison of experimental CoM trajectories and forces with simulated data using the corresponding model parameters for simulation. Top: forefoot running. Bottom: rearfoot running. Four randomly selected subsequent steps are displayed. The simulation runs without reset, thus deviations in positions accumulate. The lateral forces and positions are not very well captured, however the absolute lateral motion is small compared to vertical and anterior/posterior motion.

The dramatically reduced area of support compared to quadrupedal walking and an elevated center of mass (CoM) in upright bipedal gait gives reason to assume increased instability. The system resembles an inverted pendulum that easily falls over when perturbed. However, this relation is only valid for static scenarios. In human walking, the point of application of the ground reaction force moves with respect to the CoM throughout a walking cycle (Fig. 3.3a). This fundamental difference compared to an inverted pendulum (Fig. 3.3b) is the basis for a stabilization mechanism that does not rely on the instantaneous area of support.

Assuming that the body would be supported above the CoM, like when walking with crutches or brachiating in trees, the inverted pendulum could be transformed into a regular physical pendulum. Perturbations could then be tolerated because they would result in pendulum-like swinging motions allowing the system to react adequately if necessary. Appropriate support can also be mimicked inherently by the system by redirecting the ground reaction force to a point above the CoM. Small perturbations would automatically lead to torques restoring posture similar to the function of a physical pendulum (Fig. 3.3a). The concept of mimicking a physical pendulum can be found in different contexts (Fig. 3.3c) and is here termed the virtual pendulum (VP) concept.

Turning an inverted pendulum into a VP differs from the approach of using postural feedback for explaining dynamic stability during bipedal gait. The VP approach does not include sensory feedback on the current posture (body pitch). In contrast to a feedback- stabilized inverted pendulum as displayed in Figure 3.3b where acting forces intersect below the CoM at the contact point with the ground, forces intersect above the CoM in VP systems. A moving point of origin of force with respect to the body as typical for legged locomotion is an important prerequisite for a VP. In human walking, a force intersection point clearly above the CoM can be observed, indicating the realization of the VP concept. Here, the VP concept is

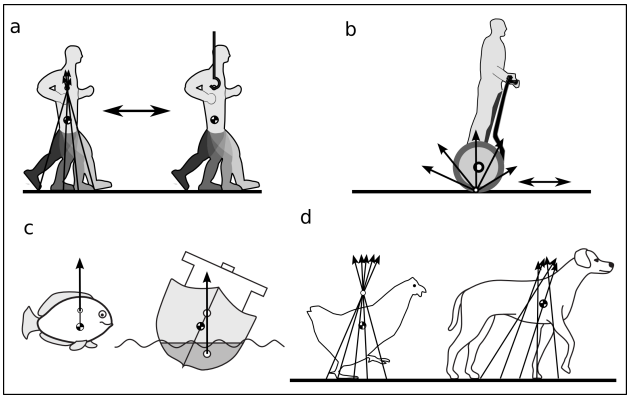

Figure 3.3: **The virtual pendulum (VP) concept** (a) A physical pendulum is mimicked when the ground reaction forces (GRFs) intersect above the center of mass (CoM). Such systems are termed VPs. This behavior is found in human walking (cf. Fig. 3.5) and is in contrast to a feedback-stabilized inverted pendulum (b). Whereas in (a) the origin of force moves with respect to the body, in the inverted pendulum shown in (b) the direction of the force is adjusted to maintain the upright posture. Hence, in (b), the postural stability is achieved by appropriate acceleration, whereas in VP systems the coupling of posture to motion can be much weaker (see text). (c) A VP is found in different systems, for example, in fish and ships, in which the GRF is replaced by the buoyancy force, or in other animals such as walking dogs and running chickens (see also Fig. 3.5). A single intersection point is not necessary for a VP system and cannot always be found (see Fig. 3.5 and text).

represented by one single point, which is termed the virtual pivot point VPP.

In biomechanics, conceptual models are widely used to elucidate specific aspects of bipedal gait. The simplest walking model consists of a point-mass on rigid legs (Alexander, 1976) and predicts walking and running to be optimal modes of locomotion (Srinivasan and Ruina, 2005). Despite the explanatory power of the model for many aspects (Kuo, 2007; Donelan et al., 2002; Cavagna et al., 1977), the lack of compliance in the legs does not allow this model to predict typical experimental ground reaction force patterns that can be considered the fingerprint of a gait. Human-like ground reaction force patterns are generated by the bipedal spring-mass-model (Geyer et al., 2006; Blickhan, 1989; McMahon and Cheng, 1990; Blickhan and Full, 1993; Seyfarth et al., 2002), in which the rigid legs of the simplest model are replaced by springs. Here, we follow the tradition of conceptual models and extend this model by replacing the point-mass of the original model with a rigid body, thereby moving the CoM above the hip as is the case in humans (Fig. 3.3a, Fig. 3.4a). The body essentially represents an unstable inverted pendulum that needs to be stabilized on top of two legs. Stability is implemented using the VP concept. A hip torque during stance of each leg is introduced to redirect its ground reaction force to a VPP somewhere along the body's long axis as shown in Fig. 3.4a. Here, we demonstrate how the VP concept explains dynamic stability during upright bipedal gait and provide experimental evidence that this concept is not exclusive to human walking. Further, we discuss the importance of this concept for the development of upright human walking.

Methods The model's equations of motion are

$$\begin{aligned} m\ddot{x} &= F_x \\ m\ddot{y} &= F_y \\ J\ddot{\varphi} &= r_{\mathrm{VPP}}\left(\sin(\varphi)F_y - \cos(\varphi)F_x\right) \end{aligned} \tag{3.1}$$

with mass $m = 80\,\mathrm{kg}$ and moment of inertia $J = 5\ \mathrm{kg\ m^{-2}}$. r_{VPP} denotes VPP height, F_x and F_y denote the horizontal and vertical GRF, respectively. GRF is the sum of leg spring force F_S pointing along the leg axis and force F_τ induced by the hip torque and acting perpendicular to the massless leg spring. The magnitude of F_S is given by $F_S = k(L_0 - L)$, with k denoting spring stiffness and L_0 and L denoting spring rest length and current length, respectively. The magnitude of F_τ is $F_\tau = F_S \tan(\gamma)$. Here, positive values of F_τ correspond to a clockwise rotation of F_S. The corresponding hip torque τ is calculated by $\tau = LF_S \tan(\gamma)$. The initial conditions for Fig. 3.4b were $\dot{y} = 0, \dot{\varphi} = 0.1\mathrm{rad\,s^{-1}}, \varphi = 0$. Initial height was calculated such that the energy stored in the spring equaled 3J. The remaining energy from a total of 900 J was used for motion in walking direction. The model was implemented in Matlab® R2009a using the Simulink 7 toolbox (The Mathworks Inc., Natick, MA, United States of America).

To compare hip torques predicted by the VPP model with hip torques observed in human gait, previously collected data from Lipfert (2010) for 21 healthy subjects walking and running on a treadmill were analyzed. Inverse dynamics were calculated by a sequential algorithm, taking soft tissue dynamics into account (Günther et al., 2003). Calculated hip torques were normalized to each subject's body weight, leg length and gait cycle, and then averaged to give an overall mean including all steps of all subjects. CoM motion was obtained by integrating the GRFs twice. Initial values for velocity were estimated from kinematic measurements. For human walking, the height of the sacrum was taken as initial CoM height (Gard et al., 2004). For dogs and chickens, initial CoM heights were estimated according to literature (Lee et al., 1999; Daley et al., 2006).

Modeling results The model generated walking solutions similar to those of the underlying spring-mass template, which can adjust to subtle changes in the ground level (Fig. 3.4d). Even though no damping was introduced, body pitch oscillation after perturbation

diminished over time which is different to the behavior of a physical pendulum. In this model, stability of the underlying gait model appears to affect postural sway.

Replacing the point mass of the template by a trunk offers a new reference frame given by the body's long axis which can be used to align the leg in preparation of touch-down. Hence, body-specific sensory signals instead of global information (e.g. gravity direction) can be used for leg placement. The results of our simulation showed that this feature may not only preserve but even increase the stability of the model (Fig. 3.4b).

In the model, a second functional role of the trunk lays in the adjustment of speed during locomotion: Because the ground reaction force is always directed to the VPP, forward and backward lean of the trunk must be accompanied by acceleration and deceleration of the system, respectively. Thus, adjusting the VPP location offers a simple way to change the speed of the model. With respect to model performance, adding a trunk to the model appears to be a greater chance than challenge when the VP concept is applied.

Despite its simplicity, the VPP model is capable of predicting hip torque patterns similar to those observed in human walking (Fig. 3.4c). In this model, the similarity is lost when replacing the VP scheme by a pitch-proportional hip torque control scheme using a global reference frame. However, the loss of similarity by direct feedback on the posture is not lost in all cases as shown, for instance, by the model of Geyer and Herr (2010). When applying the VP concept, the ground reaction force remains aligned towards the body until the leg spring is unloaded, which is an important feature to prevent slipping. With these mechanically attractive and biologically reasonable properties, the VP concept appears suitable for describing human gait and may be used as a basis for more detailed models of human locomotion.

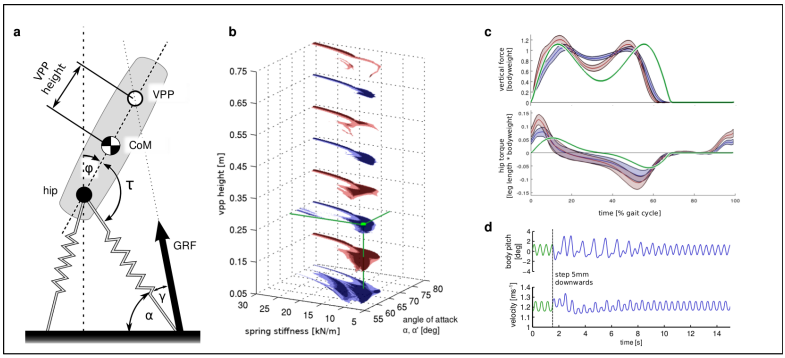

Figure 3.4: **Results of the VPP model**
(a) The VPP model consists of a rigid body above two massless leg springs. A hip torque is introduced to redirect the GRF to the VPP located above the CoM. **(b)** This graph shows parameter configurations for which the model reached at least 10 steps (light areas), 25 steps (medium areas) or 50 steps (dark areas) from non-steady state (see Methods section.). The simulation was stopped after 50 steps. For a motivation of this steps-to-fall method, see Seyfarth et al. (2002). In red areas, the leg is aligned with respect to the ground (angle of attack α), whereas in blue areas the leg is aligned with respect to the body (angle of attack α', where $\alpha = \alpha' + \phi$). For visual presentation, areas are drawn every 10 cm. The configuration at the location shown in green (spring stiffness: 13 kN m^{-1}, $\alpha' = 69\,\mathrm{deg}$, VPP height = 0.25 m) was used for calculation shown in **c** and **d**. **(c)** The model generated hip torque and GRF patterns that resemble those of human walking (BW, bodyweight). The solid green lines depict simulation results, and the blue and red areas correspond to the mean and standard deviation of our experimental data at 1.1 and 1.6 ms^{-1}, respectively. **(d)** Starting from a periodic solution (green region), a small disturbance of a 5 mm step is negotiated by the model without any parameter adaptation, indicating that the VP concept provides basic postural stability. Here, the model shows partially stable solutions (Holmes et al., 2006), that is, after a small perturbation, the model generally approaches another solution.

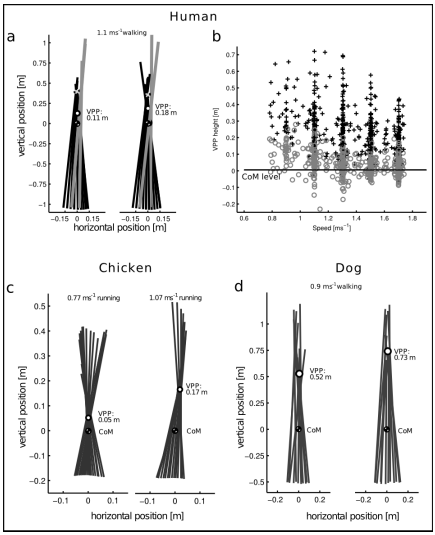

Figure 3.5: **The VPP in experimental data**
(a) Two subsequent steps typical for human walking are shown. Here, the coordinate system originates at and moves with the CoM. Lines show the total ground reaction force at different times, originating at the center of pressure and pointing along the line of action of the force. The ground reaction forces are clearly focused above the CoM. The white circle shows the calculated effective VPP (see text). If the impact force around touchdown (gray lines) is omitted, a very clear intersection point would occur (here, grey circles at 0.39 and 0.35 m, respectively). The impact can then be regarded as disturbance to the system. **(b)** Calculated VPP positions from six subjects walking on an instrumented treadmill at different speeds are shown. Grey circles show calculated VPP heights with impact forces, black crosses show VPP heights without impact forces. **(c)** In running chickens, a clear VPP was observed. In our data, VPP height is strongly coupled to running speed. **(d)** Although less focused than in running chickens or walking humans, walking dogs also show a VPP. However, in different dog gaits, no VPP could be detected.

VPP location In experimental studies, the VPP for each step can be defined as the single point where (1) the total transferred angular momentum remains constant and (2) the sum-of-squares- difference to the original angular momentum over time is minimal, if the ground reaction force would be applied at exactly this point. For human walking, the correspondingly calculated VPP is located 5-70 cm above the CoM (Fig. 3.5a, b). A similar range of VPP location is also predicted by the model where most stable solutions can be found for VPP heights of approximately 1-50 cm (Fig. 3.4b). If VPP height reaches the boundary of this range, only few gait patterns remain stable. For a given VPP location, the model is stable for a range of different leg stiffness and angles of attack (Fig. 3.4d). The results of the model showed that hip torque magnitude and VPP location are tightly related. Thus, experimentally measured VPP location may be a sensitive measure to assess human gait in general and during development and in health and disease.

Stabilizing posture by applying the VP concept is not unique to human walking. Similar observations have been made with other animals including dogs when walking on a treadmill (Fig. 3.5d) and chickens when walking and running over-ground (Fig. 3.5c).

Discussion Similar to the spring-mass model, the VP concept describes a mechanical behavior rather than an explicit movement trajectory. The VP concept combined with the spring-mass-model can tolerate small disturbances and compensates for such disturbances by its inherent mechanical properties without the need for active regulation. This observation is a possible explanation of why natural walking feels effortless.

For each model, there is a trade-off between its simplicity and its limitations. This model was limited to the parasagittal plane, and additional stability challenges originating from 3D motion were neglected. In addition, the model did not contain a foot, and the trunk, arms, head and leg masses were combined in a rigid trunk. These additional aspects can be modeled using different modeling

approaches (Geyer and Herr, 2010; Hof et al., 2005; Bullimore and Burn, 2006; Andrada, 2008) that are often linked to the basic models. However, in this study, we followed the tradition of conceptual models focusing on the point of interest.

The existence of a VP in different animals suggests that the VP might be the result of mechanical circumstances rather than being a primarily intended locomotion pattern. In the following, this theory is discussed using the example of bipedal human walking. For a VPP in human walking, torques extending the hip are required in the first part of stance, and torques flexing the hip are required in the last part of stance. These torques reduce the horizontal forces. Further, these torques generate leg retraction and protraction as required at the time of transition between contact and swing. Hip extension torques prior to ground contact, as are observed in experimental data (Fig. 3.4c), retract the leg and hence prepare the leg for ground contact. Apparently, the hip torques required for leg protraction and retraction during steady locomotion also provide the VP and facilitate postural stability. Thus, utilizing the VP concept requires almost no additional effort.

The VP concept can be considered a general template for locomotion, similar to the spring-like leg behavior found in a large variety of animals (Blickhan and Full, 1993; Farley et al., 1993; Alexander, 1988). Nature seems to take advantage of the attractive properties of mechanical templates, that facilitate stable gait without the need for precise trajectory planning (Geyer et al., 2006; Seyfarth et al., 2002). Jointly implemented as VPP model, these two templates combined are able to describe upright human walking.

Moreover, the supportive function of the VP may have assisted the erection of hominine walking. Recent research suggests that humans did not evolve from a knuckle-walking ancestor (Kivell and Schmitt, 2009). Instead, the erection of locomotion likely took place in an arboreal environment, similar to the environment in which orang-utan still live today: When brachiating through trees, straighter legs and a more upright posture can be observed as an

adaptation to more flexible branches (Thorpe et al., 2007), making the gait kinematically more similar to modern human walking. This theory is supported by observations of fossils of the recently presented early hominine Ardipithecus Ramidus "Ardi", who appears to have retained arboreal locomotion capabilities but did not rely on physical suspension (Lovejoy et al., 2009b). Based on (1) the presence of a VPP in various animal and human gaits, (2) the illustrated mechanism that facilitates the VPP in human walking and (3) the presumed similarity of ancestral and modern human gait (Thorpe et al., 2007), it can be concluded that "Ardi" may have overcome the apparent instability of upright gait by utilizing the VP concept. If this theory holds true, instability was likely not an obstacle in the evolution of human bipedalism.

3.4 Conclusion

The general aim of a template is to explain and understand the behavior of a biological system in terms of a simple mechanical analogy. Starting from mere similarity to the experiments, investigations in simulation allow to draw further conclusions (see also section 4.4). Further, templates allow to characterize gait with few parameters, thus enabling the comparison of gaits across different species (Blickhan and Full, 1993; Bullimore and Donelan, 2008). These features make templates a useful tool for understanding locomotion.

Template models should not be taken too literally. Generally, the idea behind a template is to depict a specific functionality of the analyzed system, to a certain degree. In simulation, they allow to investigate the effects of the specific modeled functionality. When extensions of templates are proposed, we must take care that these extensions do not spoil the understanding gained by the original template. For example, allowing a general modification of stiffness $k(L, t)$, *any* arbitrary force pattern could be created in the model. However, this comes at the cost of having arbitrary motions, and it

will be hard to conclude anything from such model. Instead, any modification or extension of templates should start with defining the specific functionality that one would like to investigate.

In this chapter, a new template for describing the pitch stabilization in human walking was introduced. Its functionality resembles those of a regular pendulum. We have seen that despite the neutral stability of its archetype (an undamped pendulum), the VP template on top of a SLIP walking model is asymptotically stable. Because a VP can easily be implemented in biology, we could draw conclusions on the evolution of upright human walking. The experimental results have been recently confirmed by Gruben and Boehm (2011).

At this point, we should remember that templates should not be taken too literally. We do not expect that humans have massless springs below their CoM, nor do we expect that we imagine being a pendulum while we are walking. Instead, templates offer a simple mechanical analogy that resembles the characteristic features of the gait. We do not (yet) know to what extent humans rely on the features provided by the template's dynamics (e.g. stability without parameter adjustment), and to what extent additional control schemes are applied. This question is approached in section 4.4, where we will find a way to incorporate experimentally observed adaptation schemes within the framework of templates. This allows using templates for describing and analyzing the complex phenomenon of human locomotion, even if they are not literally implemented.

4

QUANTITATIVE GAIT ANALYSIS

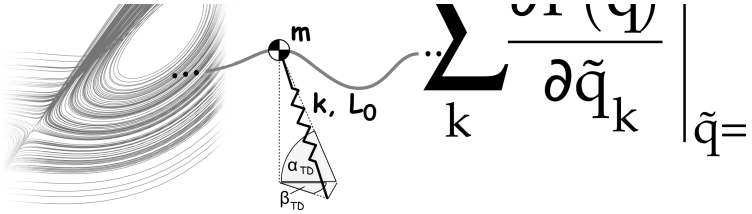

Science is facts; just as houses are made of stones, so is science made of facts; but a pile of stones is not a house and a collection of facts is not necessarily science.

Henri Poincaré (1854 - 1912)

4.1 Introduction

Human running is not a strictly periodic motion: it has some cycle to cycle variability. We seek to characterize the structure of that variability and to understand how humans react to it. Here, we assume that the variability around the limit cycle arises from dynamical noise (for example, nervous system noise (see Faisal et al., 2008; Priplata et al., 2002; Collins et al., 2003)). Thus, we consider the variability due to disturbances, and by analyzing the variability we investigate how human runners cope with disturbances.

The first step of our analysis is the identification of a periodic reference motion that we can interpret as time-varying limit cycle. In section 4.2, we argue that our assumption of noise-driven dynamics around a time-varying limit cycle is reasonable. Next, we subtract the limit cycle and continue our investigation of the residuals, at first without reference to any specific model. Then, we fit a Floquet model to the dynamics in section 4.3 to characterize the stability of the off-limit cycle motion by means of eigenvalues. Finally, we use the SLIP template to analyze the experimentally observed gait in section 4.4. We consider the extent to which the SLIP can be considered as autonomous system, and present a method to identify individualized controllers for this system.

We will summarize and discuss the findings in section 4.5.

4.2 Model-free gait characterization

4.2.1 Introduction

Human treadmill running is not strictly periodic. This becomes intuitively clear when we think about phenomena like muscle fatigue, sweating (loss of mass) or the fact that people might reduce their level of alertness when they are used to the environment or increase it suddenly, for example when they approach the side of the belt.

Also, free running in a naturally uneven environment like a forest is not a periodic motion at all, because the runner has to adapt to the terrain at every step. Consequently, we can assume that variability is an inherent feature of human running.

In this section we investigate the basic structure of this variability. Although human running is initiated by the brain which is probably the most complex structure in the universe (Kömpf, 2007), there has long been evidence that reflexes also play an important role in human running (Dietz et al., 1979). Several simulation models of human locomotion that include physiological features like neuronal delays have been proposed. In one model, Taga (1994) has shown that depending on the time delay, the system shows either a stable limit cycle or behaves in a chaotic fashion. Generally, we cannot be sure what kind of dynamics we can expect. To shed light on these questions, here we investigate some key characteristics of human treadmill running.

We perform several analyses: Section 4.2.2 computes temporal characteristics. Next, section 4.2.3), examines the left-right symmetry of the motion. Section 4.2.4 analyzes the statistical distribution of the residuals around the averaged motion. Further, in section 4.2.5 we investigate whether or not the data collapse to a low dimensional manifold in state space, which would be a sign of a strange attractor of a probably chaotic motion because strange attractors often possess a low dimensional structure. Finally, in the discussion we summarize and interpret the results.

4.2.2 Stationarity and temporal scaling

Here, we analyze stationarity and temporal scaling (that is, self-similarity in time) of the kinematics. To analyze stationarity, we use a simple yet conclusive approach:

- Data are sampled at 50 Poincaré-sections per gait cycle. To reduce dimensionality, we select a subset of 15 linear combina-

tions of marker coordinates and the corresponding velocities (see Fig. 2.18):

'l_kne_y - r_kne_y'
'l_anl_y - l_kne_y' 'r_anl_y - r_kne_y'
'l_mtv_z - l_hee_z' 'r_mtv_z - r_hee_z'
'l_trc_y - l_kne_y' 'r_trc_y - r_kne_y'
'l_kne_x - r_kne_x'
'l_trc_x - l_kne_x' 'r_trc_x - r_kne_x'
'l_anl_x - l_kne_x' 'r_anl_x - r_kne_x'
'l_mtv_x - l_hee_x' 'r_mtv_x - r_hee_x'
'com_z'

yielding a 30-dimensional state space. The suffixes _x, _y, _z indicate the lateral, anteroposterior or vertical coordinate, respectively (see Fig. 2.19).

- The averages of each Poincaré-section are subtracted.
- Velocities are scaled such that their average variance equals the average variance of position data.
- For each stride, the 30-dimensional data of all 50 sections, which in total represent the residuals around the average gait cycle, are concatenated into a single 1500-dimensional vector, representing this stride as a point in a 1500-dimensional stride space.
- A principal component analysis (PCA) is performed on these data in the stride space.
- The scores on the first principal axes, which capture a large part of the total variance, are displayed.
  In our data, the first 5 components account for $\approx 50\%$ of the total variance of the data. To account for 90% variance, ≈ 40 components must be taken into account.

The result of this approach for four subjects is displayed in Fig. 4.1. We immediately see the nonstationarity in the scores of the first principal axis. On the other principal axes, nonstationarity is not that apparent but we can see it when we look at the "local averages." This is apparent for the first principal component in each

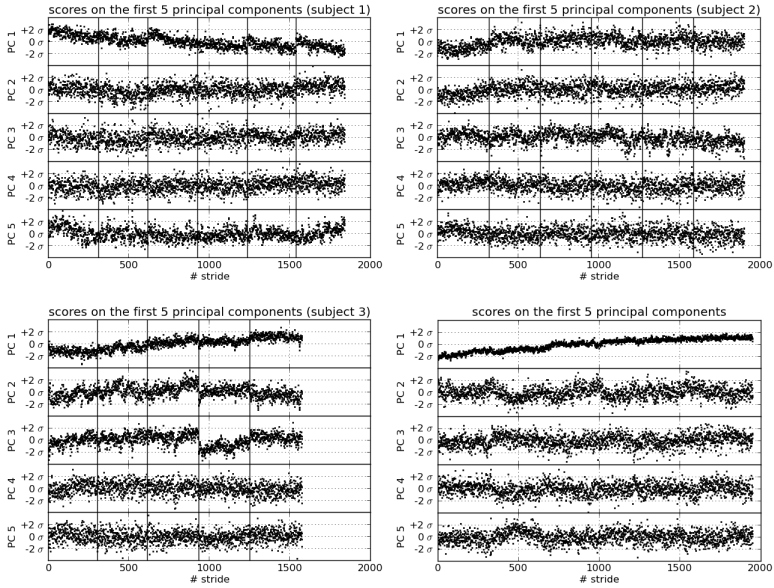

Figure 4.1:
Scores on the first principal components of residuals of an average gait cycle for four subjects, in units of the corresponding standard deviation σ. In one subject, one trial was discarded, resulting in fewer strides. Solid vertical lines indicate the borders of each individual trial. Non-stationarity is clearly visible as a slow trend in the data.

subject, but also present in in the other principal components. For example, in subject 2 the average score on PC 3 between stride 600 and 1100 is clearly higher than between stride 1500 to 1800. Because nonstationarity is clearly evident in at least one component in every subject, statistical tests are omitted.

Next, we investigate whether there are long-range correlations in the increments by applying the detrended fluctuation analysis (DFA), which is also applicable in the presence of trends. DFA scaling exponents α are computed for four subjects for which data quality was sufficiently high. The averaged scaling exponents α over 50 Poincaré-sections and 15 selected markers are 0.71, 0.65, 0.70 and 0.72, indicating the presence of long-range correlations in the data. No DFA is performed on velocities because of their presumably higher level of noise. For two representative subjects, details of the DFA are displayed in Fig. 4.2.

4.2.3 Symmetry of the motion

Intuitively, we might assume that human running is a symmetric motion. Following this assumption, it would be reasonable to split a stride into two steps for further analysis, as this would on the one hand double the amount of available data and shorten the "cycle time", which would facilitate a potential recovery of off-limit cycle dynamics. To briefly analyze the left-right symmetry, we overlay the kinematics of selected corresponding markers after a shift of half a gait cycle. The results are displayed in Fig. 4.3, indicating that symmetry is not perfect. Instead of thinking about statistical tests and arguing about the influence of errors in marker placement, we will perform a second investigation of symmetry in section 4.4.3 (which will confirm our current impression of asymmetry).

4.2.4 Statistical properties of residuals

When we assume that the dynamics are noise-driven, we expect that the residuals have a gaussian distribution. Although other distributions also might originate from noise-driven dynamics, we have no reason to assume any other distribution here.

To account for the nonstationarity described in section 4.2.2, we apply a 61-strides centered moving average detrending prior to the

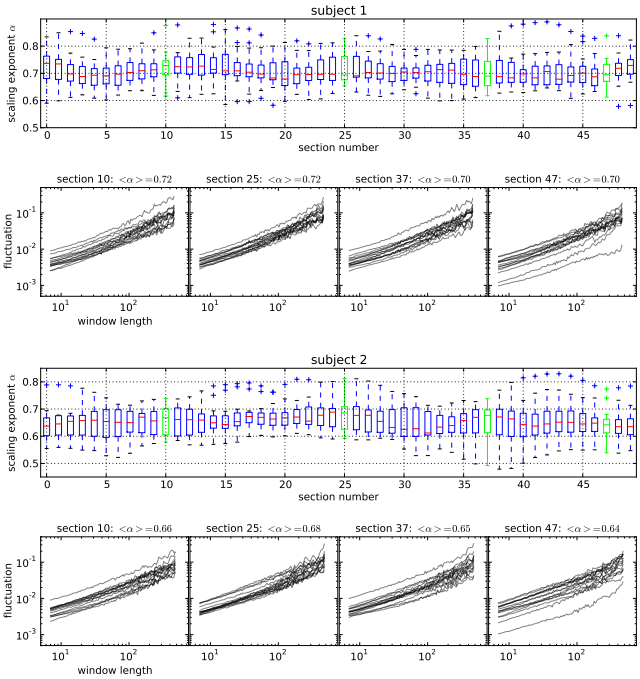

Figure 4.2:
Detrended fluctuation analysis of kinematic data around the average gait cycle (residuals) for 15 selected markers at 50 equally spaced Poincaré-sections. For four selected Poincaré-sections, the fluctuation over the window size is plotted. A decrease of the slope for larger window lengths, which would indicate a false-positive result, is not visible.

analysis. We use the same data definition, sampling rate and principal components analysis as in section 4.2.2, and plot the (normalized) scores on the first 50 principal axes in a QQ-Plot against a

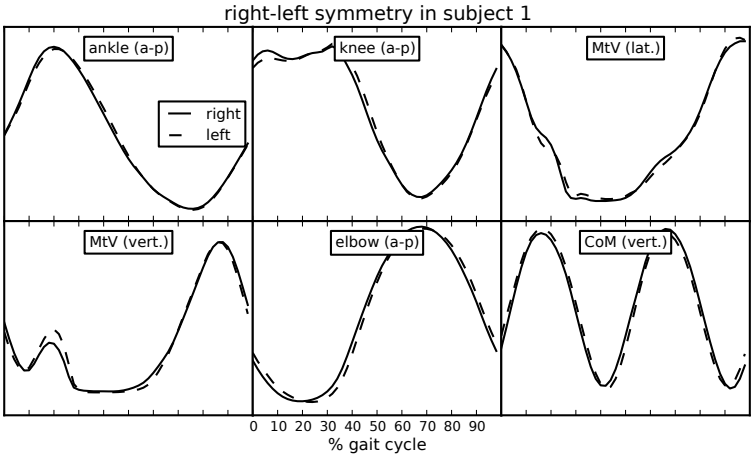

Figure 4.3:
Left-right asymmetry in the motion of makers for one representative subject. Here, the averaged motion of individual markers with respect to the CoM is plotted. "a-p", "lat." and "vert." indicate anterior-posterior, lateral and vertical direction, respectively. The corresponding phase of "left" markers were shifted by 50% of the gait cycle for comparison. In the lower right subpanels, the vertical CoM motion is displayed twice, once regularly and once shifted in time by 50% of the gait cycle. The asymmetry is small compared to the amplitude of the motion.

Gaussian distribution. The result in Fig. 4.4 shows very good agreement of our data with the Gaussian distribution.

The Gaussian distribution is known to describe various sources of noise. As our data show a Gaussian distribution, this supports our assumption that dynamics off the limit cycle might be driven by noise. Here, by 'noise' we mean random fluctuations in the dynam-

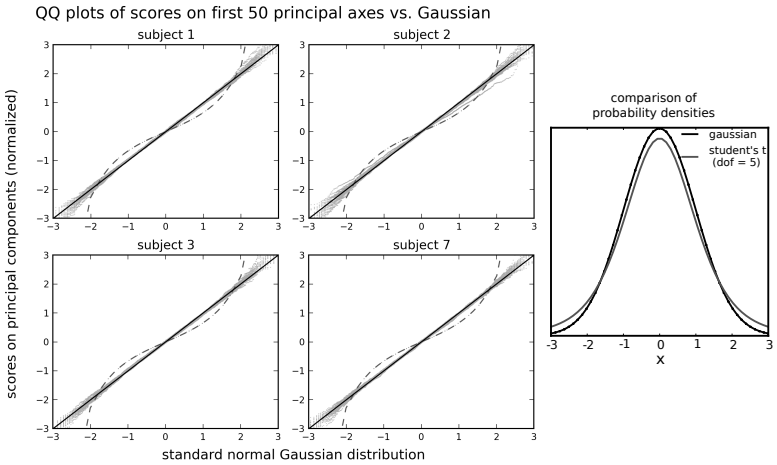

Figure 4.4:
Left: Q-Q-plots of the scores on the first 50 principal components of the stride vector space after a 61-frames centered moving average detrending, compared to a standard normal Gaussian $\mathcal{N}(0,1)$. The first 50 components account for $\approx$ 93% of the total variance of a stride. In the range between -3 to 3 times standard deviation, a very good agreement can be observed; in the quantiles from -2 to 2, where $\approx$ 95% of all values reside, deviations are hardly visible. The black line depicts $x = y$. For comparison, also a t-distribution with 5 degrees of freedom is given (dashed line). The probability densities of the gaussian and this specific t-distribution appear to be similar at a first glance (right), yet the QQ-plot can reveal the difference.

ics that do not originate from the deterministic part of the system, but will excite the dynamics of it.

4.2.5 Spatial scaling

Another possible explanation for stride to stride variability would be an aperiodic chaotic motion. Typically, such a chaotic motion results in the collapse of the dynamics onto a low-dimensional (possibly fractal) set in the state space. This hypothesis can be investigated by analyzing the spatial scaling behavior (see section 2.1.10).

We cannot precisely distinguish between a trend and effects from chaotic dynamics. Here, we used a rather simple floating average detrending procedure. However, this detrending might destroy the fine structure of the data that we are interested in when we are trying recover the attractor. Thus, here we only investigate the hypothesis that the observed data, including the apparent trend, do in fact stem from a low-dimensional chaotic attractor. That is, we do not detrend the data prior to this analysis.

Results of the dimension estimation method described in section 2.1.10 are expemplarily given for two subjects in Fig. 4.5, indicating that a hypothetical attractor would have a dimension of $\approx$ 8 and is thus not low-dimensional. We can interpret the result of a dimension of ≈ 8 also in another way: when we assume that the deviations are not equally spread around the limit cycle in every dimension, but instead only 8 dimensions have large amplitude, we would observe just the same result.

4.2.6 Conclusion

In this section, we computed several model-free characteristics of human running in order to gain knowledge of the kind of system that was observed.

The temporal analysis revealed nonstationarity as well as long-range correlations. Generally, both are typical for complex systems or simple open systems - in which case the environment would also have to be included in a model, yielding again a complex system. This is not surprising because humans are indeed complex systems.

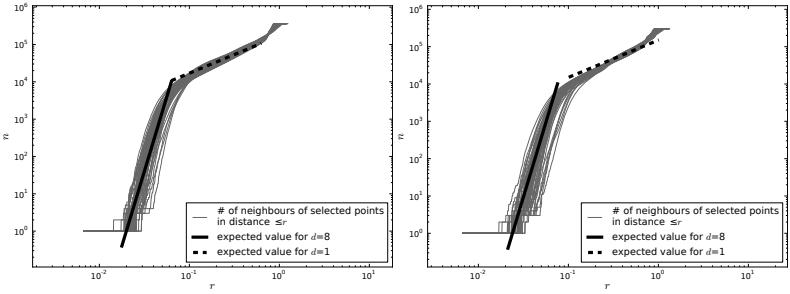

Figure 4.5:
Double-logarithmic plot of the number of neighbors n in a given radius r for 50 randomly chosen points in the experimentally observed running data. Here, two representative graphs for two subjects are presented, each computed of 360,000$\times$30 data points distributed over $\approx$ 1800 gait cycles. The spatial scaling for the measured data does not reveal a low-dimensional attractor. For larger diameters, the decrease of the slope towards 1 can be explained by the dominance of the (1-dimensional) limit cycle structure at that scale. For smaller scales, a much steeper slope ($d \approx 8$) is observed, which is what we would expect from noisy data. Data were not detrended prior to analysis.

When analyzing step-to-step behavior, we must keep in mind that there is also a complex motion that alters the limit cycle with time.

Ashkenazy et al. (2002) presented a model to explain the observed long-range correlations in human gait dynamics, which is based on the assumption that there is a (possibly) random choice between different oscillating circuits that drive the motion. The presented results are in line with this hypothesis: a possible explanation for the slow trends observed in the gait pattern would be a continuous adaptation of physiological gait parameters, like a modulation of reflex strengths (see for example Duysens et al. (1993)). When we consider a gait as resulting from a neuromechanical os-

cillator, an alteration of the oscillator's parameters could be identified with the change of choice of a oscillating circuit in Ashkenazy's model. This indicates that the trend and the long-range correlation might possibly have the same physiological origin.

The question of symmetry has been addressed before in literature (for a review, see for example Sadeghi et al. (2000)). Often, symmetry has been assumed, but our data indicate in line with the results of Sadeghi et al. (2000) that instead asymmetry is natural in human running. This finding is further supported by results in section 4.4. As a consequence, all investigations that explicitly or implicitly refer to a cyclic motion (for example, stability analysis; see sections 4.3 and 4.4.3) must consider a complete stride and not a single step as reference.

The Gaussian distribution of the residuals around the (local) average motion, together with the failed detection of a low-dimensional manifold containing the dynamics, indicate that the dynamics might be induced by noise instead of being signs of a chaotic motion. Although noise superimposed on a chaotic motion cannot be excluded as explanation of the dynamics, larger deviations from the Gaussian distribution would be likely in that case. Thus, in the following we consider dynamic noise as main source of variability in our experimental data.

Summarizing all this information, we can now formulate a general approach to model the dynamics: We can assume that there is a stable limit cycle, that slowly varies with time. The excitation of the dynamics is assumed to be dynamical noise, which leads to a stochastic model of the form $\mathrm{d}x = f(x)\mathrm{d}t + \mathrm{d}\eta$ with η denoting the noise. When we further assume that the amplitude of the off-limit cycle dynamics is sufficiently small, we can formulate a linear model; in the case of return maps at phase φ we obtain an autoregressive model of the form $x_{n+1} = A(\varphi)x + \eta$, which is the approach in section 4.3.

Before we continue, we need to state another implicit assumption: we assume that the dynamics around the limit cycle do not

change when the limit cycle itself changes, that is, the matrix $A(\varphi)$ of the autoregressive model is explicitely independent of time. In practice, this means we consider the data as stationary after the detrending (including removal of the limit cycle). We search for models to describe the short-time dynamics of these residuals, but we must keep in mind that there are additional slow dynamics which are not captured by our models.

4.3 Linear Gait analysis

4.3.1 Motivation

We have found evidence in section 4.2 that human gait can be modeled as an asymptotically stable limit cycle, which however changes on a slow time scale. Following this approach, the natural first order approximation of the dynamics is a linearization, that is, we model the dynamics around the limit cycle as a linear system (see for example Revzen and Guckenheimer (2011) or Hurmuzlu and Basdogan (1994)). As we have a periodic base motion, namely the limit cycle, we assume that the system around the limit cycle does not depend on time but on phase:

$$\dot{x} = A(\varphi)x, \tag{4.1}$$

where x denotes the state of the system, and $A(\varphi)$ describes the linear approximation of the dynamics at phase φ. This kind of system is known as Floquet system, who was the first to describe it (Floquet, 1883). One of its properties is that it is equivalent up to a transformation of coordinates to a linear time invariant (LTI) system, which in turn can be characterized by its eigenvalues.

As we assume that we have a periodic system, we are interested in return maps B which map the state at phase φ exactly one stride (2π) ahead. The eigenvalues of B describe the stability of the system and the decay time of disturbances. They are called Floquet

multipliers. The similarity to an LTI system implies that the eigenvalues are independent of the chosen section φ. However, this is not necessarily true for recovered return maps.

4.3.2 Methods

We use the same part of the state space as described in section 4.2.2 to reduce the data dimension, and detrend the data (this includes removing the mean) using a 61-strides centered moving average detrending. Detrending is performed individually for each Poincaré-section. We compute return maps for the residuals as described in section 2.1.2. Further, we apply the bootstrap procedure to obtain a distribution of eigenvalues. This distribution will then be subject to analysis of a significant slow-dynamics subspace (see section 2.1.5). Finding such a subspace would be a first step to recover the off-limit cycle dynamics of the human runner (Revzen and Guckenheimer, 2011).

To verify the code, we first apply the analysis to an artificial simulated Floquet system with a randomly selected system matrix that is driven by noise. The corresponding stochastic differential equation $\mathrm{d}x = Ax\mathrm{d}t + \mathrm{d}\eta$ is then integrated numerically using the method described by Bastani and Hosseini (2007), implemented in Python (http://www.scipy.org) by Shai Revzen. The results in Fig. 4.6 indicate that the implementation is able to recover the eigenvalues of a Floquet system from measurement data, and that the 61-strides detrending hardly affects the recovered eigenvalues at all.

4.3.3 Results

A consequence of the similarity to a linear time-invariant system is that the eigenvalues of the system must not change when regression is performed on different Poincaré-sections. This is not necessarily true for the recovered eigenvalues, because of independent bootstraps at different phases. Also, interpolation of the data might pro-

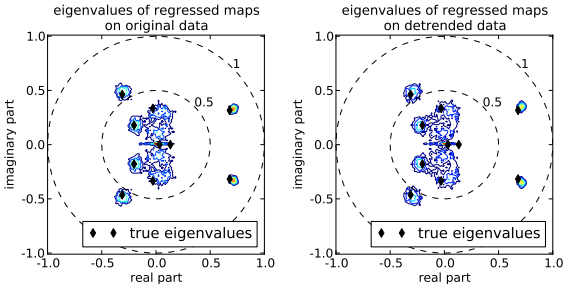

Figure 4.6:
Verification of the eigenvalue recovery algorithm on simulated data on a noise-driven Floquet system. The true Floquet multipliers are displayed in black diamonds.
Left: on original simulation data, Right: on simulation data after a 61-frames centered moving average detrending was applied to the data.

duce some phase dependent changes in the eigenvalues. A similar study for walking already found a phase dependence of the recovered eigenvalues (Hurmuzlu and Basdogan, 1994).

Results in Fig. 4.7 indicate that the eigenvalue distributions vary with phase. Yet, the center and diameter of the distribution are roughly similar, indicating that statements regarding the decay time of disturbances should still be approximately correct.

We compute the eigenvalue distributions of the return maps for four subjects at one selected Poincaré-section with high total variance, and perform the test for a significant slow-dynamics subspace (see section 2.1.5). Results are displayed in Fig. 4.8. We see that for all subjects, a large fraction of the distribution is within the $\frac{1}{e} \approx .3$-circle, indicating that most disturbances decay within one stride. The diameter of the distributions is clearly larger than the expected diameter r_0 for structure-free data of the the same dimension, com-

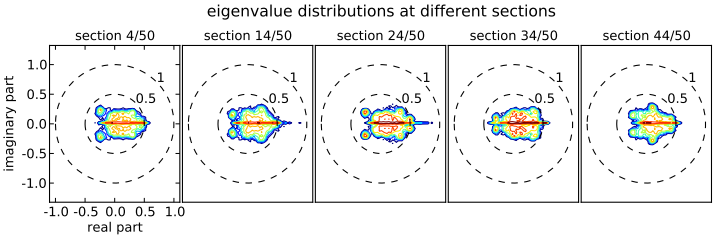

Figure 4.7:
Eigenvalue distribution of the return map for experimental data starting at different phases, for one selected subject (2). Clearly, the distribution changes with phase. For all sections, the vast majority of the distribution is $< .5$ in this example.

puted according to section 2.1.4. Although the distributions seem to have a shape that is different from a disc which would be expected for random data, the template dimension estimation fails to find a significant slow-dynamics subspace for all subjects except subject 1. That is, there is no clear jump in the matching quality of the general null model (that is, random matrices) to the data. In subject 1, a circular distribution cannot capture the largest eigenvalue very well, yielding a clear increase in model fit residuals Ξ_d for this dimension. However, as in this subject a very strong trend is present, this large real positive eigenvalue might correspond to leftovers from the drift instead of being part of the off-limit cycle dynamics.

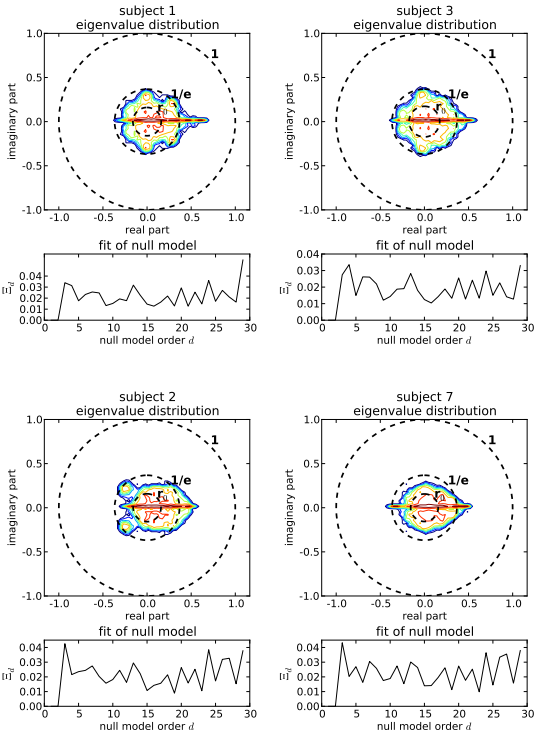

Figure 4.8:
Upper subpanels: The eigenvalue distributions of return maps for one stride. r_0 depicts the expected radius for structure-free input data (see section 2.1.4). For comparison, the circle with diameter e^{-1} is given.
Lower subpanels: Model fit residuals Ξ_d for fitting a circular law model to the lowest d eigenvalues. To account for the restriction to a Poincaré-section, the dimension with lowest variance has been removed from the data.

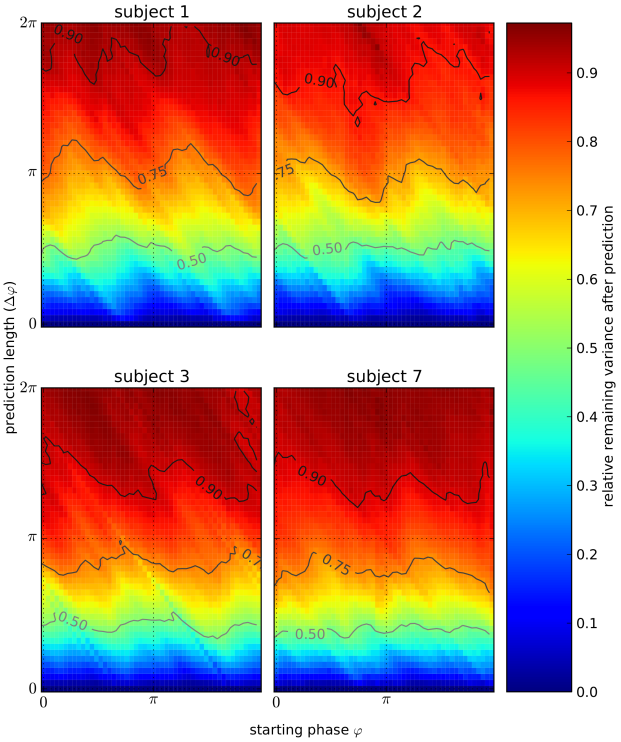

Figure 4.9:
Relative remaining variance after prediction as a function of the starting section and the prediction length (that is, the phase difference between input and prediction output). After one step ($\Delta\varphi = \pi$), a comparatively large fraction of the variance can be predicted using a linear model, whereas after one stride ($\Delta\varphi = 2\pi$), only a small fraction can be predicted. These qualitative results are independent from the starting section.

The recovered eigenvalues do not tell us all about the actual lifetime of disturbances. On the one hand, small eigenvalues do not imply a rapid convergence towards the limit cycle - here, we would also have to analyze the singular values of the matrix. On the other hand, the recovered magnitude of the eigenvalues is not very precise. This is clear when we compare the diameter of the eigenvalue distribution with the diameter r_0 that we would expect if we had only noise and no structure at all (Fig. 4.8). Thus, we can expect that disturbances decay within few steps, but we cannot get the exact decay time from the recovered eigenvalues.

Instead of using the eigenvalues, we can directly analyze the lifetime of disturbances using prediction. First, we fit a model to predict data at phase ϕ_2 from data at phase ϕ_1. Second, we predict the data and compare the variance of the data after prediction to the variance of the data prior to prediction. When we assume that there is dynamical noise driving the motion, the total variance is the sum of the variance of the deterministic dynamics plus the variance of noise-induced dynamics. To analyze the lifetime of disturbances, we now compare these two variances. In detail, we fit a linear model $\hat{A}$ to predict data x at phase φ_2 using data at phase φ_1: $\hat{x}(\varphi_2) = \hat{A}x(\varphi_1)$, and compute the relative remaining variance after prediction $r = \frac{\text{var}(\hat{x}(\varphi_2) - x(\varphi_2))}{\text{var}(x(\varphi_2)}$. The results are presented in Fig. 4.9. We clearly see that for short times, we can predict nearly all of the variance, indicating a good signal-to-noise ratio. After one step, there is still a substantial amount of variance ($\approx 20\% - 25\%$) that can be predicted. After a stride, only $\approx 5\% - 10\%$ of the variance can be predicted. This indicates that disturbances decay typically within one stride.

4.3.4 Conclusion

We see that eigenvalues of the linearized return maps are mostly located in a disc of diameter $.5$ in the complex plane. The majority have even magnitude $\lesssim 1/e \approx .3$, indicating that disturbances typ-

ically decay within a single stride. Analyzing the prediction quality as a function of prediction length shows even more clearly that disturbances decay within one stride, and that after one step there is still some variance that can be predicted. This is in good agreement with the results of Carver et al. (2009), who hypothesized a single-step or two-step deadbeat control strategy for running, depending on the constraints.

In addition to the quick decay of disturbances shown in this section, we saw in section 4.2 the presence of a slow drift. This indicates control action on two different time scales, indicating (at least) two levels of control. We assumed that the short-time dynamics, which we can now call "quick" dynamics do not change when the limit cycle itself changes. This means that the disturbance rejection mechanism stays roughly the same under different conditions, an assumption that appears reasonable but might be challenged by further studies.

The dependence of the eigenvalue distribution on phase indicates that there are parts of the dynamics that cannot be captured by this linear approach. These dynamics may correspond to nonlinearities of the system like sensory thresholds.

Testing for a template dimension that separates the dynamics into a "slow" and "fast" part did not result in a clear separation. However, this does not imply that our maps consist of random data. To the contrary, as the typical diameter of the eigenvalue distribution is clearly larger than the expected diameter for structure-free data r_0, we can positively state that there is a (possibly quite small) fraction of the dynamics that can be recovered by a linear fit to the data. Further evidence for this will be given in the following section 4.4.

4.4 SLIP based gait analysis

4.4.1 Motivation

As we have already seen in previous sections, human running is complex and unsteady even under stationary experimental conditions. But does this imply that a good model to describe and analyze human locomotion also must be complex?

In chapter 3 we discussed how human running motion can be described using minimalistic template models, thereby reducing the continuous dynamics to a set of few parameters. Here, we focus on the SLIP model, as there is a way to precisely compute the corresponding model parameters for an experimentally observed step (see section 3.2). This small, easily interpretable set of parameters enables a gait analysis in a low-dimensional space.

When we describe the motion using a template model, the equations of motions are given, and only a few parameters are left to be determined. If we knew how these parameters are adjusted step by step, we would learn a lot about human gait control at this level of abstraction. Here we investigate these step by step SLIP paramater changes.

4.4.2 Methods

Extended SLIP model for data description

The spring-loaded inverted pendulum (SLIP) (Blickhan, 1989; McMahon and Cheng, 1990) is a widely used model to describe bouncy gaits such as human running in a highly reductive manner, allowing the reduction of the center of mass (CoM) dynamics to a few model parameters. Here, we will use a 3D version of the model (see Fig. 4.10 and also Carver et al. (2009); Peuker et al. (2012)).

Denoting CoM position with $[x, y, z]^T$ and foot position (tip of leg) with $[x_F, y_F = 0, z_F]^T$, the equations of CoM motion in stance are:

$$\begin{aligned} \ddot{x} &= \tilde{F}_s L^{-1}(x - x_F) \\ \ddot{y} &= \tilde{F}_s L^{-1} y - g \\ \ddot{z} &= \tilde{F}_s L^{-1}(z - z_F), \end{aligned} \tag{4.2}$$

with current leg length $L = \sqrt{(x - x_F)^2 + y^2 + (z - z_F)^2}$, spring force $\tilde{F}_s = \frac{k}{m}(L_0 - L)$ and gravitational acceleration $g = 9.81\, ms^{-2}$. In flight, the mass follows a ballistic motion ($\ddot{y} = -g$, $\ddot{x} = \ddot{z} = 0$), and leg orientation is fixed to $\alpha_{\mathrm{TD}}, \beta_{\mathrm{TD}}$ (see Fig. 4.10).

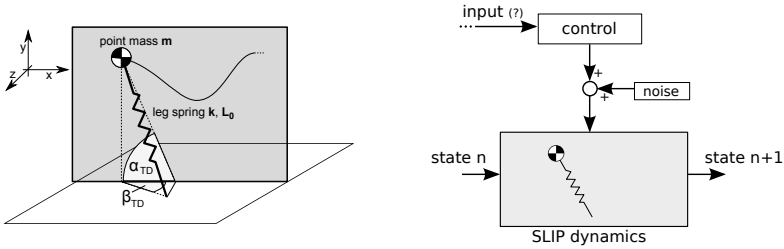

Figure 4.10:
Left: scheme of the 3D SLIP model. During swing, the leg parameters spring rest length L_0 and stiffness k as well as the leg orientation angles α_{TD} and β_{TD} are adjusted. Additionally, an energy input δE during stance is introduced to allow energy adjustments. Right: Scheme of the SLIP-based view of the gait controller. The system state at apex n, consisting of $[y, \dot{x}, \dot{z}]^T$ is mapped to the next apex state by the SLIP dynamics. In this view, the parameters of the SLIP model are adjusted by a controller, and have random variation due to noise. Identification of the controller input is part of this work.

In normal running, there is a single point around mid-stance with $\dot{y} = 0$. At this point, we allow a specified amount of energy δE to be introduced by changing the spring rest length L_0 and stiffness

k. With the additional requirement that the ground reaction force should not be altered, the new parameters L_0' and k' are

$$L_0' = \frac{2\delta E}{k(L_0 - L)} + L_0 \tag{4.3}$$

$$k' = k\frac{L - L_0}{L - L_0'}. \tag{4.4}$$

During flight, the leg parameters are adjusted for next stance. In our approach, we approximate the CoM dynamics of a human runner by the SLIP model, whose parameters are set by a controller and have an additional noise component (Fig. 4.10B).

Parameters for each step in experimental data were computed using the algorithm outlined in section 3.2 (see also Ludwig et al., 2012 (accepted)).

Experimental setup

We use the experimental data described in section 2.3 and calculate CoM motion as described in section 2.2. Due to inappropriate behavior during the experiment like voluntary changes of gait or technical failures of the measurement system, four subjects had to be excluded, leaving six subjects for analysis.

Data stationarity

Although stationary conditions were provided during the experiment, this does not imply a stationary gait. As we saw already in section 4.2, we can expect a drift of the gait pattern. Here, we test the existence of a drift in the parameters by computing a 61-strides centered moving average for all SLIP apex states and all parameters.

We compare the standard deviation of this trend to the standard deviation of 10,000 null-models which are each constructed as centered moving average of a random permutation of the original data. Figure 4.11 visualizes the original trend and one randomly chosen

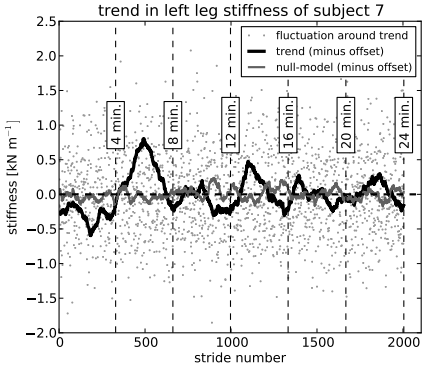

Figure 4.11:
Slow drift in the parameters is illustrated here for the stiffness of the left leg in a selected subject. For all subjects, significant trends were found.

null model. A significant drift with $p < .001$ is detected when less than 10 null-models had a larger standard deviation than the original data. In agreement with section 4.2.2, we find significant trends in the parameters k, α, β, L_0 and apex height y for all subjects on both sides. To account for the drift in general, we perform a 61-frames centered moving average detrending for all states and all parameters.

Regression and prediction

For each prediction, we split input and output data into a regression and a prediction part using the bootstrap method which yields approximately the fraction $1 - e^{-1}$ for regression and the remainder for prediction. Iteration of this procedure with different splittings allows the parameter-free estimation of confidence intervals.

Let $A \in \mathbb{R}^{n \times k}$, $B \in \mathbb{R}^{n \times d}$ denote the (re-sampled) input and output data of length n and dimension d or k, respectively, and X is the least squares solution of $||AX - B||_F$ (see section 2.1.2). We then try to predict the remainder of the original input and output data A', B', which were not used for regression: $\hat{B}' = A'X$. We analyze the quality of this out-of-sample prediction by the remaining relative variance after prediction r, which we compute as

$$r = \frac{\operatorname{trace}(\operatorname{cov}(B' - \hat{B}'))}{\operatorname{trace}(\operatorname{cov}(B'))}. \tag{4.5}$$

Note that r is equivalent to the relation of the sum of squares of elements of $(B' - \hat{B}')$ and B'. The bootstrap procedure yields a distribution of r which reflects the probability of r having a specific value, thus giving a confidence interval for r.

4.4.3 Results

Symmetry of leg parameter

To investigate the symmetry of leg parameters, we compute for each stride the difference between a selected parameter of the right and left leg. This quantity is by construction insensitive to slow trends, in contrast to the comparison of mean and variance of both sides. The corresponding distributions are displayed in Fig. 4.12, indicating that human gait on the SLIP level of abstraction is not exactly symmetric. This is in line with our results in section 4.2.3.

Independence of lateral motion

Viewed from behind, running motion can be approximated as an inverted pendulum, whose supporting point is altered at every step. The motion of this inverted pendulum is slow, because it is almost upright and the moment of inertia is comparatively high. Because of that, leg adjustments in the lateral direction might be dominated

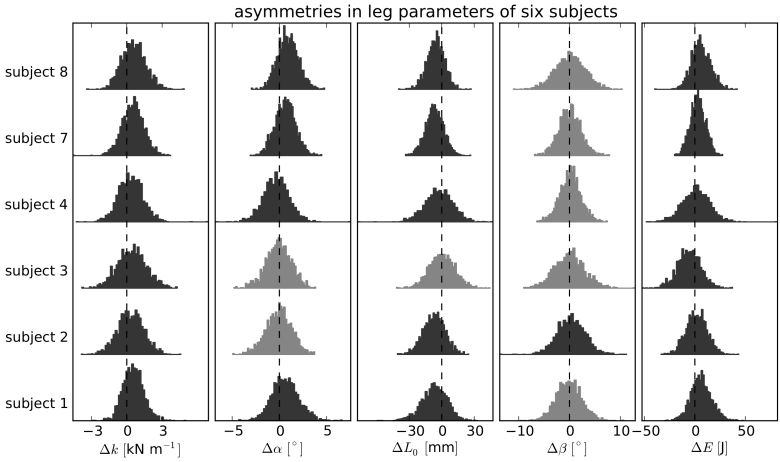

Figure 4.12:
The distribution of differences of leg parameters between left and right leg in consecutive steps is displayed for six subjects. Asymmetry was investigated using a t-test with $p < 10^{-4}$. Dark histograms indicate significant asymmetry.

by intentional maneuvering instead of step to step control, which would result in (potentially incomplete) separation of the dynamics in sagittal and lateral motion.

To test this hypothesis on the level of SLIP, we compute the correlation of the control output that mainly affects the lateral dimension, namely β, with all other control outputs. Results are displayed in Fig. 4.13, indicating that the control output for β is largely independent of the other control outputs. We can interpret this as evidence for a separation of lateral control from control in the sagittal plane.

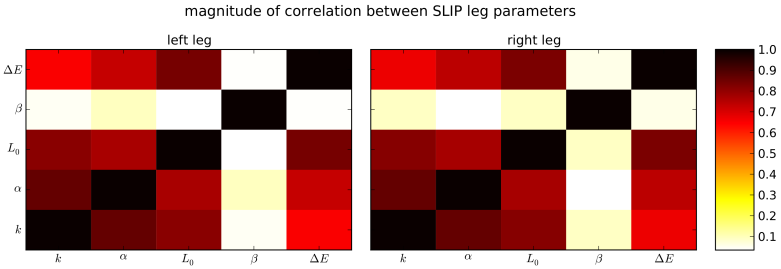

Figure 4.13:
The magnitude of the correlation between the SLIP parameters, averaged over 6 subjects. The lateral angle of attack β has very low correlation with every other parameter.

Identification of control input

In many investigations of the SLIP model, the SLIP parameters are assumed to be constant. In other cases, control schemes are investigated that take only SLIP state and parameters as input (for example in Blum et al. (2010); Carver et al. (2009)), yielding an autonomous system with a possibly extended state vector. Here, we investigate whether this is also the case in humans, that is, if the leg parameters are adjusted taking only SLIP-related information into account.

One approach to answer this question is predicting the SLIP parameters of a step with different inputs, with SLIP-based information or full-state information. The data for prediction must be available at the apex before that step.

The first candidate is an 8 dimensional augmented SLIP state from the SLIP state $[y, \dot{x}, \dot{z}]$ and the 5 SLIP parameters from the previous step. We will call this the 'augmented SLIP'. As second candidate, we take the full phase space data at apex as predictor. Finally, we perform an analysis like that described in section 2.1.3 to extract the main factors from kinematic data, approximate the

identified factors with original state space coordinates, and predict the SLIP parameters using a highly reduced state space (here: 7 dimensional). Anticipating the results from this analysis, we will call this the 'CoM + ankle SLIP'.

The results of the analysis described in section 2.1.3 are displayed in Fig. 4.14. Here, the lateral angle of attack β has been excluded from the analysis because of the independence of β from the other 4 SLIP parameters. Fig. 4.14 suggests that we take the CoM height and the ankle positions and velocities in running direction into account (note the different coordinate systems of SLIP and measured data, which were both selected according to standards in the respective literature). Taking additionally the remainder of the SLIP apex state, namely the CoM velocity in lateral and anterior direction, yields our 7-dimensional, reduced predictor. Because we are mainly interested in the sagittal plane dynamics, we chose not to take any more information than the lateral CoM velocity into account for predicting the lateral angle of attack.

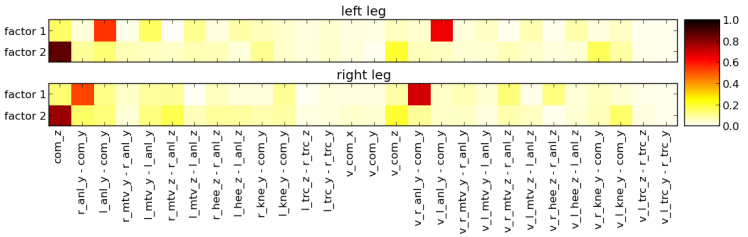

Figure 4.14:
The magnitude of the two main factors required to predict the 2D SLIP parameters (that is, without β), averaged over 6 subjects. Labels are explained in Fig. 2.18. A leading v_ denotes the derivative of the corresponding coordinate.

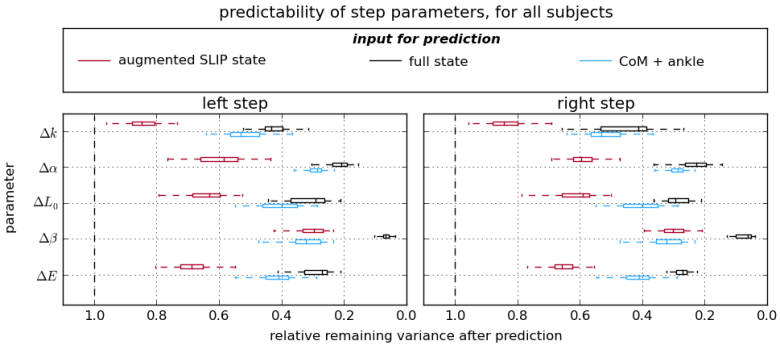

Figure 4.15:
Comparison of the predictability of the SLIP parameters using either SLIP-related data or kinematic data at the apex prior to touchdown for prediction. The achievable variance reduction is best using the full kinematic state. Taking only seven selected dimensions which have been identified before into account ("CoM + ankle"), close to optimal variance reduction can be achieved. Although the augmented SLIP state has one more dimension than the "CoM + ankle" selection, it contains less information about the SLIP leg parameter in next stance.

The predictability of the SLIP parameters from the selected inputs is given in Fig. 4.15. Clearly, the SLIP related parameters fail to predict a comparatively large fraction of what could be predicted using information from the full state. As expected, using the state of 'CoM + ankle SLIP' for prediction performs well for sagittal plane motion, and performs comparable to the 'augmented SLIP' input for the lateral angle of attack. Still, a remarkable fraction of the variance of the SLIP parameters can be computed from the 'augmented SLIP' state. That is, when we restrict ourselves to the 'augmented SLIP' state as input instead of the full state or 'CoM + ankle SLIP', we can approximate the experimentally observed control output,

although with less accuracy than we could achieve using the full state. However, using this 'augmented SLIP' approximation of the gait controller yields an autonomous closed-loop system, for which we can then analyze the stability. We perform a stability analysis of 'augmented SLIP' in section 'Stabilization by Control'.

Autonomy of the 'CoM + ankle SLIP'

We found in the previous section that knowing the state of the CoM and the ankles, including the corresponding velocities, allows comparatively good prediction of the SLIP parameters during next stance. This raises the question whether this leads to an autonomous system, that is, whether 'CoM + ankle SLIP' can be regarded as autonomous (and possibly serve as new template). Here, we investigate this question by predicting these parameters, once using only these parameters at the previous apex, and once using the full state at the previous apex. If differences are small, this indicates that the information required to predict the motion is mostly included in the 'CoM + ankle SLIP' itself. The results of predicting the 'CoM + ankle SLIP' states are given in Fig. 4.16.

The results in,4.16 show that the state of 'CoM + ankle SLIP' can be predicted using information from only that system almost as well as using information from the full state. Only small differences remain. This suggests that 'CoM + ankle SLIP' is a good starting point for deriving a new template model.

Stabilization by Control

The reduced system's state at the apex is $x_n = [y, \dot{x}, \dot{z}]^T$. The SLIP dynamics f map the state to the next state, using a set of parameters p: $x_{n+1} = f(x_n, p_n)$.

In section 4.4.3, we found that the controller output can be (partially) described using the current apex state x_n and the SLIP pa-

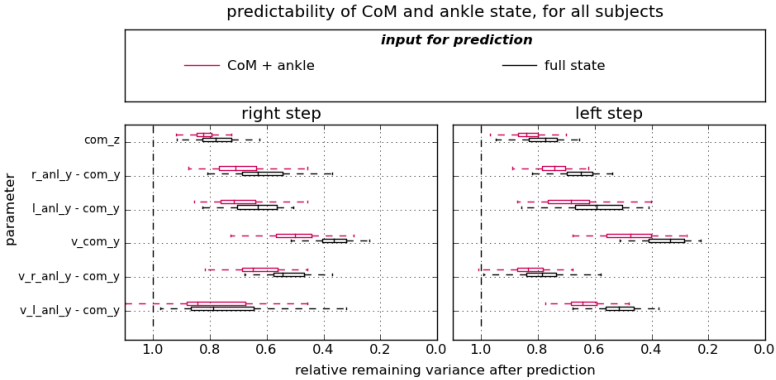

Figure 4.16:
Prediction of 'CoM + ankle SLIP' states using the full state or the 'CoM + ankle SLIP' at the previous apex as input. The prediction quality is computed for 6 subjects. Both inputs, the full state and the 'CoM + ankle SLIP' state perform similar.

rameters from the previous step p_{n-1}, yielding the augmented system state

$$\tilde{x}_n = \begin{bmatrix} x_n \\ p_{n-1} \end{bmatrix} \tag{4.6}$$

and the corresponding discrete time evolution function F:

$$\tilde{x}_{n+1} = F(\tilde{x}_n) = \begin{bmatrix} f(k(\tilde{x}_n), g(\tilde{x}_n)) \\ g(\tilde{x}_n) \end{bmatrix}, \tag{4.7}$$

where $k(\tilde{x}_n) = x_n$ extracts the current state from the augmented state, and $g(\tilde{x}_n)$ defines how the SLIP parameters are set (that is, $g(\tilde{x}_n)$ is the controller we are interested in).

The stability of a given periodic solution can be computed from the eigenvalues of a linearization of the stride map $S = F_r \circ F_l$, where the subscripts r, l indicate a right or left step, respectively.

The linearization $DS = DF_r \cdot DF_l$ can be computed from the linearized step maps F:

$$\frac{\mathrm{d}F}{\mathrm{d}\tilde{x}_n} = \underbrace{\frac{\partial F}{\partial k}\frac{\mathrm{d}k}{\mathrm{d}\tilde{x}_n}}_{\delta x} + \underbrace{\frac{\partial F}{\partial g}\frac{\mathrm{d}g}{\mathrm{d}\tilde{x}_n}}_{\delta g} = \begin{bmatrix} \frac{\partial f}{\partial k} \\ 0 \end{bmatrix} [\mathbb{1}|0] + \begin{bmatrix} \frac{\partial f}{\partial g} \\ \mathbb{1} \end{bmatrix} \underbrace{\begin{bmatrix} \frac{\mathrm{d}g}{\mathrm{d}\tilde{x}_n} \end{bmatrix}}_{A} \tag{4.8}$$

The complete linearized step map now reads

$$DS = \delta x_r \delta x_l + \delta x_r \delta g_l + \delta g_r \delta x_l + \delta g_r \delta g_l, \tag{4.9}$$

with subscripts r, l denoting the right and left step, respectively. Here, the term $\delta x_r \delta x_l$ represents the linearized model without feedback control. The matrix $A := \frac{\partial g}{\partial \tilde{x}_n}$ which represents the linear approximation of the gait controller of this autonomous system is obtained by regression from the experimentally observed sequence of augmented states.

In order to interpret the eigenvalues as statements of the stability of the system, we must evaluate the linearization at a periodic solution whose stability we then can assess. We obtain the reference solution by searching for initial conditions that are mapped to themselves by the SLIP model, when we use the average experimentally observed SLIP parameters in a left and a subsequent right step. For all subjects, we compute an individual periodic reference solution. As a consistency check, we verify that the initial conditions of the computed reference solution are within one standard deviation of the average apex state.

Having found the corresponding periodic reference solution, we evaluate the model sensitivities $\frac{\partial f}{\partial k}$ and $\frac{\partial f}{\partial p}$ numerically at these reference points. From these sensitivities, we compute the complete linearization according to Eq. 4.9.

We analyze the effect of the controller A on stability by computing the eigenvalues of DS with and without control. The results in Fig. 4.17 show that the experimentally observed controller is able

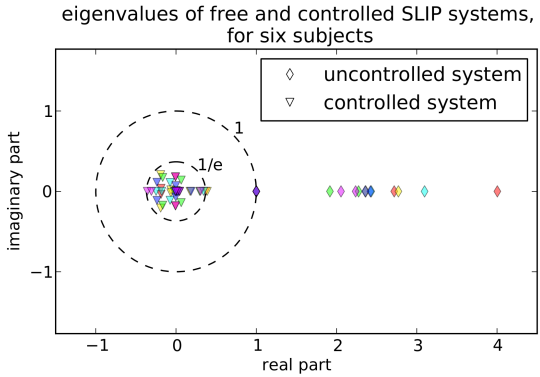

Figure 4.17:
Eigenvalues of the SLIP system with and without feedback are given for six subjects. Each subject is has a different color, consistent for both systems (controlled and uncontrolled). In the uncontrolled system, all eigenvalues in the observed situation are ≥ 1, with exactly one eigenvalue at 1 corresponding to the existence of periodic solutions for every energy within a certain range.
Adding control to the system, stability is achieved. Note that the augmented system state has 8 instead of 3 dimensions.

to shift the eigenvalues of the previously unstable system clearly inside the unit circle, thus rendering the system stable. The obtained eigenvalues are within the range of the observed Floquet multipliers in section 4.3 (Fig. 4.8).

Comparison with direct prediction

As humans are free to deviate from the SLIP model (even in a systematic manner), some information might be lost when we implicitly constrain the CoM dynamics to those of the model. To estimate this potential loss of information, we predict the apex state after

one step in two ways: Once using the augmented system state $\tilde{x}_n$ as input for the controller and simulating the SLIP model with the parameters set by the controller, and once using $\tilde{x}_n$ directly for prediction.

The results are computed for four subjects and are presented for one subject in Fig. 4.18. The possible variance reduction is very similar in both approaches. However, the predictions themselves are only similar for large magnitudes. For small magnitudes, the predictions obtained from these approaches are clearly much less correlated. This qualitative result is valid for all subjects and shows that the behavior of the controlled SLIP is similar to the behavior of the human runner, indicating that the observed maps contain information of how the subject copes with disturbances. However, we must also keep in mind that in this investigation only an incomplete input for the SLIP was used (see Fig. 4.15).

Laterality and inter-subject similarity

To investigate similarities and differences between subjects we must normalize the SLIP parameters. Here, we follow the approach of Blickhan and Full (1993), and normalize spring stiffness to $m\,g L_0^{-1}$ (m: subject's mass) and leg length to the mean initial leg length. After normalizing each subject's data, we rescale every dimension with a certain factor (that is the same for all subjects) such that the variance in each dimension is approximately equal (in all subjects).

We analyze left-right asymmetry of control and inter-subject differences by comparing the similarity of the control outputs (that is, the similarity of predicted SLIP parameters). For this, we compute the control outputs twice, once by an out-of-sample prediction using maps obtained from the same context (same subject or same leg), and once by a prediction using maps obtained from a different context. Because of the independence of β from other parameters (see Fig. 4.13) we remove it for this analysis.

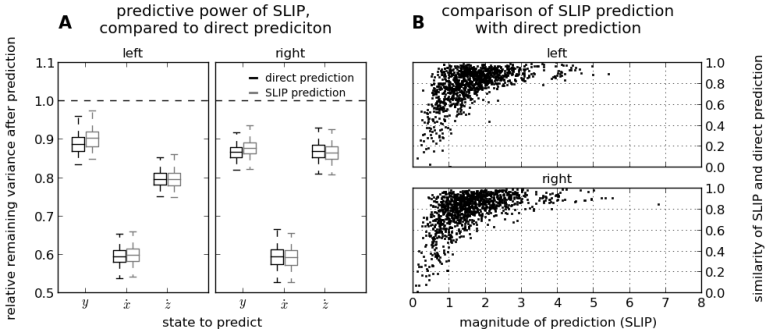

Figure 4.18:
Predictability of the adaptation of next apex state using direct prediction or SLIP based prediction. Results are given for one representative subject (3). (**A**) Direct prediction yields similar variance reduction compared to SLIP based prediction. (**B**) 'Similarity' of predictions for 1190 randomly selected steps is computed for each prediction as $1-|x_{\mathrm{SLIP}}-x_{\mathrm{direct}}|(|x_{\mathrm{SLIP}}|^2+|x_{\mathrm{direct}}|^2)^{-1/2}$, with x_{SLIP}, x_{direct} denoting the SLIP based and direct prediction, respectively. The mean values of x_{SLIP} and x_{direct} have been subtracted, and physical dimensions were selected such that the standard deviation of predicted positions and velocities is 1. A similarity value of 1 indicates the same prediction. For large predictions we find high similarity values. For visual interpretation of similarity values, see Fig. 4.19 (**C**).

When we transfer a specific bootstrapped set of maps into another context (that is, another subject or the opposite leg), we use only its element-wise average. To compare the predictions and compute their similarity, we have to compute the same prediction for one specific input twice, once using the corresponding in-context map, and once using the transferred out-of-context map. We compute the similarity for all predictions, and average over all predictions and all bootstrap repetitions. The results are presented in Fig. 4.19.

Individual differences and differences between left and right leg are clearly visible. Also, the amount of asymmetry in control output depends on the subject. However, the values of similarity are $\gtrsim .4$ and often even $\approx .7$, indicating that control action is not completely different (see Fig. 4.19**C**). This indicates that subjects might have some commonalities in control.

4.4.4 Conclusion

In this section, we have seen how we can analyze human running and control therein using templates. This allows new insights into the organization of human locomotor control on a specific level of abstraction. We further found that the autonomous model is insufficient to fully capture the control output from human runners. However, applying this partial representation of the controller in simulation renders the previously unstable system stable. This highlights that the variability of the leg parameters is neither random nor destabilizing the system, but can be interpreted to a large part as control action.

We also found that the lateral control β appears to be independent of the remaining control action, and that it could be well predicted when the lateral CoM velocity is present in the predictor. This is in line with findings of Hof et al. (2005), who proposed that in order to achieve lateral stability it is sufficient to place the leg at some region ("XCoM") which predominantly depends on the lateral velocity.

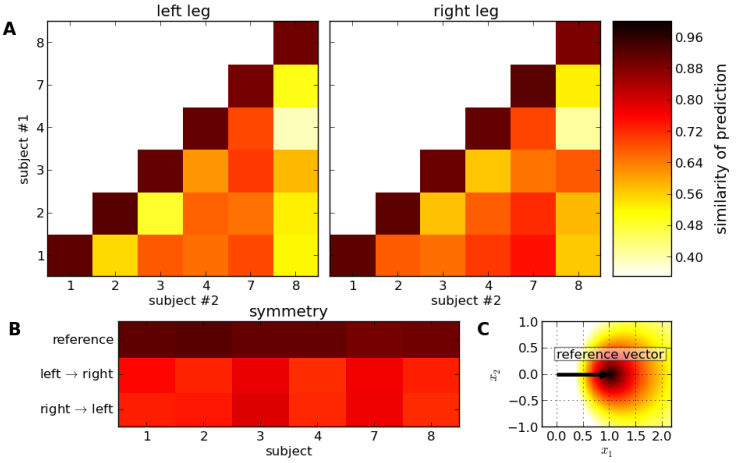

Figure 4.19:
Average similarity of normalized autonomous SLIP controller output (excluding β) in cross-subject or cross-legs prediction. Similarity of two vectors y_1, y_2 is defined as $1 - |y_1 - y_2|(|y_1|^2 + |y_2|^2)^{-1/2}$. (A) Inter-subject comparison for predicting the leg parameters. Differences between subjects are clearly visible. (B) Symmetry of control in each subject. Asymmetry of control is present for all subjects, but less pronounced in subjects 3 and 7. (C) Reference values for "similarity". Color encodes the similarity of the vector $[x_1, x_2]$ to the vector $[1, 0]$.
(Similarity on the diagonal in (A) and upper row in (B) is not exactly 1 because the individual maps deviate from the averaged map.)

Instead of using the full state for optimal prediction, we could identify reduced control input for the sagittal plane SLIP parameters (that is, without β). Close to optimal prediction of SLIP parameters

can be achieved using information of the ankle positions and velocities at apex and the CoM itself. Although we can predict the leg parameters in subsequent stance quite well from these values, they are not necessarily a control input for a nervous system controller. They could instead be the result of an already determined control action.

It is also likely that the true human gait controller has a completely different structure than our identified controller. Here, we assumed that the controller gets information at the apex and adapts the leg parameters accordingly. Let's assume that the controller would act far before apex, and its actions generally would largely affect the ankle joint position and velocity. Then, the ankle joint would contain the information of the actual control output. Our "controller" would then just be a mapping from the true output, measured at the apex, to its effect in the subsequent stance. However, this would not render the identified controller useless: One might think of an adjustable prosthesis, whose parameters are set by some controller. If we could set the prosthesis' parameters in a SLIP-like way, that is, adjust its stiffness, energy input and potentially even modify the angle of attack, we could use the identified "controller" to adjust the technical device in a way similar to how a human would do.

The identified partial closed-loop controller leads to a closed-loop system with eigenvalues less than $1/e(\approx .3)$ for all six investigated subjects, corresponding to a decay time of disturbances of no more than a single gait cycle. This is in line with results from the linear gait analysis of the full state in section 4.3. Although no deadbeat control is present (which would anyway be hardly possible to detect with this linear approach), disturbances decay to $< 1/e$ within two steps. This is also in comparatively good agreement with the predictions of Carver et al. (2009).

4.5 Summary

In this chapter, we could identify some structure in the variability of human running, by different means and with different meanings.

Generally, fractal structures are very hard to identify in the presence of noise. As our analysis in section 4.2 of the spatial distribution of the residuals did not find traces of a fractal-like structure, we did not further pursue this "chaotic systems" approach. Instead, the spatial distribution indicated that the dynamics are probably noise-induced around an asymptotically stable, time-varying limit cycle. In section 4.3, we fitted a Floquet model to the dynamics around a limit cycle, which indicated that disturbances typically decay within one stride. Due to the low magnitude and phase dependence of the eigenvalues, the Floquet structure (that is, loosely speaking, how eigenvectors of the system at a given phase evolve with time) is not clearly present, and we did not try to extract it. Instead, we pursued another approach to characterize the human disturbance rejection mechanism in section 4.4: We reduced the dynamics to the CoM motion, which we then further analyzed using the SLIP template. Using this approach, we could find a linear approximation of the human gait controller on that level of abstraction. We saw that the SLIP system is not autonomous but takes non-SLIP related input into account. However, even when the SLIP input is reduced to achieve an autonomous closed-loop system, this part of the controller achieves high stability.

We further found that SLIP could be extended by adding information about the ankles positions and velocities, without loosing much information of the full state for predicting SLIP parameters for next stance. This suggests that adding ankles is a good starting point for creating a new, improved template for human running.

The physiological realization of control was not investigated, and it is not clear that the identified control output is achieved by neural actions. For example, a stabilizing change of angle of attack α_{TD} as function of apex height y could be achieved by leg retraction in

flight, without any additional nervous control action at all (Seyfarth et al., 2003).

We could find individual differences not only in gait but also in control action, and left-right symmetry was violated both in motion and control. This is in line with literature and the notion of a dominant leg (Sadeghi et al., 2000). Our results show that, despite of temptation, great care must be taken when averaging data over subjects, over time (without appropriate account for the drift), or over left and right steps.

5

General discussion

Only he is free who cultivates his own thoughts, and strives without fear to do justice to them.

Berthold Auerbach (1812 - 1882)

5.1 Summary: viewing the whole picture

The topic of this thesis is an analysis of human locomotion. Here, instead of a merely descriptive approach I tried to work out *how* human locomotion can be understood. Besides other analyses, the main tool to achieve that goal was the notion of templates (Full and Koditschek, 1999), which allow an intuitive grasp of what is happening. The dynamics of templates can be understood, and one might regard this as partial understanding of the dynamics of the original system, which is human locomotion. Of course, such an approach can only explain parts of what is truely happening and thus will always be incomplete.

In order to explain the dynamics of the center of mass CoM, the motion of the CoM has to be measured precisely. In practice, this is difficult because both kinematic estimates and estimates based on the ground reaction forces induce systematic errors, however of a different kind. These difficulties were mostly resolved by a new algorithm to combine the best of both estimates, which is presented in section 2.2. It is based on the assumption that errors in the kinematic estimate mainly affect frequencies higher than the dominant frequency of the motion, whereas errors in the force measurement mainly effect low frequencies. When only the “good” parts of the signals, which can be separated in the frequency domain, are combined, an improved estimate can be obtained. This algorithm was verified on simulation data and is a fundamental requirement for the template based gait analysis we used.

In many biomechanical studies, the spring-loaded inverted pendulum (SLIP, Blickhan (1989); McMahon and Cheng (1990)) is used to approximate the dynamics of human running. Recently, Geyer et al. (2006) demonstrated that this model is also capable of creating a walking gait. Some extensions of the SLIP model have been proposed (e.g. Seipel and Holmes, 2007; Maykranz et al., 2009) but so far, the main point of interest has been the CoM dynamics, neglecting the extended trunk and the problem of regulat-

ing the angular momentum. To approach this topic, a novel template, namely the virtual pendulum, is introduced in section 3.3. The virtual pendulum can explain the postural stabilization of a SLIP that is loaded with a rigid body on top (the VPP model) by a feature that is experimentally observed in human walking, namely an intersection point of the ground reaction forces above the CoM which can be regarded as virtual pivot point of a virtual pendulum. Because of the similarity of experimentally observed and simulated ground reaction forces, this approach is suitable to approach the problem of postural stabilization in human walking, just as a SLIP is suited to explain the CoM dynamics.

So far, only templates that create a gait similar to typical human locomotion had been introduced. The relevance of these templates, that is to what extend they can capture features of human gait besides a certain similarity, has not been addressed sufficiently. In section 4.4, this relevance is demonstrated by presenting a novel template-based gait analysis.

However, before we could perform the template-based gait analysis, we had to investigate basic characteristics of the dynamics of human running, that is, whether we observe a stable limit cycle or possibly a strange attractor, and what stability we can expect. These analyses were performed in sections 4.2 and 4.3. It turned out that noise-driven dynamics around a stable limit cycle are a reasonable description, and that the eigenvalues of the computed return maps are quite low, indicating high stability of the gait (which is what we would expect because human running on a treadmill is apparently not a very fragile motion). Further, we saw a slow drift of the gait cycle, which indicates that despite of stationary conditions, human running is not necessarily stationary. This is also not surprising because it reflects the adaptability of the human locomotor system, but this finding has to be taken into account when computing average values or residuals.

In section 4.4, after all this preparation, the template-based gait analysis is finally presented. For this, not only the mean gait pattern,

expressed as periodic solution corresponding to the mean (template-based) gait parameters, is computed, but also the linear return map that tells us how parameters are adapted when a certain deviation from the limit cycle occurs. Because these adaptations capture (at least parts of) the reactions to disturbances, they are of vital importance when stability is analyzed. When the experimentally observed adaptations are not taken into account in simulation, the (uncontrolled) SLIP might be stable or unstable, however its reaction to disturbances will not represent the reactions of the human, and thus its (in)stability will have no relevance for the human gait.

We also identified the variables that determine the parameter adaptation of the subsequent stance. Because there are factors that cannot be expressed in the SLIP model, we must conclude that the SLIP model cannot be regarded as an autonomous, independent subsystem which describes the CoM dynamics. However, in our case, taking only that information which is available to the SLIP into account yields a controller that renders the system stable, with eigenvalues comparable to the eigenvalues of a full state return map. Following the templates and anchors approach of Full and Koditschek (1999), the next step would be to identify an extended model which also describes human running well but yields nearly autonomous dynamics when applied to humans (in the way described in section 4.4).

We must admit that results from our SLIP-based gait analysis only reflect parts of the true system, and quantitative assessments like eigenvalues cannot be considered as precise. Still, as some part of the human's disturbance rejection mechanism (that is, the leg parameter adaptation), is captured, the enhanced model is a valuable step towards a deeper understanding of human locomotion.

5.2 Templates for understanding human locomotion?

What is the benefit of using templates for describing human locomotion? Why using explicit mechanical models instead of, for example, cubic spline approximations to the dynamics? The most important point of using templates is to get a model whose behavior can be analyzed mathematically and that can be understood. In a subsequent step, this understanding on a mechanical level then paves the way for a transfer of human-like mechanism into technical devices like robots (e.g. Radkhah et al., 2011; Poulakakis and Grizzle, 2007).

Using templates reduces the description of the motion to a small set of parameters and initial conditions. These parameters can then be used for further investigation, as in the present thesis, or serve as reference for technical models. Here, we found almost along the way that lateral motion is approximately independend from sagittal plane motion, a result that is also in line with previous findings of Hof et al. (2005) and gives a justification for sagittal plane analyses. It might have been possible to find this result without templates, but in the simple world of the SLIP template, it was straight-forward to obtain.

Despite - or because of their simplicity, templates can be used to analyze the contribution of selected features to the gait. For example, Maykranz et al. (2009) investigated the effect of adding a foot to the leg, finding that just its presence can account for landing-takeoff asymmetry that is observed in human running but not reproduced in one-step periodic solutions of the SLIP. Merker et al. (2011) investigated whether asymmetry is generally a bad feature (as one might intuitively assume) and showed that this is not the case, but that in fact a small asymmetry can enhance stability and robustness of the gait. Seyfarth et al. (2003) demonstrated that the experimentally observed swing-leg retraction shortly before touchdown can dramatically increase gait stability. Although these studies are valid in a strict sense only for the investigated model, it is

likely that their findings also apply to some extent to human running.

Yet this kind of question is not the only possible question to be addressed using templates. One might for example ask: Using SLIP-like running dynamics, is there a lower bound in disturbance rejection time? Or could, given an infinite-gain control, any disturbance be rejected within any time span? This question was analyzed by Carver et al. (2009), who showed that depending on the kind of control target, at least one or two steps are required to fully reject disturbances of the CoM motion. The authors then argued that this was due to the underactuation at the ground contact, a constraint which is also present in humans. Thus, their results can almost completely be transferred to human running. Here, in sections 4.3 and 4.4.3, we found results that are in good agreement with these predictions, although not completely confirming their very specific hypothesis of a two-step deadbeat control.

And there is yet another possible use of templates: as shown in section 3.3, the postural stabilization of human walking comes almost at no cost, eventually as a by-product of leg placement. This simple realization lets us conclude that the evolution of an upright gait did probably not invoke the solution of a difficult stabilization problem. Here, a template helped to gain insight into the evolution of humans.

A crucial point when analyzing an analogy instead of the original is to require similarity in the behavior (Kalveram and Seyfarth, 2009). Similarity is required in the features that are being analyzed. For example, the argument of Carver et al. (2009) is based on the underactuation at the ground contact. Here, similarity with humans is given, which enables the transfer of the conclusion to humans. However, when stability is addressed, we have to precisely distinguish between what mechanisms might exist and what mechanisms are actually applied. We found in section 4.4 that there is some adaptation of the leg parameters which can be regarded as control action. This existing adaptation scheme has then to be

taken into account when using templates to analyze the stability of human gait.

Using the experimentally identified controller in simulation, it is in principle possible to infer the individual disturbance rejection mechanism and the stability of the gait of a subject. A key requirement for analyzing stability of a system is that this system is autonomous, that is that there are no external inputs. If there were, we are not able to say what's going to happen because we do not know these inputs. In section 4.4, we found that an autonomous SLIP cannot represent all leg adaptations of a human runner. Consequently, the SLIP equipped with the controller cannot be used to (fully) assess the stability of an individual human runner. This does not imply that templates are inadequate here, it just means that following the templates and anchors approach, an extended template that is able to capture humans' reactions to a larger extent is required. Our findings suggest that such an extended gait model should include the ankle joints.

Summarizing, templates are well suited to enhance the understanding of human locomotion. Care has to be taken that findings in template analyses do really apply to human locomotion.

5.3 Physiological aspects of templates and control

The SLIP template is based on the assumption of elastic legs. Elasticity of legs has been found in animals (Alexander and Bennet-Clark, 1977; Alexander, 1988) and humans (Witte et al., 1997). But this does not necessarily imply that humans have a linear spring in mind when running. Geyer et al. (2003) showed that a simple muscle-reflex model that incorporates a physiological muscle model equipped with a modified stretch-reflex behaves very similar to a linear spring in steady state running and hopping. Not only the elastic properties of a muscle-tendon complex but also reflexes are

physiologically important parts of locomotion. But how do they fit to the notion of templates?

Several modeling studies have demonstrated that reflexes, in combination with a neuronal oscillator, can produce a remarkably stable gait (e.g. Taga, 1994; Yakovenko et al., 2004), with an emphasis that reflexes may play a crucial role in gait pattern generation and adaptation. Geyer and Herr (2010) even proposed a model of human walking that relies on reflexes and does not include a central pattern generator. This model shows good agreement with experimental data, highlighting the potential importance of reflexes once more. This is also in line with findings of Ivanenko et al. (2002), who demonstrated the importance of a mechanical feedback for gait pattern creation in a simulated reduced gravity experiment. The latter two studies suggest that a large part of the gait pattern generation in humans might stem from an oscillating system that involves reflexes as well as mechanical feedback from foot- floor interactions. It should be noted that reflexes are not fixed but versatile: Several studies have found changes in reflex strengths in different tasks like walking, running, standing or sitting (Duysens et al., 1993; Dietz et al., 2001). This indicates that humans might switch on a set of reflexes to create a beneficial basic gait pattern.

Reflexes come with an inherent coupling of sensory feedback with muscle activation. It is not surprising that they could also account for stiffness adaptation. For example, when the runner is too high at the apex, the resulting higher landing velocity might lead to larger and faster leg compression which in turn could evoke larger muscle activation, leading to a higher leg stiffness in the language of the SLIP. Thus, instead of sensing the body's height at apex and adjusting the leg correspondingly, this could be facilitated by reflexes. Reflexes could also facilitate the realization of a VPP in walking, especially in larger disturbances: imagine when the trunk is moving too fast forward, a stretch reflex in the hip extensors would lead to the result that we expect from the VPP scheme. Summarizing, the properties of muscle-tendon-reflex systems can be the biological re-

alization of what we describe with templates, including parts of the corresponding control scheme.

Relying on the favorable properties of the template's dynamics – which might be realized by nature in different ways – might also reduce supraspinal control effort – for example, there is no need to compute a target trajectory. Mergner (2010) found that in human stance control "behavioral flexibility and fault tolerance goes together with computational parsimony, an equally important biological constraint". Bauby and Kuo (2000) also suggested that "humans may harness passive dynamic properties of the limbs in the sagittal plane, but must provide significant active control in order to stabilize lateral motion". The latter is in line with our finding of independence of lateral control from sagittal-plane control in section 4.4. In line with this is a finding (however in balancing tasks) from Cabrera and Milton (2004). They demonstrated that latency increases with skill level, supposing that neural control involves longer intervals of prediction-free control which are interrupted by consciously generated movements. All these results suggest that humans may indeed take advantage of the benefits of a basic gait pattern, that can be described in the language of templates. Potential benefits of such a basic gait pattern have been widely analyzed (e.g. Seyfarth et al., 2002; Geyer et al., 2006; Rummel et al., 2010).

We see that there is no need for an exact realization of a template in biological systems, but there are mechanisms that lead to the template's behavior. Further, we must keep in mind that the parameter adaptation scheme (section 4.4) is not necessarily a representation of higher level control, but could also instead capture leg adaptations that are due to intrinsic physiological properties like reflexes. But although we might not yet fully understand the relation between the template and its anchor (the biological system), analyzing properties of the (possibly new or extended) template sheds light on nature's highly flexible, adaptive and computationally parsimonious solution to the challenge of legged locomotion, a challenge that is still not mastered by artificial systems.

5.4 Possible applications in machines

Before the Olympic Games 2008, there was a long debate whether or not Oscar Pistorius, also known as the “Blade runner”, should be allowed to compete. This topic was subject to controversial scientific discussion (e.g. Lechler and Lilja, 2008; Potthast and Brueggemann, 2010). The curious question was whether a “disabled” athlete, namely Oscar Pistorius, has an unfair advantage by using prostheses instead of legs.

The prostheses he used are passive devices of carbon fibers. But prostheses are not limited to passive devices. There are some active devices available, and several research projects aim at building a powered prosthesis that should mimic the features of the lost limb (e.g. Eilenberg et al., 2010; Hitt et al., 2010; Grimmer and Seyfarth, 2011). In these devices, a central question is how to adapt the devices to the specific situation. Several approaches have been proposed in these projects. As most of these devices contain adjustable elastic elements and the possibility to inject or remove energy, a SLIP-like description of the control input stands to reason. Using that framework, human- like step to step adaptations of leg parameters could in principle be estimated following the approach from section 4.4. Further, additionally the VPP constraint on the desired ground reaction forces could also yield a control target for active prostheses or orthoses.

Not only prostheses might benefit from transferring the human leg parameter adaptation scheme into technical devices. There is also the field of bipedal robots, where implementing elastic legs is meanwhile as common as having rigid legs. Examples of elastically operating robots are Thumper (Poulakakis and Grizzle, 2007), Mabel (Grizzle et al., 2009), ATRIAS (Grimes and Hurst, 2012 (accepted)) and BioBiped1 (Radkhah et al., 2011). In the BioBiped project, a SLIP-like behavior is aimed at. Here, both the human leg adaptation scheme and the VPP could be transferred to that robot.

5.5 Possible applications in gait analysis

Several new potential measures can be derived from the present work to characterize gait and compare gaits between subjects. As a matter of fact, templates allow rescaling and thus a comparison of gaits under different subjects, even under different species (Blickhan and Full, 1993). This renders template-related quantities for describing and comparing gaits highly informative.

What are these new potential measures? In section 3.3, the VPP was introduced, and a method how to calculate it from individual experimental steps is presented. Its location, the step to step variability of its location and the "precision", that is the residual sum of squares of external torque, are potential measures for quantifying postural stability in walking. However, it must be noted that so far, no investigation exists on whether or not these measures are meaningful in a clinical context. Further, a VPP location can only be found in walking but not in running.

The other potential new measure is the SLIP parameter adaptation scheme. As it is possible to normalize gait and SLIP parameters, individual adaptation schemes can be compared. Also, stability can partially be inferred when using the closed-loop system proposed in section 4.4.3. However, in this case also the clinical relevance is an open question, and generally persons with an increased risk of falling might typically be unable to run at all.

Another important finding for gait analysis was the individuality of symmetry and control. It implies that averaging over subjects and over left and right legs must be done with great care, as it might yield artifacts depending on the scientific question. Further, a slow drift of the gait pattern was found, and had to be removed prior to further analyses. After a short break, a discontinuity in the dynamics exists (cf. Fig. 4.1), indicating that data from one long trial cannot be compared directly with data from many short trials.

Summarizing, the presented work contains potential new ways to describe and quantify human gait, but their clinical relevance

has to be evaluated. However, from a research point of view, applying these measures might be very interesting, as they allow the reduction of several aspects of human gait to a small number of parameters without loosing too much information.

5.6 Résumé

It is an ambitious goal to understand human locomotion in full detail. Here, I presented an approach that is based on minimalistic template models. Although the biological realization of what is analyzed with templates may be quite different, they can be used to describe the resulting motion. In this work, the main contributions for template-based gait analysis are the presentation of a novel template to explain postural stability (the VPP) and a method to adapt the existing SLIP template to match not only the average human motion but also to capture the reactions to disturbances with this model. Much work is left, and even new questions and challenges came up during this work. However, we did achieve substantial progress on the long road towards understanding human locomotion.

BIBLIOGRAPHY

R.M. Alexander. Mechanics of bipedal locomotion. *Perspectives in experimental biology*, 1:493–504, 1976.

R.M. Alexander. Walking and running: Legs and leg movements are subtly adapted to minimize the energy costs of locomotion. *American Scientist*, 72(4):pp. 348–354, 1984. ISSN 00030996. URL `http://www.jstor.org/stable/27852758`.

R.M. Alexander. *Elastic mechanisms in animal movement*. Cambridge University Press Cambridge, 1988.

R.M. Alexander. Energy-saving mechanisms in walking and running. *Journal of experimental biology*, 160(1):55–69, 1991.

R.M. Alexander and H.C. Bennet-Clark. Storage of elastic strain energy in muscle and other tissues. *Nature*, 265(5590):114–117, Jan 1977.

E. Andrada. *A New Model Of The Human Trunk Mechanics In Walking*. PhD thesis, Ilmenau, Univ.-Verl., 2008.

Y. Ashkenazy, J.M. Hausdorff, C.P. Ivanov, and H.E. Stanley. A stochastic model of human gait dynamics. *Physica A: Statistical Mechanics and its Applications*, 316(1-4):662–670, 2002.

ASIMO, 20.11.2011. URL http://asimo.honda.com/downloads/pdf/asimo-technical-information.pdf.

A. Astolfi and R. Ortega. Immersion and invariance: a new tool for stabilization and adaptive control of nonlinear systems. *IEEE Transactions on Automatic Control*, 48(4):590–606, 2003. doi: 10.1109/TAC.2003.809820.

A.F. Bastani and S.M. Hosseini. A new adaptive runge-kutta method for stochastic differential equations. *Journal of computational and applied mathematics*, 206(2):631–644, 2007.

C.E. Bauby and A.D. Kuo. Active control of lateral balance in human walking. *Journal of biomechanics*, 33(11):1433–1440, 2000.

P. Bhounsule and A. Ruina. Cornell ranger: energy-optimal control. In *Dynamic Walking*, 2009.

R. Blickhan. The spring-mass model for running and hopping. *J Biomech*, 22(11-12):1217–1227, 1989.

R. Blickhan and R.J. Full. Similarity in multilegged locomotion: Bouncing like a monopode. *Journal of Comparative Physiology A: Neuroethology, Sensory, Neural, and Behavioral Physiology*, 173 (5):509–517, 1993.

Y. Blum, S.W. Lipfert, J. Rummel, and A. Seyfarth. Swing leg control in human running. *Bioinspir Biomim*, 5(2):026006, Jun 2010. doi: 10.1088/1748-3182/5/2/026006. URL http://dx.doi.org/10.1088/1748-3182/5/2/026006.

C.W. Braune and O. Fischer. Der Gang des Menschen Theil 3: Betrachtungen über die weiteren Ziele der Untersuchung und Überblick über die Bewegungen der unteren Extremitäten. In *Abhandlungen der Mathematisch-Physischen Classe der Königlich Sächsischen Gesellschaft der Wissenschaften*, pages 87–170, 1900.

S.M. Bruijn, D.J.J. Bregman, O.G. Meijer, P.J. Beek, and J.H. van Dieën. Maximum lyapunov exponents as predictors of global gait stability: A modelling approach. *Med Eng Phys*, 34:428–436, Aug 2012. doi: 10.1016/j.medengphy.2011.07.024. URL `http://dx.doi.org/10.1016/j.medengphy.2011.07.024`.

S.R. Bullimore and J.F. Burn. Consequences of forward translation of the point of force application for the mechanics of running. *Journal of theoretical biology*, 238(1):211–219, 2006.

S.R. Bullimore and J.M. Donelan. Criteria for dynamic similarity in bouncing gaits. *Journal of theoretical biology*, 250(2):339–348, 2008.

J.L. Cabrera and J.G. Milton. Human stick balancing: Tuning lèvy flights to improve balance control. *Chaos*, 14:691–698, 2004.

S.G. Carver, N.J. Cowan, and J.M. Guckenheimer. Lateral stability of the spring-mass hopper suggests a two-step control strategy for running. *Chaos: An Interdisciplinary Journal of Nonlinear Science*, 19(2):026106, 2009.

P. Castagno, J. Richards, F. Miller, and N. Lennon. Comparison of 3-dimensional lower extremity kinematics during walking gait using two different marker sets. *Gait and Posture*, 3(2):87–87, 1995.

G.A. Cavagna. Force platforms as ergometers. *Journal of Applied Physiology*, 39(1):174, 1975.

G.A. Cavagna, N.C. Heglund, and C.R. Taylor. Mechanical work in terrestrial locomotion: two basic mechanisms for minimizing energy expenditure. *American Journal of Physiology-Regulatory, Integrative and Comparative Physiology*, 233(5):R243–R261, 1977.

J.J. Collins, A.A. Priplata, D.C. Gravelle, J. Niemi, J. Harry, and L.A. Lipsitz. Noise-enhanced human sensorimotor function. *Engineering in Medicine and Biology Magazine, IEEE*, 22(2):76–83, 2003.

S. Collins, A. Ruina, R. Tedrake, and M. Wisse. Efficient bipedal robots based on passive-dynamic walkers. *Science*, 307(5712): 1082, 2005.

R.H. Crompton, L. Yu, W. Weijie, M. Günther, and R. Savage. The mechanical effectiveness of erect and 'bent-hip, bent-knee' bipedal walking in australopithecus afarensis. *Journal of human evolution*, 35(1):55, 1998.

R.H. Crompton, E.E. Vereecke, and S.K.S. Thorpe. Locomotion and posture from the common hominoid ancestor to fully modern hominins, with special reference to the last common panin/hominin ancestor. *Journal of anatomy*, 212(4):501–543, 2008.

M.A. Daley, J.R. Usherwood, G. Felix, and A.A. Biewener. Running over rough terrain: guinea fowl maintain dynamic stability despite a large unexpected change in substrate height. *Journal of experimental biology*, 209(1):171, 2006.

W.T. Dempster. Space requirements of the seated operator. *WADC Technical Report 55159*, (WADC-55-159, AD-087-892):55–159, 1955.

V. Dietz, D. Schmidtbleicher, and J. Noth. Neuronal mechanisms of human locomotion. *Journal of Neurophysiology*, 42(5):1212–1222, 1979. URL `http://jn.physiology.org/content/42/5/1212.abstract`.

V. Dietz, K. Fouad, and C.M. Bastiaanse. Neuronal coordination of arm and leg movements during human locomotion. *European Journal of Neuroscience*, 14(11):1906–1914, 2001.

J.B. Dingwell and J.P. Cusumano. Nonlinear time series analysis of normal and pathological human walking. *Chaos*, 10(4):848–863, 2000.

J.B. Dingwell and H.G. Kang. Differences between local and orbital dynamic stability during human walking. *Journal of biomechanical engineering*, 129:586, 2007.

J.B. Dingwell, J.P. Cusumano, P.R. Cavanagh, and D. Sternad. Local dynamic stability versus kinematic variability of continuous overground and treadmill walking. *Journal of biomechanical engineering*, 123:27, 2001.

J.M. Donelan, R. Kram, and A.D. Kuo. Mechanical and metabolic determinants of the preferred step width in human walking. *Proceedings of the Royal Society of London. Series B: Biological Sciences*, 268(1480):1985, 2001.

J.M. Donelan, R. Kram, and A.D. Kuo. Mechanical work for step-to-step transitions is a major determinant of the metabolic cost of human walking. *Journal of Experimental Biology*, 205(23):3717–3727, 2002.

E.L. Du Brul. The general phenomenon of bipedalism. *American Zoologist*, 2(2):205–208, 1962.

M. Duarte and V.M. Zatsiorsky. Long-range correlations in human standing. *Physics Letters A*, 283(1-2):124–128, 2001.

J. Duysens, A.A.M. Tax, M. Trippel, and V. Dietz. Increased amplitude of cutaneous reflexes during human running as compared to standing. *Brain research*, 613(2):230–238, 1993.

M.H.A. Eames, A. Cosgrove, and R. Baker. Comparing methods of estimating the total body centre of mass in three-dimensions in normal and pathological gaits. *Human movement science*, 18(5): 637–646, 1999.

C. Eckart and G. Young. The approximation of one matrix by another of lower rank. *Psychometrika*, 1:211–218, 1936. ISSN 0033-3123. URL `http://dx.doi.org/10.1007/BF02288367`. 10.1007/BF02288367.

J.P. Eckmann and D. Ruelle. Ergodic theory of chaos and strange attractors. *Reviews of modern physics*, 57(3):617, 1985.

B. Efron. Bootstrap methods: another look at the jackknife. *The annals of Statistics*, 7(1):1–26, 1979.

B. Efron. Missing data, imputation, and the bootstrap. *Journal of the American Statistical Association*, pages 463–475, 1994.

B. Efron and R. Tibshirani. Bootstrap methods for standard errors, confidence intervals, and other measures of statistical accuracy. *Statistical science*, 1(1):54–75, 1986.

M.F. Eilenberg, H. Geyer, and H. Herr. Control of a powered ankle–foot prosthesis based on a neuromuscular model. *Neural Systems and Rehabilitation Engineering, IEEE Transactions on*, 18(2):164–173, 2010.

A.A. Faisal, L.P. Selen, and D.M. Wolpert. Noise in the nervous system. *Nat Rev Neuroscience*, 9(4):292–303, 2008. doi: 10.1038/nrn2258.Noise.

C.T. Farley, J. Glasheen, and T.A. McMahon. Running springs: speed and animal size. *Journal of experimental Biology*, 185(1):71–86, 1993.

G. Floquet. Sur les équations différentielles linéaires à coefficients périodiques,. *Annales de l'École Normale Supérieure*, 12:47–88, 1883.

C. Forsell and K. Halvorsen. A method for determining minimal sets of markers for the estimation of center of mass, linear and angular momentum. *Journal of biomechanics*, 42(3):361–365, 2009.

R.J. Full and D.E. Koditschek. Templates and anchors: neuromechanical hypotheses of legged locomotion on land. *Journal of Experimental Biology*, 202(23):3325–3332, 1999. URL `http://jeb.biologists.org/content/202/23/3325.abstract`.

S.A. Gard, S.C. Miff, and A.D. Kuo. Comparison of kinematic and kinetic methods for computing the vertical motion of the body

center of mass during walking. *Human movement science*, 22(6): 597–610, 2004.

H. Geyer and H. Herr. A muscle-reflex model that encodes principles of legged mechanics produces human walking dynamics and muscle activities. *Neural Systems and Rehabilitation Engineering, IEEE Transactions on*, 18(3):263–273, 2010.

H. Geyer, A. Seyfarth, and R. Blickhan. Positive force feedback in bouncing gaits? *Proceedings of the Royal Society of London. Series B: Biological Sciences*, 270(1529):2173–2183, 2003.

H. Geyer, A. Seyfarth, and R. Blickhan. Spring-mass running: simple approximate solution and application to gait stability. *Journal of theoretical biology*, 232(3):315–328, 2005.

H. Geyer, A. Seyfarth, and R. Blickhan. Compliant leg behaviour explains basic dynamics of walking and running. *Proc Biol Sci*, 273 (1603):2861–2867, Nov 2006. doi: 10.1098/rspb.2006.3637. URL `http://dx.doi.org/10.1098/rspb.2006.3637`.

A.L. Goldberger, L.A.N. Amaral, J.M. Hausdorff, P.C. Ivanov, C.K. Peng, and H.E. Stanley. Fractal dynamics in physiology: alterations with disease and aging. *Proceedings of the National Academy of Sciences of the United States of America*, 99(Suppl 1): 2466, 2002.

G. Golub and C. Reinsch. Singular value decomposition and least squares solutions. *Numerische Mathematik*, 14:403–420, 1970. ISSN 0029-599X. URL `http://dx.doi.org/10.1007/BF02163027`. 10.1007/BF02163027.

K.P. Granata and T.W. Lockhart. Dynamic stability differences in fall-prone and healthy adults. *J Electromyogr Kinesiol*, 18(2): 172–178, Apr 2008. doi: 10.1016/j.jelekin.2007.06.008. URL `http://dx.doi.org/10.1016/j.jelekin.2007.06.008`.

P. Grassberger and I. Procaccia. Measuring the strangeness of strange attractors. *Physica D: Nonlinear Phenomena*, 9(1-2):189–208, 1983.

C. Grebogi, E. Ott, S. Pelikan, and J.A. Yorke. Strange attractors that are not chaotic. *Physica D: Nonlinear Phenomena*, 13 (1-2):261 – 268, 1984. ISSN 0167-2789. doi: 10.1016/0167-2789(84)90282-3.

J.A. Grimes and J.W. Hurst. The design of ATRIAS 1.0 a unique monopod, hopping robot. In *Proceedings of the 15th Int. Conference of CLAWAR, Johns Hopkings University, Baltimore, USA*, 2012 (accepted).

M. Grimmer and A. Seyfarth. Stiffness adjustment of a series elastic actuator in an ankle-foot prosthesis for walking and running: The trade-off between energy and peak power optimization. In *Robotics and Automation (ICRA), 2011 IEEE International Conference on*, pages 1439–1444. IEEE, 2011.

J.W. Grizzle, J. Hurst, B. Morris, H.W. Park, and K. Sreenath. Mabel, a new robotic bipedal walker and runner. In *American Control Conference, 2009. ACC'09.*, pages 2030–2036. IEEE, 2009.

K.G. Gruben and W.L. Boehm. Force direction pattern stabilizes sagittal plane mechanics of human walking. *Human Movement Science*, 2011.

K. Gruber, H. Ruder, J. Denoth, and K. Schneider. A comparative study of impact dynamics:: wobbling mass model versus rigid body models. *Journal of Biomechanics*, 31(5):439–444, 1998.

J. Guckenheimer. Isochrons and phaseless sets. *Journal of Mathematical Biology*, 1(3):259–273, 1975.

J. Guckenheimer and P. Holmes. *Nonlinear oscillations, dynamical systems, and bifurcations of vector fields*, volume 42. Springer-Verlag, 1983.

M. Günther and R. Blickhan. Joint stiffness of the ankle and the knee in running. *Journal of biomechanics*, 35(11):1459–1474, 2002.

M. Günther, V.A. Sholukha, D. Kessler, V. Wank, and R. Blickhan. Dealing with skin motion and wobbling masses in inverse dynamics. *Journal of Mechanics in Medicine and Biology*, 3(3/4): 309–336, 2003.

E.M. Gutierrez-Farewik, A. Bartonek, and H. Saraste. Comparison and evaluation of two common methods to measure center of mass displacement in three dimensions during gait. *Human movement science*, 25(2):238–256, 2006.

K. Halvorsen, M. Eriksson, L. Gullstrand, F. Tinmark, and J. Nilsson. Minimal marker set for center of mass estimation in running. *Gait & posture*, 30(4):552–555, 2009.

J.M. Hausdorff, C.K. Peng, Z. Ladin, J.Y. Wei, and A.L. Goldberger. Is walking a random walk? evidence for long-range correlations in stride interval of human gait. *Journal of Applied Physiology*, 78 (1):349–358, 1995.

J.M. Hausdorff, P.L. Purdon, C.K. Peng, Z. Ladin, J.Y. Wei, and A.L. Goldberger. Fractal dynamics of human gait: stability of long-range correlations in stride interval fluctuations. *Journal of Applied Physiology*, 80(5):1448–1457, 1996.

J.M. Hausdorff, S.L. Mitchell, R. Firtion, C.K. Peng, M.E. Cudkowicz, J.Y. Wei, and A.L. Goldberger. Altered fractal dynamics of gait: reduced stride-interval correlations with aging and huntington's disease. *Journal of Applied Physiology*, 82(1):262, 1997.

J.M. Hausdorff, Y. Ashkenazy, C.K. Peng, P.C. Ivanov, H.E. Stanley, and A.L. Goldberger. When human walking becomes random walking: fractal analysis and modeling of gait rhythm fluctuations. *Physica A: Statistical mechanics and its applications*, 302 (1):138–147, 2001.

J.K. Hitt, T.G. Sugar, M. Holgate, and R. Bellman. An active foot-ankle prosthesis with biomechanical energy regeneration. *Journal of Medical Devices*, 4:011003, 2010.

A.L. Hof, M.G.J. Gazendam, and W.E. Sinke. The condition for dynamic stability. *Journal of biomechanics*, 38(1):1–8, 2005.

P. Holmes, R.J. Full, D. Koditschek, and J. Guckenheimer. The dynamics of legged locomotion: Models, analyses, and challenges. *SIAM Review*, 48:207–304, 2006.

Y. Hurmuzlu and C. Basdogan. On the measurement of dynamic stability of human locomotion. *Journal of Biomechanical Engineering*, 116:30, 1994.

Y.P. Ivanenko, R. Grasso, V. Macellari, and F. Lacquaniti. Control of foot trajectory in human locomotion: role of ground contact forces in simulated reduced gravity. *Journal of neurophysiology*, 87(6):3070–3089, 2002.

J.H. Jules Henry Poincaré. Sur le problème des trois corps et les équations de la dynamique. divergence des séries de m. lindstedt. *Acta Mathematica*, 13:1–270, 1890.

M.P. Kadaba, H.K. Ramakrishnan, and M.E. Wootten. Measurement of lower extremity kinematics during level walking. *Journal of Orthopaedic Research*, 8(3):383–392, 1990.

R.E. Kalman. A new approach to linear filtering and prediction problems. *Journal of basic Engineering*, 82(Series D):35–45, 1960.

K.T. Kalveram and A. Seyfarth. Inverse biomimetics: How robots can help to verify concepts concerning sensorimotor control of human arm and leg movements. *Journal of Physiology-Paris*, 103 (3):232–243, 2009.

J.W. Kantelhardt, E. Koscielny-Bunde, H.H.A. Rego, S. Havlin, and A. Bunde. Detecting long-range correlations with detrended fluctuation analysis. *Physica A: Statistical Mechanics and its Applications*, 295(3):441–454, 2001.

H. Kantz and T. Schreiber. *Nonlinear time series analysis*, volume 2000. Cambridge university press Cambridge, 1997.

S. Kiebel and A.P. Holmes. The general linear model. *Human brain function*, 2:725–760, 2003.

T.L. Kivell and D. Schmitt. Independent evolution of knuckle-walking in african apes shows that humans did not evolve from a knuckle-walking ancestor. *Proceedings of the National Academy of Sciences*, 106(34):14241–14246, 2009.

D. Kömpf, editor. *100 Jahre Deutsche Gesellschaft für Neurologie [1907 - 2007]*. Dt. Ges. für Neurologie, Berlin, 2007.

A.D. Kuo. The six determinants of gait and the inverted pendulum analogy: A dynamic walking perspective. *Human movement science*, 26(4):617–656, 2007.

K. Lechler and M. Lilja. Lower extremity leg amputation: an advantage in running? *Sports Technology*, 1(4-5):229–234, 2008.

D.V. Lee, J.E. Bertram, and R.J. Todhunter. Acceleration and balance in trotting dogs. *Journal of Experimental Biology*, 202(24):3565, 1999.

S.W. Lipfert. *Kinematic and dynamic similarities between walking and running*. Verlag Dr. Kovač, 2010.

D. Liu and E. Todorov. Evidence for the flexible sensorimotor strategies predicted by optimal feedback control. *J Neurosci*, 27(35): 9354–9368, Aug 2007. doi: 10.1523/JNEUROSCI.1110-06.2007. URL `http://dx.doi.org/10.1523/JNEUROSCI.1110-06.2007`.

E.N. Lorenz. Deterministic nonperiodic flow. *Journal of the Atmospheric Sciences*, 20(07), 1963.

C.O. Lovejoy, B. Latimer, G. Suwa, B. Asfaw, and T.D. White. Combining prehension and propulsion: the foot of ardipithecus ramidus. *Science*, 326(5949):72, 2009a.

C.O. Lovejoy, G. Suwa, S.W. Simpson, J.H. Matternes, and T.D. White. The great divides: Ardipithecus ramidus reveals the postcrania of our last common ancestors with african apes. *Science*, 326(5949):73, 2009b.

C.O. Lovejoy, G. Suwa, L. Spurlock, B. Asfaw, and T.D. White. The pelvis and femur of ardipithecus ramidus: the emergence of upright walking. *Science*, 326(5949):71, 2009c.

C. Ludwig. Möglichkeiten zur Einschränkung der Variabilität des Laufmusters. (in german). Master's thesis, Friedrich-Schiller-University, Jena, Germany, 2010.

C. Ludwig, A. Seyfarth, and H.-M. Maus. Multiple-step model-experiment matching allows precise definition of dynamical leg parameters in human running. *Journal of Biomechanics*, 2012 (accepted).

O. Mack. Investigations of piezoelectric force measuring devices for use in legal weighing metrology. *Measurement*, 40(7-8):746–753, 2007.

H.-M. Maus, S.W. Lipfert, M. Gross, J. Rummel, and A. Seyfarth. Upright human gait did not provide a major mechanical challenge for our ancestors. *Nat Commun*, 1:70, 2010. doi: 10.1038/ncomms1073. URL `http://dx.doi.org/10.1038/ncomms1073`.

H.-M. Maus, A. Seyfarth, and S. Grimmer. Combining forces and kinematics for calculating consistent centre of mass trajectories. *J Exp Biol*, 214(Pt 21):3511–

3517, Nov 2011. doi: 10.1242/jeb.057422. URL http://dx.doi.org/10.1242/jeb.057422.

D. Maykranz, S. Grimmer, S. Lipfert, and A. Seyfarth. Foot function in spring mass running. *Autonome Mobile Systeme 2009*, pages 81–88, 2009.

T.A. McMahon and G.C. Cheng. The mechanics of running: how does stiffness couple with speed? *J Biomech*, 23 Suppl 1:65–78, 1990.

T. McGeer. Passive dynamic walking. *The International Journal of Robotics Research*, 9(2):62–82, 1990.

C.P. McGowan, R.V. Baudinette, J.R. Usherwood, and A.A. Biewener. The mechanics of jumping versus steady hopping in yellow-footed rock wallabies. *Journal of experimental biology*, 208 (14):2741, 2005.

T. Mergner. A neurological view on reactive human stance control. *Annual Reviews in Control*, 34(2):177–198, 2010.

A. Merker, J. Rummel, and A. Seyfarth. Stable walking with asymmetric legs. *Bioinspiration & Biomimetics*, 6:045004, 2011.

A.E. Minetti and G. Belli. A model for the estimation of visceral mass displacement in periodic movements. *Journal of biomechanics*, 27 (1):97–101, 1994.

B.M. Nigg and W. Herzog. *Biomechanics of the musculo-skeletal system*. Wiley Chichester, 1999.

J.D. Ortega and C.T. Farley. Minimizing center of mass vertical movement increases metabolic cost in walking. *Journal of Applied Physiology*, 99(6):2099, 2005.

N.H. Packard, J.P. Crutchfield, J.D. Farmer, and R.S. Shaw. Geometry from a time series. *Physical Review Letters*, 45(9):712–716, 1980.

C.K. Peng, S.V. Buldyrev, S. Havlin, M. Simons, H.E. Stanley, and A.L. Goldberger. Mosaic organization of dna nucleotides. *Phys Rev E Stat Phys Plasmas Fluids Relat Interdiscip Topics*, 49(2):1685–1689, Feb 1994.

J. Perry. *Gait analysis: normal and pathological function*. Thorofare, NJ : SLACK, 1992.

Petman. URL `http://www.bostondynamics.com/robot_petman.html (20.11.2011)`.

F. Peuker, C. Maufroy, and A. Seyfarth. Leg-adjustment strategies for stable running in three dimensions. *Bioinspiration & Biomimetics*, 7(3):036002, 2012.

R.R. Playter and M.H. Raibert. Control of a biped somersault in 3d. In *Intelligent Robots and Systems, 1992., Proceedings of the 1992 lEEE/RSJ International Conference on*, volume 1, pages 582–589. IEEE, 1992.

H. Pontzer, D.A. Raichlen, and M.D. Sockol. The metabolic cost of walking in humans, chimpanzees, and early hominins. *Journal of human evolution*, 56(1):43–54, 2009.

W. Potthast and G.P. Brueggemann. Comparison of sprinting mechanics of the double transtibial amputee oscar pistorius with able bodied athletes. In *XXVIII International Symposium of Biomechanics in Sports*, pages 121–124, 2010.

I. Poulakakis and J.W. Grizzle. Monopedal running control: Slip embedding and virtual constraint controllers. In *Proc. IEEE/RSJ Int. Conf. Intelligent Robots and Systems IROS 2007*, pages 323–330, 2007. doi: 10.1109/IROS.2007.4399559.

A. Priplata, J. Niemi, M. Salen, J. Harry, L.A. Lipsitz, and J.J. Collins. Noise-enhanced human balance control. *Physical Review Letters*, 89(23):238101–238101, 2002.

V. Racic, J.M.W. Brownjohn, and A. Pavic. Reproduction and application of human bouncing and jumping forces from visual marker data. *Journal of Sound and Vibration*, 329(16):3397–3416, 2010.

K. Radkhah and O. von Stryk. Actuation requirements for hopping and running of the musculoskeletal robot biobiped1. In *IEEE/RSJ Int. Conf. on Intelligent Robots and Systems (IROS), Invited paper*, page to appear, 2011.

K. Radkhah, C. Maufroy, H.-M. Maus, D. Scholz, A. Seyfarth, and O. von Stryk. Concept and design of the biobiped1 robot for human-like walking and running. *International Journal of Humanoid Robotics*, 8 (3):439–458, 2011.

M.H. Raibert. *Legged Robots that balance*. The MIT Press,Cambridge, MA, 1985.

S. Revzen and J.M. Guckenheimer. Finding the dimension of slow dynamics in a rhythmic system. *Journal of The Royal Society Interface*, 2011. doi: 10.1098/rsif.2011.0431.

S. Revzen and J.M. Guckenheimer. Estimating the phase of synchronized oscillators. *Physical Review E*, 78(5):051907, 2008.

F.J. Romeiras and E. Ott. Strange nonchaotic attractors of the damped pendulum with quasiperiodic forcing. *Physical Review A*, 35(10):4404, 1987.

J. Rummel, Y. Blum, and A. Seyfarth. Robust and efficient walking with spring-like legs. *Bioinspir Biomim*, 5(4):046004, Dec 2010. doi: 10.1088/1748-3182/5/4/046004. URL `http://dx.doi.org/10.1088/1748-3182/5/4/046004`.

H. Sadeghi, P. Allard, F. Prince, and H. Labelle. Symmetry and limb dominance in able-bodied gait: a review. *Gait & Posture*, 12(1): 34–45, 2000.

F. Saibene and A.E. Minetti. Biomechanical and physiological aspects of legged locomotion in humans. *European journal of applied physiology*, 88(4):297–316, 2003.

M. Saini, D.C. Kerrigan, M.A. Thirunarayan, and M. Duff-Raffaele. The vertical displacement of the center of mass during walking: a comparison of four measurement methods. *Journal of biomechanical engineering*, 120:133, 1998.

T. Sauer, J.A. Yorke, and M. Casdagli. Embedology. *Journal of Statistical Physics*, 65(3):579–616, 1991.

S. Schmitt and M. Günther. Human leg impact: energy dissipation of wobbling masses. *Archive of Applied Mechanics*, pages 1–11, 2010.

W.J. Schwind and D.E. Koditschek. Approximating the stance map of a 2-dof monoped runner. *Journal of Nonlinear Science*, 10(5): 533–568, 2000.

V. Segers, P. Aerts, M. Lenoir, and D. De Clerq. Dynamics of the body centre of mass during actual acceleration across transition speed. *Journal of Experimental Biology*, 210(4):578, 2007.

J. Seipel and P. Holmes. A simple model for clock-actuated legged locomotion. *Regular and chaotic dynamics*, 12(5):502–520, 2007.

A. Seyfarth, H. Geyer, M. Günther, and R. Blickhan. A movement criterion for running. *J Biomech*, 35(5):649–655, May 2002.

A. Seyfarth, H. Geyer, and H. Herr. Swing-leg retraction: a simple control model for stable running. *J Exp Biol*, 206(Pt 15):2547–2555, Aug 2003.

G. Shan and C. Bohn. Anthropometrical data and coefficients of regression related to gender and race. *Applied ergonomics*, 34(4): 327–337, 2003.

K. Sreenath, H.W. Park, I. Poulakakis, and J.W. Grizzle. A compliant hybrid zero dynamics controller for stable, efficient and fast bipedal walking on mabel. *The International Journal of Robotics Research*, 30(9):1170–1193, 2011.

K. Sreenath, H.-W. Park, and J.W. Grizzle. Design and experimental implementation of a compliant hybrid zero dynamics controller with active force control for running on MABEL. In *IEEE International Conference on Robotics and Automation (ICRA)*, 2012.

M. Srinivasan and A. Ruina. Computer optimization of a minimal biped model discovers walking and running. *Nature*, 439(7072): 72–75, 2005.

D.H. Sutherland. The evolution of clinical gait analysis: Part ii kinematics. *Gait & posture*, 16(2):159–179, 2002.

G. Taga. Emergence of bipedal locomotion through entrainment among the neuro-musculo-skeletal system and the environment. *Physica D: Nonlinear Phenomena*, 75(1-3):190–208, 1994.

F. Takens. Detecting strange attractors in turbulence. *Lecture Notes in Mathematicks*, 898:366–381, 1981.

T. Tao, V. Vu, and M. Krishnapur. Random matrices: Universality of esds and the circular law. *The Annals of Probability*, 38(5): 2023–2065, 2010.

J. Theiler, S. Eubank, A. Longtin, B. Galdrikian, and J.D. Farmer. Testing for nonlinearity in time series: the method of surrogate data. *Physica D: Nonlinear Phenomena*, 58(1-4):77–94, 1992.

S.K.S. Thorpe, R.L. Holder, and R.H. Crompton. Origin of human bipedalism as an adaptation for locomotion on flexible branches. *Science*, 316(5829):1328, 2007.

W.J. Wang and R.H. Crompton. The role of load-carrying in the evolution of modern body proportions. *Journal of anatomy*, 204 (5):417–430, 2004.

W.J. Wang, R.H. Crompton, Y. Li, and M.M. Günther. Energy transformation during erect and 'bent-hip, bent-knee' walking by humans with implications for the evolution of bipedalism. *Journal of human evolution*, 44(5):563–579, 2003.

C.V. Ward. Interpreting the posture and locomotion of australopithecus afarensis: Where do we stand? *American journal of physical anthropology*, 119(S35):185–215, 2002.

L.M. Ward and P.E. Greenwood. 1/f noise. *Scholarpedia, 2(12):1537.*, 2(12):1537, 2007.

T. Weaver and R. Klein. The evolution of human walking. In *Human Walking*. Lippincott: Williams & Wilkins, 2006.

E.R. Westervelt, J.W. Grizzle, and D.E. Koditschek. Hybrid zero dynamics of planar biped walkers. *Automatic Control, IEEE Transactions on*, 48(1):42–56, 2003.

H. Whitney. Differentiable manifolds. *The Annals of Mathematics*, 37(3):645–680, 1936.

E.T. Whittaker. *A treatise on the analytical dynamics of particles and rigid bodies: with an introduction to the problem of three bodies*. Cambridge Univ Press, 1904.

M.W. Whittle. Three-dimensional motion of the center of gravity of the body during walking. *Human movement science*, 16(2-3): 347–355, 1997.

M.B. Wilk and R. Gnanadesikan. Probability plotting methods for the analysis for the analysis of data. *Biometrika*, 55(1):1–17, 1968.

S.B. Williams, J.R. Usherwood, K. Jespers, A.J. Channon, and A.M. Wilson. Exploring the mechanical basis for acceleration: pelvic limb locomotor function during accelerations in racing greyhounds (canis familiaris). *Journal of Experimental Biology*, 212 (4):550–565, 2009.

D.A. Winter. *Biomechanics and motor control of human movement*. John Wiley & Sons Inc, 2009.

H. Witte, S. Recknagel, J.G. Rao, M. Wüthrich, and C. Lesch. Is elastic energy storage of quantitative relevance for the functional morphology of the human locomotor apparatus? *Acta anatomica*, 158(2):106–111, 1997.

S. Yakovenko, V. Gritsenko, and A. Prochazka. Contribution of stretch reflexes to locomotor control: a modeling study. *Biological cybernetics*, 90(2):146–155, 2004.